Mechanical behaviour of tools for shearing Ultra High-Strength Steels: influence of the microstructure on fracture and fatigue micro-mechanisms of tool steels and evaluation of micro-mechanical damage in tools

Ingrid Picas

Supervisors: Dr. Daniel Casellas Padró
Prof. José Manuel Prado Pozuelo

A Thesis submitted for the degree of Doctor in the Universitat Politècnica de Catalunya, Fundació CTM Centre Tecnològic.

Manresa, September 2012

4. DISCUSSION

In the previous chapter the results obtained in the course of this investigation regarding:

- the microstructure of the studied tool steels,
- their macro- and micro-mechanical properties,
- crack nucleation and growth under monotonic loads (*R*-curve),
- fatigue crack nucleation and propagation mechanisms,
- mechanical and tribological behaviour of industrial and laboratory tools,
- effects of the shearing process parameters and
- tool life prediction models,

have been discussed separately, in their corresponding sections. However and given the existing relationships amongst them, in the present chapter they are settled all together in order to help obtaining explanations, from an in-depth micro-mechanical point of view, of the failure mechanisms governing the behaviour of shearing tools and improve the microstructural design of tool steels as well as the performance of tools.

This global approach involves considering the problem of the failure of industrial tools from its root causes; namely the reason why cracks nucleate and propagate in tool steels, when, where and how they do it depending on the applied mechanical solicitations and the microstructural features, process parameters or tribological mechanisms. That should bring to light the guidelines to enhance the performance of such tools and broaden the possibilities of the shearing processes to manufacture new and more challenging components. Therefore, the objective of the following sections is not to review the aforementioned results, but to reveal the significance of the findings obtained to understand the failure of industrial tools.

This chapter has been structured in three different sections, each one of these dealing with the topics: fracture and fatigue micro-mechanisms of tool steels, the case of real tools with an in-depth study of the failure mechanisms from micro-mechanical point of view and the suitability of the life predicting models for these tools.

4.1 Fracture and fatigue micro-mechanisms of tool steels

4.1.1 Crack nucleation under monotonic load

Failure of ingot cast tool steels was already reported by many authors to be initiated by cleavage fracture of primary carbides rather than matrix rupture ([BER98], [ANT97], [RAM99] amongst others). That is verified in this investigation since failure initiation sites of 1.2379, UNIVERSAL and K360 are certainly

located at broken primary carbides. Interestingly, no primary carbide decohesion is observed in any of the studied samples.

Under monotonic load the stresses at which the first carbides break, σ^{RC}, i.e. when the first cracks nucleate in the microstructure, vary depending on the carbide type, size, morphology and distribution in the matrix. As the load goes up during the test cracks grow from these broken primary carbides through the microstructure until they attain a critical size and the sample fractures (see section 3.2.3).

As shown in section 3.2.3, in 1.2379, σ^{RC} values of M_7C_3 carbides are 700 – 900 MPa and 500 – 700 MPa for D2 and D3 sample configurations respectively. In K360 D2, the M_7C_3 carbides have a σ^{RC} lower than those of 1.2379 (500 – 700 MPa). This difference is attributed to the slightly higher size and more irregular shape of M_7C_3 carbides in K360 compared to those in 1.2379. MC carbides of K360 have smaller sizes and they are more rounded compared to the M_7C_3 embedded in the same steel, accordingly they show higher σ^{RC} values (1300 - 1500 MPa). UNIVERSAL D2 shows the highest σ^{RC} since its M_7C_3 carbides do not fail until 1300 – 1500 MPa and the MC at 1600 – 1800 MPa. In UNIVERSAL D3, σ^{RC} values are 1000 – 1200 MPa and 1400 – 1600 MPa for the M_7C_3 and MC carbides, respectively.

The higher σ^{RC} results of UNIVERSAL primary carbides are understood through their lower sizes, more regular and rounded shapes compared to those of 1.2379 and K360. However, apart from the size and morphological features of the primary carbides embedded in 1.2379, UNIVERSAL and K360, these carbides also present different micro-mechanical properties; namely the M_7C_3 of 1.2379 have higher E and H than those of K360 and UNIVERSAL, while the MC carbides of the aforementioned steels show higher E and H than the M_7C_3 of 1.2379. Carbides of UNIVERSAL show the highest K_C values, what also contributes to increase their σ^{RC} with respect to the other steels.

The breakage of primary carbides can also be influenced by the presence of defects at their inside. As shows Figure 4.1.1, carbides in 1.2379 and K360 present pores or holes which are probably formed during the solidification process and remained even after forging. In UNIVERSAL none of these are observed, contributing to explain why the σ^{RC} of its carbides is the highest amongst the studied ingot cast steels. However, some MC primary carbides in UNIVERSAL solidify from non metallic particles or impurities, as show Figures 4.1.1 e) and f). Such heterogeneous nucleation can be detrimental for the carbide resistance to fracture.

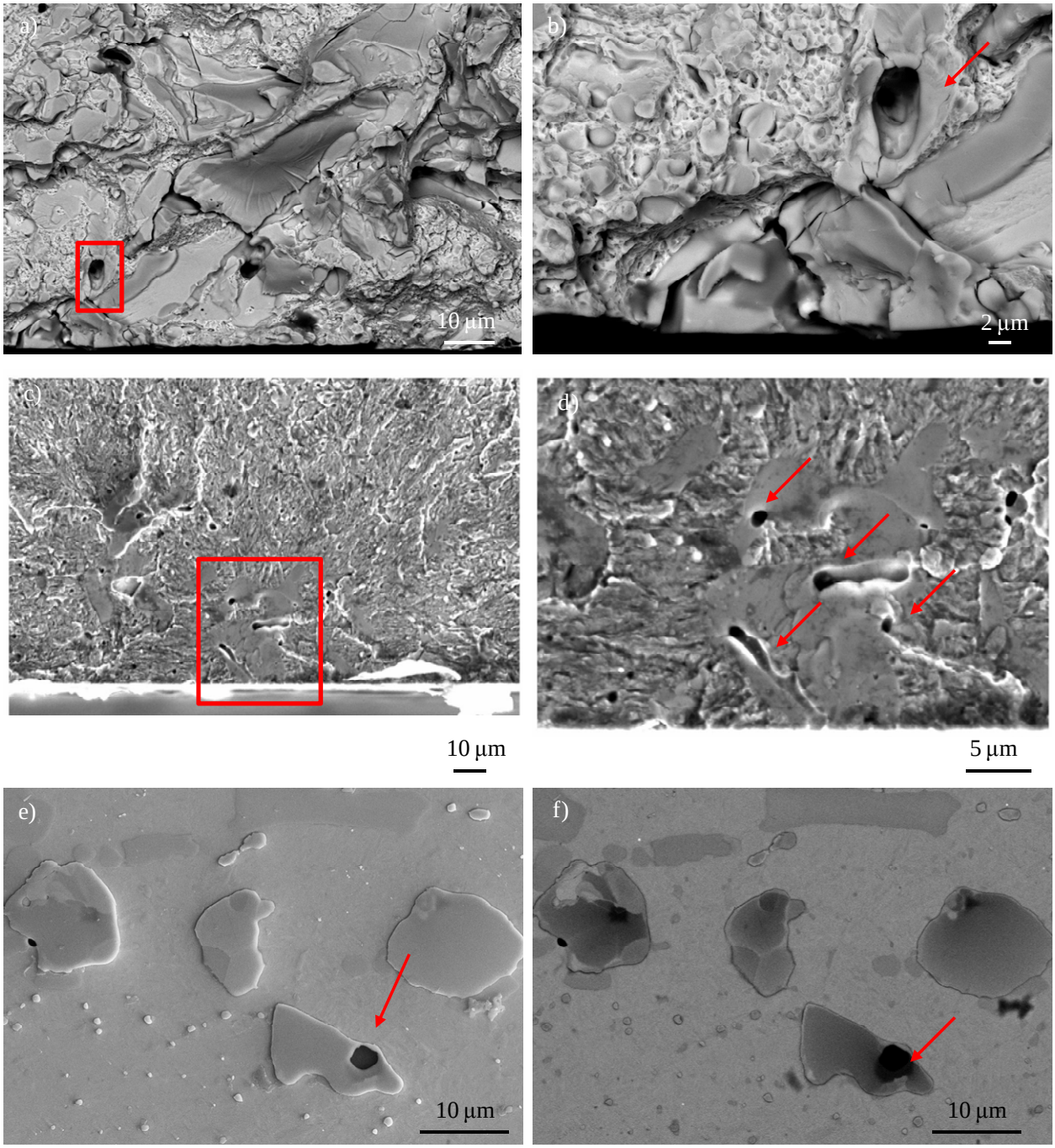

Figure 4.1.1 Examples of different types of defects observed in primary carbides: a)-b) holes in M_7C_3 carbides of 1.2379; c)-d) holes in M_7C_3 carbides of K360 and e)-f) non metallic particle at MC carbides of UNIVERSAL

Another parameter with direct effects on σ^{RC} is the distribution of primary carbides in the metallic matrix. As reported by Rammerstorfer et al. [RAM99], the matrix in carbide rich bands starts to yield at much smaller macroscopic stress levels than in carbide poor bands. As a consequence, carbides in these rich layers fracture by cleavage at lower applied stresses (that means lower σ^{RC}) than those in poor bands. This argument allows to finding an explanation of why results of σ^{RC} in D2 samples are higher than in D3. As shown previously in section 3.2.3 (Figure 3.2.15), in D2 samples matrix and primary carbide bands alternate at the zone submitted to highest stress during the three points bending test. Contrarily, in D3 a

whole carbide rich layer, or more than one, is located at this zone. Therefore, the matrix between these carbides in rich layers is prone to start yielding at lower macroscopic stress levels in D3 samples than in D2 (i.e. σ^{RC} values are lower for D3 than D2).

According to the arguments presented in the last paragraph, the properties of the matrix also contribute to determining the onset for fracture of primary carbides. After the work of Yokoi et al. [YOK03], the stress for primary carbide cracking corresponds to the yield stress of the matrix at its surrounding. Pile-up dislocations at primary carbides result in cracking and if that is the case, large carbides fracture easier due to the higher number of dislocations pile-ups at their surroundings. This means that carbide cracking is promoted when the yield stress of the matrix is low and when the carbide is large and/or it has an irregular shape.

The properties of the metallic matrix are given by the tempering treatment, in which small secondary carbides precipitate on specific crystallographic habit planes within the martensitic matrix. The size of these precipitates is strongly dictated by the tempering temperature, since at low and intermediate tempering temperatures, the substitutional alloying elements do not have sufficient mobility to form carbide particles. At higher tempering temperatures, however, diffusion accelerates, and the precipitated carbides rapidly coarsen. Therefore, a fine distribution of secondary carbides is only possible provided that the tempering temperature allows the alloying elements to diffuse very short distances.

Since these secondary carbides control the plastic deformation of the matrix (namely through their size, coherency and distribution), i.e. they determine the movement of dislocations. Dislocations movement, in turn, determines the yield stress of the matrix and the fracture of primary carbides by cleavage. The nucleation of cracks which propagate through the microstructure to unstable fracture is a consequence of the breakage of these primary carbides; hence every micro-constituent of a tool steel plays its own role when it comes to nucleation and propagation of cracks. Thus, not only primary carbides must be controlled and well adjusted depending on the desired application, but also the small secondary precipitates contribute to the failure of tool steels and are an important concern for tool steel design considerations.

The same arguments about the role of microstructural constituents are valid to explain the failure mechanisms of HWS under monotonic load, except that apart from primary carbides, inclusions are also involved in the mechanism. In this steel, the macroscopic stress has to go up to 3400 – 3600 and 3800 – 4000 MPa to nucleate any crack in the microstructure at inclusion and carbide particles respectively. Such high values of σ^{RC} compared to those obtained for ingot cast steels owe to the small, rounded, and homogeneous distribution of primary carbides in the microstructure. Such microstructure prevents the formation of dislocation pile-ups since dislocations move easier through the microstructure compared to

ingot cast steels. Inclusion particles, in turn, are brittle and have not a good cohesion with the matrix lattice; furthermore, their sizes use to be higher than those of carbides in PM steels, and that is why it is easier to nucleate cracks from them than from primary carbides.

To summarise, the nucleation of cracks in tool steels is due to the failure of primary carbides by cleavage (and inclusion particles in case of PM steels) when the matrix at their surrounding exceeds its yield stress. The yield stress of the matrix, in turn, is determined by the secondary fine carbides precipitated in the martensite matrix during tempering.

4.1.2 Subcritical growth of cracks under monotonic load

With the increase of the applied load, cracks nucleated at primary carbides or inclusion particles grow out through the matrix. As carbides are generally well adhered to the matrix, cracks easily cross through the interface. However, due to the higher toughness of the metallic matrix compared to primary carbides, if a crack is to grow any further from the carbide, an increase of load is required. This implies that the material resistance to fracture, R, also increases and consequently, that these materials have a rising R-curve behaviour.

As schematised in Figure 3.2.21, the mechanism of crack propagation under monotonic loading consists, prior to observe any crack growth at the surface, in the plastic deformation of the metallic matrix around broken primary carbides. As discussed in section 3.2.3.1 and 1.2.1.2, plastic deformation and sinking of the matrix takes place since, as a result of the opened crack in the carbide below the surface, the matrix at the surface is highly stretched. The matrix at the surface is tougher than the matrix below it because the first one is locally under plane stress conditions, while the second is under plane strain. As it is shown in Figure 1.2.5, fracture toughness in plane stress is much higher than in plane strain conditions. Therefore, the matrix at the surface has a higher toughness than below this, and it is capable of developing more plastic deformation before cracking. As a result, the crack grows easier below the surface and it forms a balloon-like shape instead of the semi-circle typically assumed.

At the initial stages of crack growth when cracks grow from the primary carbide to the metallic matrix, the shape of broken primary carbides (i.e. the shape of nucleated cracks) also contributes determining the preferred crack growth direction in the material. As at a certain applied stress K values vary in function of the crack geometry (a/c ratio), at 0º and 90º with respect to the sample surface K has different values if primary carbides are shallow or deep. Shallow carbides have $a/c < 1$ and $K^{90^\circ} > K^{0^\circ}$, meaning that cracks nucleated from them tend to grow perpendicular to the surface. In contrast, deep carbides have $a/c > 1$ and $K^{0^\circ} > K^{90^\circ}$, and if this is the case cracks spread first parallel to the surface. This “competition” between 0º and 90º crack growths lasts until K^{0° finally approaches K^{90° or vice versa and as a result, cracks attain

semi-circular shapes (a/c = 1). From this moment and so on, cracks grow in equilibrium keeping this more stable geometries near a/c ratios of 1, in which $K^{0^o} = K^{90^o}$.

Gomes et al. [GOM97] could only find very shallow cracks on the sample surface prior to unstable fracture despite corroborating that final failure initiation sites had approximately semi-circular geometries. After the explanation of the paragraph above in which cracks certainly attain semi-circular shapes provided that they have sufficiently grown, it is plausible to say that in the stepwise tests performed by Gomes et al. the last stop before unstable fracture was well-before any crack had developed semi-circular geometries. In these steels, fracture occurs in a rather unstable manner and it is almost impossible to stop stepwise tests at the moment just before failure. The achievement of this goal is only possible provided that in situ information about the cumulated damage in the microstructure is acquired, for instance, by means of acoustic emission. That is why in this work this technique has been developed and applied in fracture tests (see section 3.2.4 and 3.2.6.1), and by which stepwise tests could be monitored and halted instants before unstable failure of samples took place. Although there are many cracks that nucleate and start propagating in the sample surface, only very few (namely one or two) attain longer sizes and a/c = 1. These cracks rapidly grow further and even coalesce with other cracks, leading imminently to failure.

These findings are relevant to understanding subcritical growth of microcracks in tool steels and assess possible *R*-curve behaviours. As shown in section 3.2.6.2, ingot cast steels show a certain dependency of toughness and crack size, i.e. a rising *R*-curve, which is more accentuated depending on the steel microstructure and sample configuration (D2 or D3). HWS, in turn, has a flat *R*-curve and therefore, toughness is independent of the initial crack size. As a consequence in ingot cast steels, toughness is size dependent and that means that in function of the initial crack size, $2c_0$, and the applied stress, σ_a, the resulting fracture toughness may be lower than the toughness at the plateau, K_{IC}.

The influence of the initial crack size, in terms of $2c_0$, in the applied stress intensity factor for unstable fracture, K_R, and the corresponding applied stress level, σ_r, is shown in Figure 4.1.2 a) and b) for the studied steels, sample configurations and a/c ratios of 0,5 and 1 respectively. In these diagrams it can be observed that there is an inverse relationship between K_R, $2c_0$ and σ_r respectively. In Figure 4.1.2 K_R has been plotted vs σ_r for better convenience to rationalise the results with respect to stresses which are predicted in tools by means of FE-simulations. However, it has to be borne in mind that these stresses cannot be directly compared to the ones applied in the fracture tests carried out to determine the *R*-curves, and that the notion of *R*-curve stands for the dependency of the toughness with respect to the crack size, not to the applied stress. Anyway, the three parameters K_R, $2c_0$ and σ_r can be related through Equation 2.4.2.

If a macroscopic stress of about 1500 MPa is applied (what is has been observed to be reasonable for tools after results presented in chapter 3), the effective toughness of the material is not as predicted after E 399-90 tests, as shows Table 4.1.1, but it is lower instead. In 1.2379 and K360 the difference between K_{IC} and the estimated K_R at 1500 MPa is of about 30 %, in UNIVERSAL it is comprised between 10 and 20 % for D2 and D3 configurations respectively, and in HWS there is practically no variation of K_R with respect to K_{IC}.

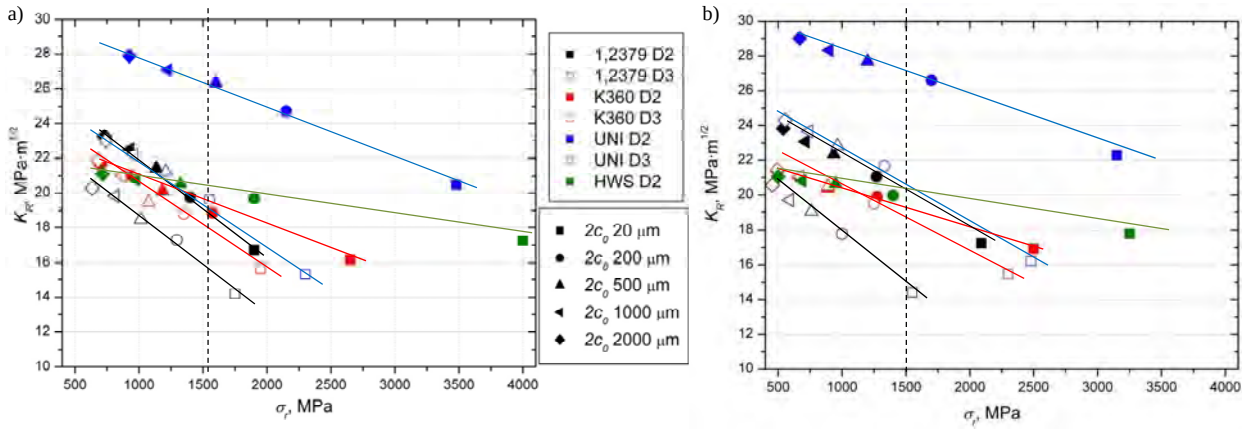

Figure 4.1.2 Applied stress intensity factors for unstable fracture, K_R, vs the corresponding applied stresses, σ_r, considering the different $2c_0$ values: a) for *a/c* 0,5 and b) for *a/c* 1. Dashed lines indicate the estimated stress level in tools of 1500 MPa

Table 4.1.1 K_{IC} (E 399-90), estimated K_R at 1500 MPa and the difference calculated between these two for the studied steels under D2 and D3 configurations and for *a/c* 0,5 and 1

		D2				*D3*		
K, MPa·m$^{1/2}$	*a/c*	*1.2379*	*K360*	*UNIVERSAL*	*HWS*	*1.2379*	*K360*	*UNIVERSAL*
K_{IC} (E 399-90)	-	28	28	29	21	22	22[(1)]	24
K_R (at 1500 MPa)	0,5	19	20	26	21	16	18	19
Difference, %	0,5	32,1	28,6	10,3	2,4	27,3	18,2	20,8
K_R (at 1500 MPa)	1	20	20	27	20	15	19	21
Difference, %	1	28.5	28.5	6.9	2.8	31.8	13.6	12.5

[(1)] K_{IC} for K360 D3 is assumed to be equal to the value of 1.2379 D3

As it follows from the results reported in Table 4.1.1, in ingot cast tool steels the reduction of toughness in case that small cracks (or high stresses) are involved and compared to the values determined for long cracks (K_{IC}), is so significant that it is possible that HWS shows a higher K_R even if it has a lower K_{IC}. Horton and Child [HOR83] reported that the reason for the differences between K_{IC} in conventional and PM steels lies in the fact that microcracks formed at or in carbides link up, with a minimum of plastic deformation of the matrix, owing to the smaller ligament sizes in the PM steel. In this sense, Muro et al. [MUR02] and Bolton and Gant [BOL98] found that the K_{IC} was controlled by the ductility of the matrix more than the primary carbides embedded, and that in turn, is a result of the heat treatment conditions and the volume fraction, size and distribution of small secondary precipitates within the martensitic lattice.

These are very important considerations that must be taken into account when designing tools made of ingot tool steels with high fracture resistance for applications under high stress levels, since small cracks nucleated in the microstructure have lower toughness values than those expected after K_{IC}. Therefore, different properties might be taken into consideration depending on the tool application and the acting stresses, since the behaviour of the tool steel can vary substantially.

From this standpoint, it is plausible to say that in tools subjected to high stresses as these for shearing UHSS, an HWS-type microstructure not only has higher resistance to crack nucleation from broken primary carbides as shown in section 3.2.3, but it also shows higher K_R than ingot cast steels if small cracks are nucleated in the microstructure. As follows from Figure 4.1.2, cracks smaller than 500 μm can already present higher K_R in HWS than in 1.2379 and K360. Nevertheless, if the applied stresses are low enough so that nucleated cracks can grow to longer sizes (more than 500 μm), an ingot cast steel type microstructure can show a better performance since K_{IC}, in this case, is higher than in HWS.

4.1.3 Fatigue crack nucleation and propagation: rationalization in basis of the mechanisms observed under monotonic load

In fatigue, crack nucleation and propagation mechanisms turn up a bit different than under monotonic conditions. However, real tools are subject to repetitive loadings so the behaviour of tool steels under these conditions is a key factor allowing to explaining the damage observed. In fatigue, the micro-mechanical mechanisms of crack nucleation and growth account for an extra consideration that is the metallic matrix may reduce its mechanical properties as long as the number of cycles increases. Such loss of mechanical properties of the metallic matrix may imply a decrease in hardness, yield stress and toughness. Softening of the metallic matrix is understood after Fukaura et al. [FUK04] by the destabilisation of the tempered martensite structure due to strain localisation processes, such as persistent slip bands (PSBs) and vein structure formation. The occurrence of these phenomena is difficult to be ascertained unless TEM or similar means are employed, but the consequences of their presence in the microstructure are tangible and they have been studied in this Thesis.

As presented in section 3.2.5, the nucleation of cracks in cyclic conditions is also a matter in which primary carbides are involved (and inclusions in case of PM steels). But contrarily to what it was explained under monotonic loads, in fatigue is not necessary that the applied stress exceeds a critical value so that the carbide breaks (such as the determined σ^{RC}). In this case, different situations are possible depending on the applied load and the microstructure of the steel. To help illustrating the effects of the applied stress level on the different microstructures considered in this Thesis, Figure 4.1.3 reassembles in a same diagram the results obtained in terms of σ^{R}, σ^{max} and σ^{RC} for the steels and configurations studied.

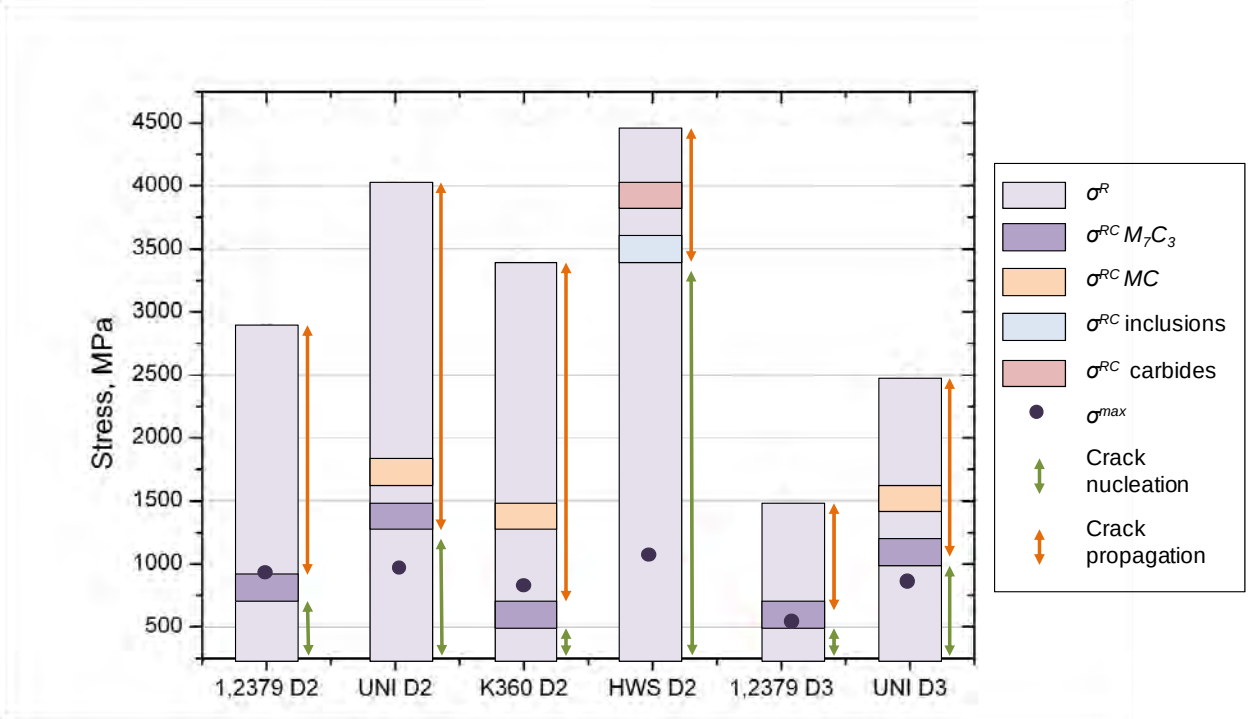

Figure 4.1.3 Plot of σ^{R}, σ^{max} and σ^{RC} for the steels considered in this Thesis. The green and orange arrows indicate the nucleation and propagation stages of cracks under monotonic loading

Consider for instance, the case of 1.2379 D2. In this steel and configuration it can be observed that $\Delta\sigma^{fat}$ and σ^{RC} lie almost on the same stress level. This implies that crack nucleation in fatigue is due to a great extent, to primary carbides broken already at the first load cycles. As shown in section 3.2.5.1, provided that the ΔK of these cracks at the broken carbide exceeds ΔK_{TH}, the rest of the fatigue life is spent in their propagation until one of them attains the critical size for failure. The nucleation stage in 1.2379 is hereby very short compared to the number of cycles concerned for propagation, as well as under monotonic loads, the applied stress at which carbide start to break are much lower than the applied stress in which samples break ($\sigma^{RC} << \sigma^{R}$ as indicate the green arrow in Figure 4.1.3).

In fatigue, initial crack propagation when cracks are still confined at the carbide cluster is rather tortuous and does not show a stable growth. Similar to monotonic loads, the shape of the fractured carbides determine the shape of initial cracks and therefore, the condition of $\Delta K \geq \Delta K_{TH}$ necessary so that propagation starts. The present Thesis has shown in section 3.2.5.1 that as long as $\Delta K < \Delta K_{TH}$, propagation does not take place. However, if the size of nucleated cracks fulfils the aforementioned condition and they successfully grow through the matrix, once they attain a certain size (usually when they propagate out from the initial cluster) the growth is more stable and steady, independently of the primary carbides ahead, as shown in section 3.2.5.2. Once a stable propagation rate is attained, cracks approach semi-circular shapes and keep growing in equilibrium for the rest of the fatigue cycles.

In case of UNIVERSAL D2, in Figure 4.1.3 it can be observed that in contrast to 1.2379 D2, $\Delta\sigma^{fat}$ is lower than σ^{RC}. Thus, the arguments proposed to explain the fatigue nucleation and propagation mechanisms in 1.2379 D2 cannot be applied in case of UNIVERSAL D2. Assuming that primary carbides do not suffer from fatigue, which is plausible as ceramic particles, at the applied stresses of $\Delta\sigma^{fat}$ they are not expected to break. However, primary carbides also appear at the failure initiation sites on fracture surfaces. That is why in case of UNIVERSAL the breakage of carbides cannot be understood because the applied stress is higher than σ^{RC} but because the strain in the matrix around the carbide is higher than the strain that carbides can withstand. As explained in section 3.2.5, this phenomenon is attributed to the loss of mechanical properties of the metallic matrix during fatigue tests.

In an attempt to shed light on this effect, the metallic matrix around fatigue cracks in UNIVERSAL was evaluated by means of instrumented indentation tests. As shown in Figure 4.1.4, there is a slight reduction of mechanical properties in the nearby of cracks, compared to the values measured further than 20 mm from the fracture surface (E was 253 ± 8 GPa and H 9,9 ± 0,4 GPa, with E_{min} and E_{max} of 235 and 263 GPa and H_{min} and H_{max} of 9,3 and 10,4 GPa).

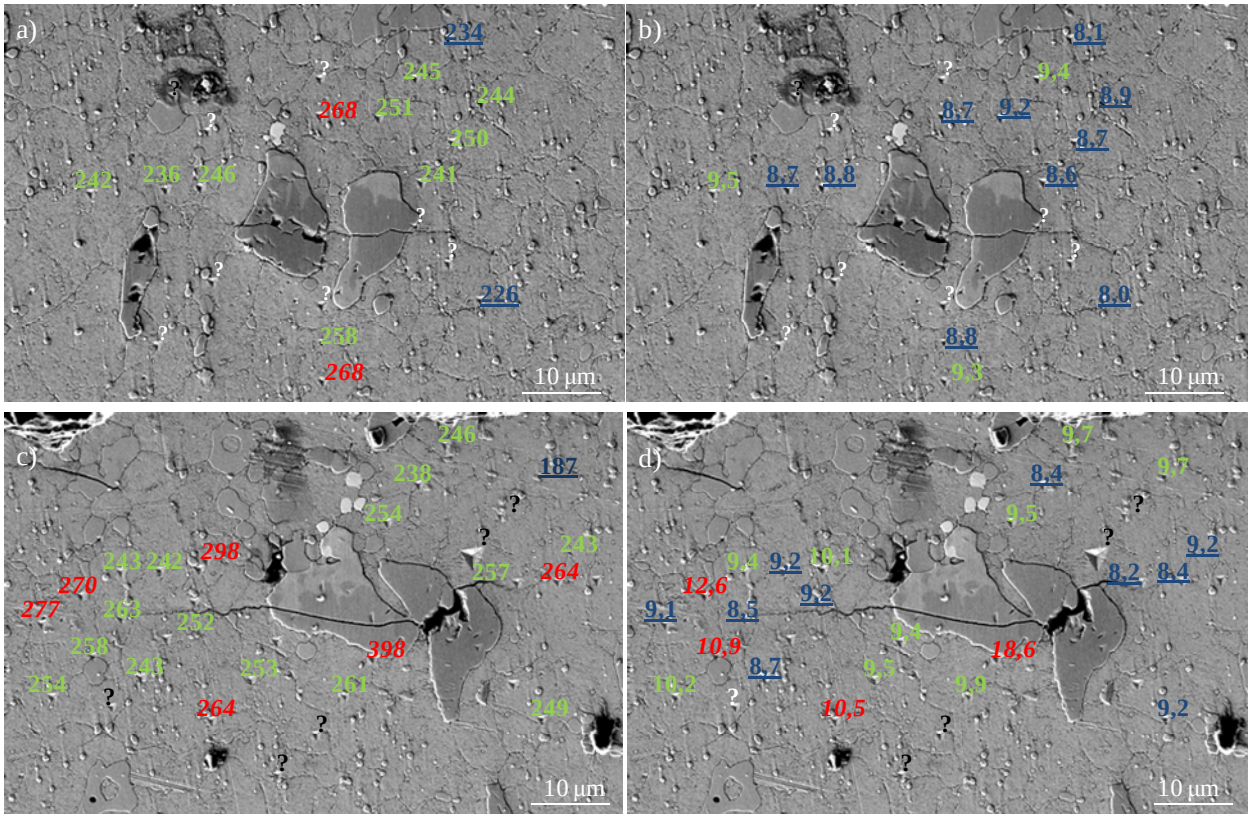

Figure 4.1.4 Micro-mechanical properties of the metallic matrix: a) and c) Young's modulus and b) and d) hardness values

To the author's knowledge, the amount of scientific publications regarding the evaluation of micromechanical properties of the matrix around broken primary carbides is scarce. However, the work of Nyström et al. [NYS95] used a similar approach, in which cyclic plastic zones around fatigue cracks of austenitic and ferritic stainless steels were studied by means of hardness measurements using an ultra-low indentation system. The strain distribution ahead of fatigue cracks was evaluated by these authors upon the assumption that a certain plastic strain amplitude implies a certain stress level, which can be correlated with the measured hardness. Close to the crack the material was observed to be heavily deformed and in the austenitic material slip band formation was frequent. Unfortunately, this phenomenon was not identified in this Thesis for tool steel materials, due to their higher hardness and low plasticity ahead of fatigue cracks. A more in-depth analysis using TEM or EBSD should be considered in order to ascertain the presence of such PSBs in the material under consideration.

Figure 4.1.5 plots the estimated stress-strain curves of a carbide and the matrix. It is assumed that carbides behave as completely elastic bodies (with E calculated by means of nano-indentation) and that they fail when σ attains σ^{RC}. For the example that is presented here, σ^{RC} and E of the M_7C_3 carbides in UNIVERSAL are considered (see Tables 3.2.4 and 3.2.6). The strain level corresponding to σ^{RC} is ε^{RC}, and it is associated with the critical strain for failure of the carbide. Regarding the properties of the metallic matrix of UNIVERSAL in turn, the elastic regime is modelled by its E, as determined by means of nano-indentation (see Table 3.2.5). It is well-known that nano-indentation overestimates E values compared to conventional tensile tests, but as the macro-mechanical properties of the matrix isolated from carbides are difficult to be determined, this value is taken into account since it is already a rather good approximation.

Similar to E, the yield stress, σ_y, of the matrix isolated from carbides is not easy to determine by means of macroscopical tests. Spherical nano-indentation tests were performed in an attempt to quantify this property and, even though further work is required to improve the accuracy of the values obtained, a σ_y of 1400 MPa was finally taken for the example of Figure 4.1.5. The plastic behaviour of the matrix is assumed as that obtained in compression tests with UNIVERSAL samples. As the contribution of primary carbides in the plastic flow is assumed to be negligible, the aforementioned approximation was found reasonable enough as to be applied.

Some experimental tests should be performed to assess the softening or loss of σ_y of the matrix with the increase of the number of cycles. However, these are time consuming experiments and out of the frame of this Thesis, that is why they are progressing as future works. In front of that lack of experimental data, two different and reduced σ_y are considered: 1100 and 900 MPa. These values are picked from the literature in [HER83], page 499, in case of softening of quenched and tempered steels, as summarised in Table 4.1.2.

Table 4.1.2 Monotonic and cyclic properties of selected engineering alloys [HER83], page 499

Material	*Condition*	σ_y*(monotonic)*/σ_y*(cyclic)*
SAE 1045	Q + T (370 ºC), 410 HBN (43,6 HRC)	1365/825
SAE 1045	Q + T (180 ºC), 595 HBN (56,8 HRC)	1860/1725
AISI 4340	Q + T (425 ºC), 409 HBN (43,6 HRC)	1370/825

It is expected that the plastic behaviour of the softened matrix changes with respect to the initial state. However, as no information could be provided in this regard, for this example it was just assumed that it remained unmodified.

If an applied stress level of 1100 MPa is considered, as shown in Figure 4.1.5, no carbides should break at the first load cycle since $\sigma_a < \sigma^{RC}$ and $\varepsilon^m < \varepsilon^{RC}$. If a reduction of mechanical properties to σ_y of 1100 MPa takes place after a certain number of cycles, still no carbides are expected to fail since $\sigma_a < \sigma^{RC}$ and $\varepsilon^{msoft1} < \varepsilon^{RC}$. However, if the reduction is to σ_y of 900 MPa, even though $\sigma_a < \sigma^{RC}$, breakage can occur since $\varepsilon^{msoft2} > \varepsilon^{RC}$.

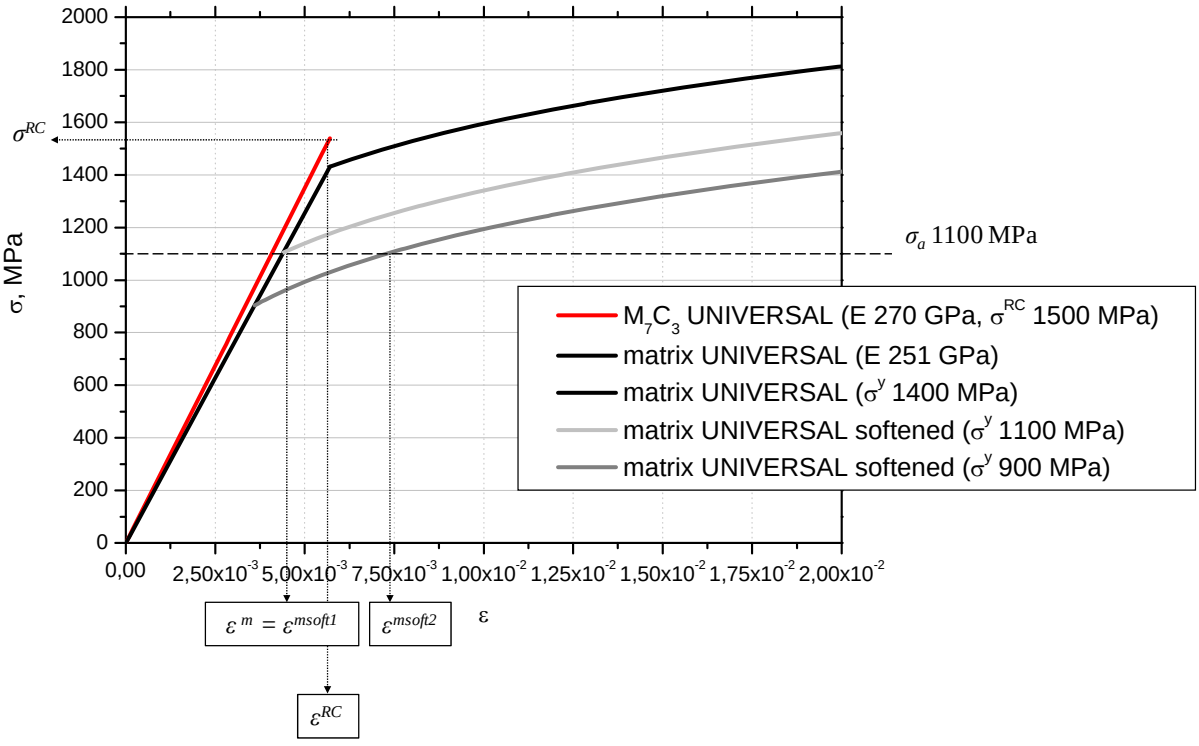

Figure 4.1.5 Schema of the stress-strain curves of carbides (red line), the matrix (black line) and to cases in which the properties of the matrix are reduced as a result of fatigue

As it follows from the results presented above, in UNIVERSAL D2 and opposite to 1.2379 D2, a certain incubation period in which the matrix properties reduce is expected to take place in fatigue prior to the nucleation of the first cracks in the microstructure. Crack propagation in turn, is explained by the same mechanisms as in case of 1.2379 D2.

These findings permit to say that a microstructure with more regular and small primary carbides, embedded in a more homogeneous manner in the matrix, such as this of UNIVERSAL, helps increasing the resistance to crack nucleation, both under monotonic (since more load must be applied) and cyclic loading (more load or number of cycles are required) compared to 1.2379. Slight improvements of crack propagation of UNIVERSAL compared to 1.2379 are observed, and they are attributed to the better properties of the metallic matrix. E and H of the matrix of UNIVERSAL and 1.2379 are similar. However, some differences are expected in terms of σ_y even though they could not be quantified in the frame of this Thesis.

The case of HWS D2 probably makes the difference with respect to the behaviours observed in ingot cast steels. HWS has a markedly lower $\Delta\sigma^{fat}$ compared to σ^{RC}, and furthermore $\Delta\sigma^{fat}$ is only slightly higher than the values determined for ingot cast steels, even though the behaviour of HWS under monotonic conditions is much superior. This finding reflects that in fatigue the advantages of the PM steels over the ingot cast reduce; i.e. the fatigue sensitivity of HWS is higher than that of ingot cast steels.

However, as in HWS no large carbides are present, failure initiation sites in fatigue are located at inclusion particles almost in all cases, for the same reasons as indicated in case of monotonic loadings (inclusions are weak points of PM steels). Then it is plausible that in front of this lack of larger stress concentrators in the microstructure, the matrix at the neighbourhood of inclusion particles is subject to more distortion and stresses rise with respect to the rest of the microstructure. After an incubation period which can vary depending on the stress applied, the size of the inclusion and its location in the sample, cracks may finally nucleate due to the degradation of the matrix properties at its surroundings.

As it follows from these arguments, the behaviour of HWS is not any different than the one of UNIVERSAL. In them both a crack finally appears when the matrix is degraded nearby an embedded particle, where stresses are magnified with respect to the applied macroscopical stress. In fact, the size of inclusions and the size of carbides of UNIVERSAL can be quite similar, but in HWS inclusions are rare and almost perfectly circular. That is why HWS shows an increased $\Delta\sigma^{fat}$ with respect to UNIVERSAL.

Crack nucleation in HWS concerns the major part of the fatigue life, as it is the case of monotonic tests (as shows the green arrow in Figure 4.1.3) since the resistance of the microstructure against crack nucleation is very high. However, once cracks are successfully nucleated, propagation stages are rather short in fatigue, as well as in monotonic conditions (orange arrow in Figure 4.1.3), since the resistance of the microstructure to the propagation of cracks is low, as discussed earlier in section 4.1.2. Even though the results of m and $Log\ A$ presented in Table 3.2.3 do not allow to extract any concluding remark regarding a faster propagation of cracks in HWS than in the other steels, in section 1.3 it was shown that it is typically reported in the literature that the resistance to fatigue crack propagation of PM steels is

lower than the ingot cast. Given that the microstructure ahead of nucleated cracks in HWS is very homogeneous, stable propagation of these into semi-circular shapes is expected already from the initial stages.

Regarding the behaviour of 1.2379 D3 and UNIVERSAL D3, the same arguments explained before for the respective materials in configuration D2 are valid; i.e. in 1.2379 D3 cracks nucleate at the first load cycles since primary carbides are broken under the applied stresses while in UNIVERSAL D3 a certain number of cycles are required prior to the nucleation of cracks. Under monotonic loads, ingot cast steels show a significant anisotropy in fracture results. In fatigue and even though these differences between D2 and D3 are rather attenuated, D2 samples show a better performance than D3 ones.

The case of K360 D2 in turn, is rather particular since two different types of fracture modes are observed. The first type corresponds to that described for 1.2379 D2, in which fracture is initiated from primary carbides at the surface and, since $\sigma^{max} \sim \sigma^{RC}$, the incubation period for crack nucleation is expected to be rather short. The second mechanism, in turn, is very different to any of the others observed in this work and it consists in internal failure at high number of cycles due to the formation of fish-eyes.

The existence of two different fatigue failure mechanisms is something well reported in the literature in case of tool and high strength bearing steels submitted to giga-cycle fatigue regimes (Sohar et al. [SOH08-1], [SOH08-2], SOH08-3] and Shiozawa et al. [SHI01], [SHI06-1] and [SHI06-2]). These authors state that when low loads are applied, failure is explained by decohesion of secondary precipitates at the surrounding of particles (primary carbides or inclusions, depending on the considered material). This phenomenon is responsible for the formation of areas with different surface roughness, attributable to subsequent stages of crack growth. These differences in roughness explain the formation of such fish-eyes at the surrounding of the initiating carbide particles.

In the present investigation, the same type of failure observed by these authors at the giga-cycle regimes is observed in case of K360 D2 at 10^6 cycles. Failure initiation sites of K360 are practically always located at M_7C_3 carbides, in only one case an MC is identified, and despite the sizes and morphologies of M_7C_3 carbides in 1.2379 and K360 are quite similar, in K360 there is a lower percentage of them in the microstructure. For this reason, at the surface of K360 fatigue samples (where stresses are maximal during a three-point bending test) there is a lower probability to find an M_7C carbide, or carbide cluster, which in addition is large enough for the initiation of a propagating crack.

If that is the case, i.e. no carbides large enough for breaking at the applied stresses are found at the surface of the sample, internal failure may take place from some large primary carbide present inside the sample. In Table 4.1.3 it can be observed that in all fatigue fractured samples of K360 D2, ΔK of the broken carbide at the failure initiation sites is higher than ΔK_{TH} (as shown in Figure 3.2.11, ΔK_{TH} for K360 D2 is 3,8 MPa·m$^{1/2}$).

Table 4.1.3 Applied stress amplitude, $\Delta\sigma$, number of cycles to failure, N, initial carbide size, a, and corresponding applied stress intensity factor, ΔK, of the samples of K360D2 broken in fatigue

Sample	*Fish-eye*	*$\Delta\sigma$, MPa*	*N, cycles*	*a, μm*	*ΔK, MPa·m$^{1/2}$*
P3F2	No	1166	15800	12	5,3
P4F1	No	999	1900	20	5,6
P9F2	No	916	30070	18	4,9
P6F1	No	832	43700	19	4,6
P4F2	No	832	52000	15	4,1
P9F1	Yes	999	283100	21	5,2
P7F2	Yes	916	702000	16	4,2

This means that carbides can break below the surface and cracks can propagate from them. Then, the particular morphology in the fish-eye region of samples showing internal failure is due to the crack propagation in absence of oxygen, instead of the decohesion process of small secondary carbides as described by the model of Shiozawa et al. [SHI06-2].

The results of section 3.2.1 and 3.2.5 with short, medium and long cracks reveal that crack propagation mechanisms are governed by the same mechanical properties as those determined by means of standard tests for long cracks. Although the initial ΔK when cracks are still in carbides could not be ascertained (since the real depth of carbides under the surface could not be evaluated) the estimated values assuming *a/c* ratio 1 are completely in agreement with the ΔK_{TH} determined for long cracks using the standard procedure E 647-00. The stable fatigue crack growth curve shows very similar behaviours for small, medium and long cracks and accordingly, their parameters *m* and *Log A* of the Paris law also resemble.

4.2 The case of real tools. An in-depth study of the failure mechanisms from a micro-mechanical point of view

In this section, the occurrence of failure in punching and slitting tools of the HPC are rationalised in basis of a micro-mechanical analysis of the fracture mechanisms. Tests with the HPC have permitted to reproduce the mechanical solicitations of industrial tools but under controlled laboratory conditions. Moreover, tools could be supervised in situ and easily replaced for examination. DP1000 2 mm thick and a cutting clearance of 10 % are used in this investigation as it was reported in section 3.3.3.

As shown in Figure 4.2.1, the main failure mechanisms identified in these tools is fracture both by chipping and micro-chipping at the cutting edge. The cases of the punching and the slitting tools are discussed respectively in sections 4.2.1 and 4.2.2.

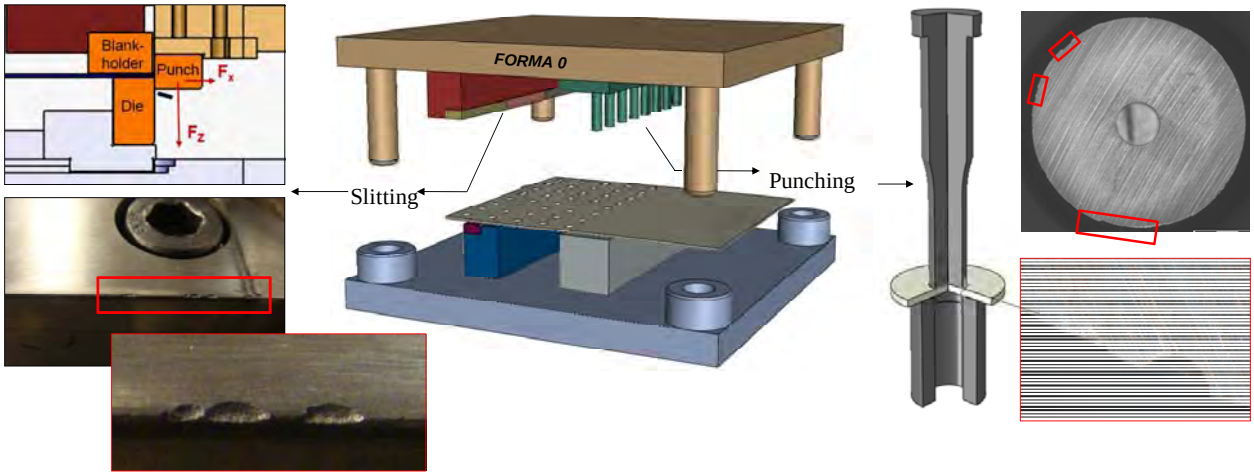

Figure 4.2.1 Schema of the two processes studied in the HPC: punching and slitting, and the failure mechanism observed, i.e. fracture by chipping and micro-chipping

4.2.1 Micro-mechanical analysis of the punching tools

As shown previously in section 3.3.3.1, the cutting edge of the punching tools employed in the HPC revealed severe damage by fractures. In Figure 4.2.2 an example of fractured punch is shown and in Figure 4.2.2 d) in cut and polished samples extracted from the punch it can be observed that many broken carbides are present below the surface as well.

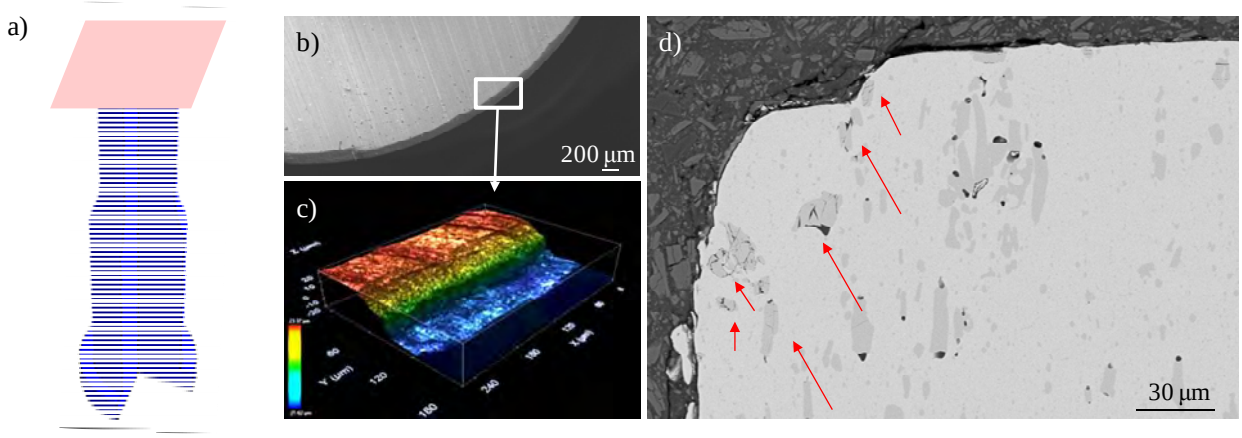

Figure 4.2.2 Main failure mechanisms observed in punching tools: a) schema of the punch to show that the image presented in Figures b) and c) corresponds to a view of the rake face; b) fractured cutting edge of a 1.2379A punch; c) topographic image of the fracture in the 1.2379A punch; d) cross sectional cut of the punch where many broken primary carbides are observed below the cutting edge

In Figure 3.3.44 it was already shown that besides damage generated at the cutting edge, many broken primary carbides and microcracks are present directly below the flank and rake faces of punches even at positions very distant with respect to the cutting edge and where fractures are observed. The nucleation and propagation of these cracks cannot be understood after the results obtained from FE-simulations since they estimate very low applied stresses in there (about 300 MPa). Thus, they ought to be explained by other mechanisms, as it will be discussed in the following lines.

Figure 4.2.3 shows the type of damage observed at the rake face of punches at distant positions from the cutting edge in direction towards the centre of the punch. At the flank face, even up to distances of more than 1 mm from the cutting edge a very similar type of damage is observed, as shows Figure 4.2.4. Broken primary carbides (with cracks parallel to the surface) are present directly below the surface (denoted in red arrows in Figures 4.2.3 and 4.2.4), as well as numerous microcracks which run parallel to the surface (blue arrows in the aforementioned figures).

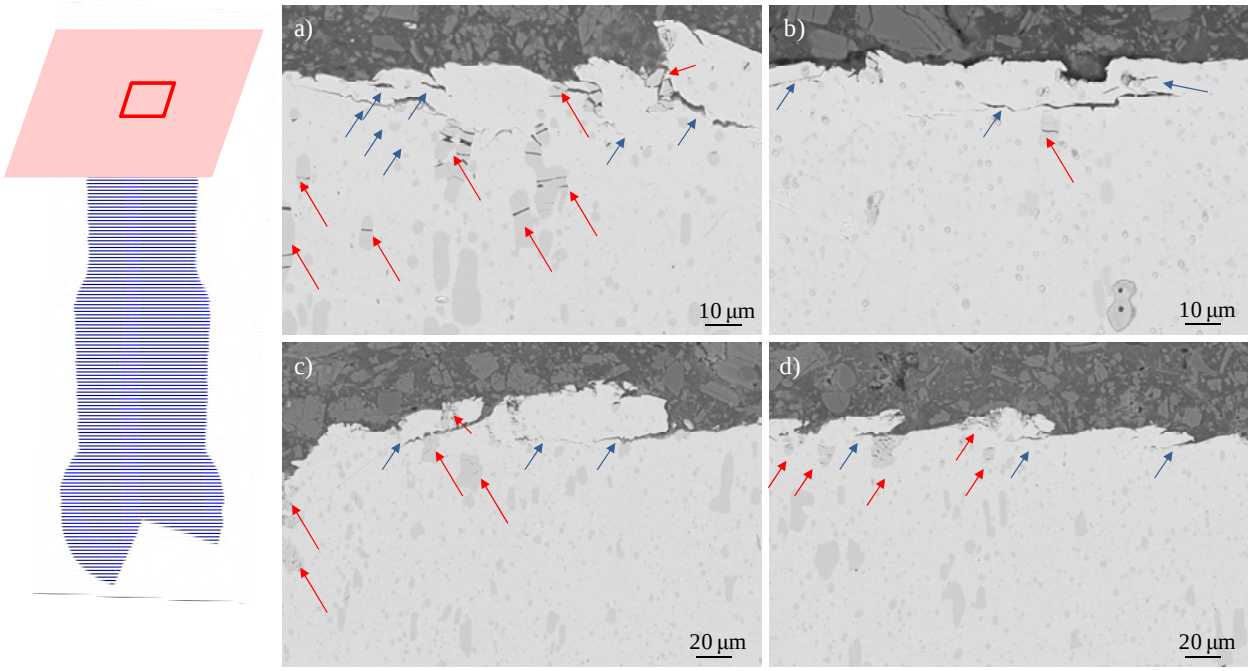

Figure 4.2.3 Damage observed at the microstructure of the punch through cross sectional cut, at the rake face and at distant positions from the cutting edge in direction to the centre. In a), b) c) and d) images, the existence of broken primary carbides is denoted with red arrows while blue arrows indicate cracks nucleated inside the material and propagating parallel to the surface

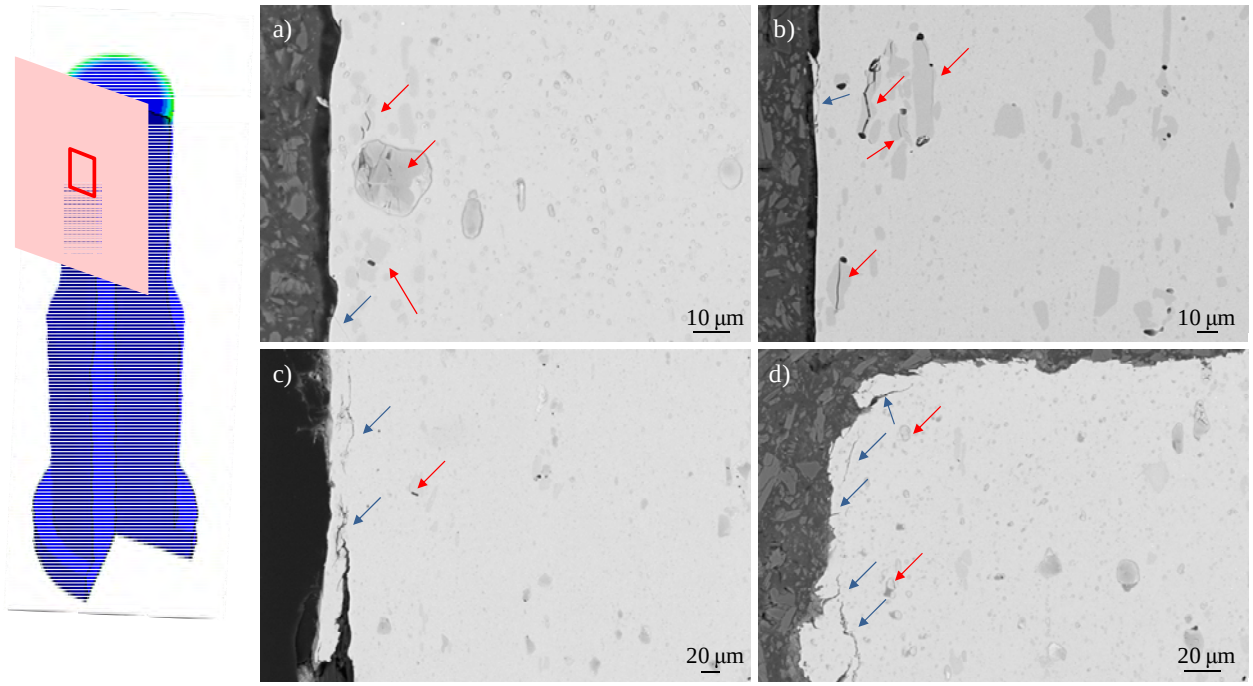

Figure 4.2.4 Damage observed at the microstructure of the punch through cross sectional cut, at the flank face and at distant positions from the cutting edge (around 1 mm). In a), b) c) and d) images, the existence of broken primary carbides is denoted with red arrows while blue arrows indicate cracks nucleated inside the material and propagating parallel to the surface

The occurrence of such type of damage which cannot be explained by means of the von Mises stresses estimated after FE-simulations, calls the role of fatigue wear mixed mechanisms. These are due to sliding and high frictional forces all along the surface of the punch in contact with the sheet material, which were not taken into account in FE-simulations. FE-simulation results are helpful determining macroscopically, the stress state of the punch and assess the severity of an operation with respect to another. It allows detecting the most requested zones in tools as well. However, from a micro-mechanical point of view, stresses predicted by means of macro FE-models cannot explain the type of damage observed.

Stachowiak and Batchelor showed that under conditions of severe sliding, material within a certain distance of the surface shifts in the direction of sliding due to deformation caused by the frictional force [STA05]. Strains caused by shearing in sliding are present some depth below the surface reaching the extreme values at the top of this, as shown schematically in Figure 4.2.5.

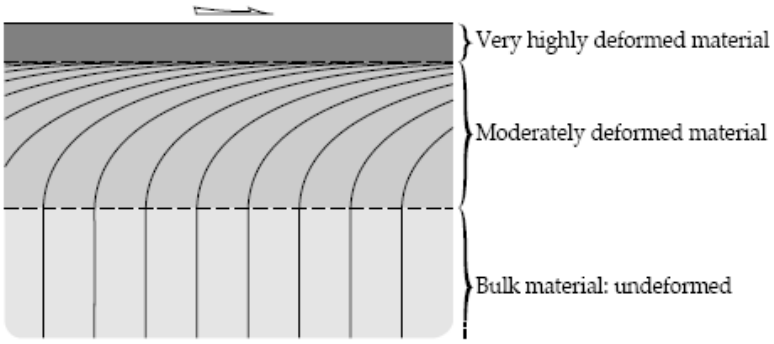

Figure 4.2.5 Strain levels in a deformed surface [STA05]

The aforementioned authors proposed a mechanism by which under such high sliding conditions, crack nucleation and propagation can be rationalised. As it follows from these authors, strain induced by sliding eventually breaks down the original grain structure at the surface to form dislocation cells. These cells can be described as submicron regions, relatively free from dislocations, which are separated by regions (walls) of highly tangled dislocations. At the interface the cells are elongated at the direction of sliding and are relatively thin resembling layers of flat "tiles". The high energy cell boundaries are probable regions for void formation, crack nucleation, and also crack propagation, as shown in Figure 4.2.6 in a 1.2379A punch.

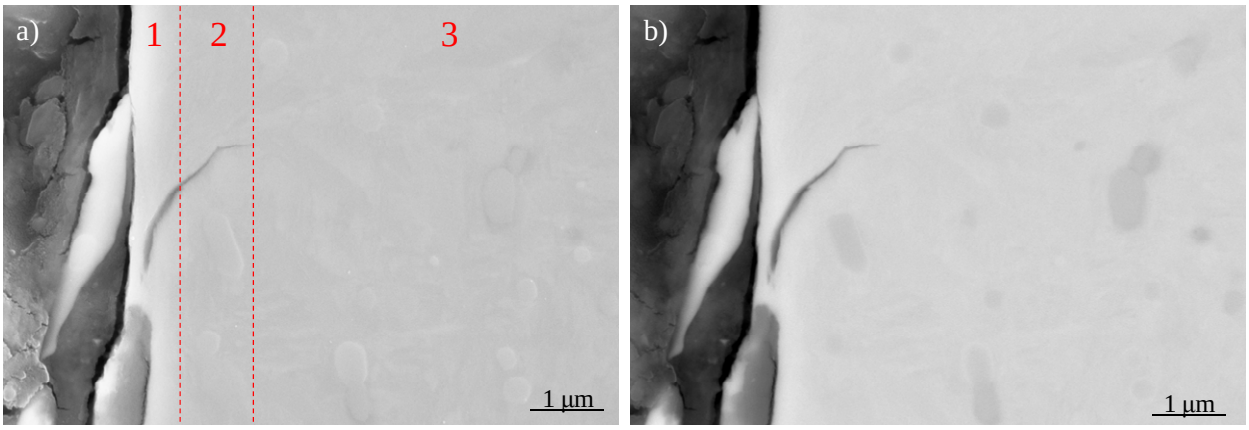

Figure 4.2.6 Strain levels in a deformed surface and formation of a crack in the flank face of a 1.2379A punch. 1: very highly deformed material, 2: moderately deformed material and 3: bulk material, undeformed

During repetitive sliding, plastic deformation of the surface layer leads the material to pile up without detaching from the surface. The piled up material does not move but instead, a protuberance of deformed surface is created that resembles a wave (as it can be observed in Figures 4.2.3 d) and 4.2.4 d)). To accommodate the "wave", very high strains are sustained leading to the cracking of the material in the "wave". During sliding, planes of weakness in the material become orientated parallel to the surface by such discussed deformation processes, and laminar pieces of material detached from the surface are formed by a surface crack reaching a plane of weakness, as schematically illustrated in Figure 4.2.7, and as shown in Figure 4.2.8 for a 1.2379B punch.

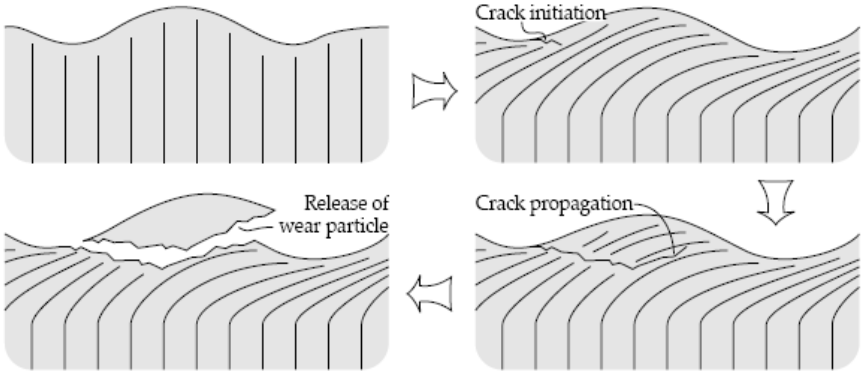

Figure 4.2.7 Schematic illustration of the mechanism of material particle release due to growth of surface initiated cracks [STA05]

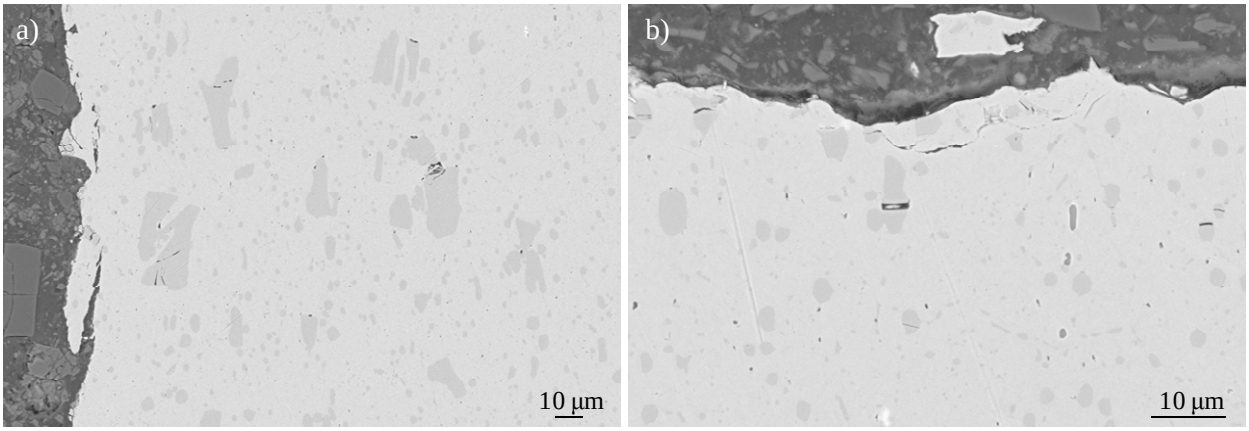

Figure 4.2.8 Mechanism of material particle release in a 1.2379B punch: a) flank side and b) rake side of the punch

Once a piece of material is released from the surface, a crater is formed as show Figures 4.2.9 b) and c) and the borders of these craters are potential initiation sites for new cracks, as denote red arrows in Figure 4.2.9 b), which propagate under the cyclic applied loads.

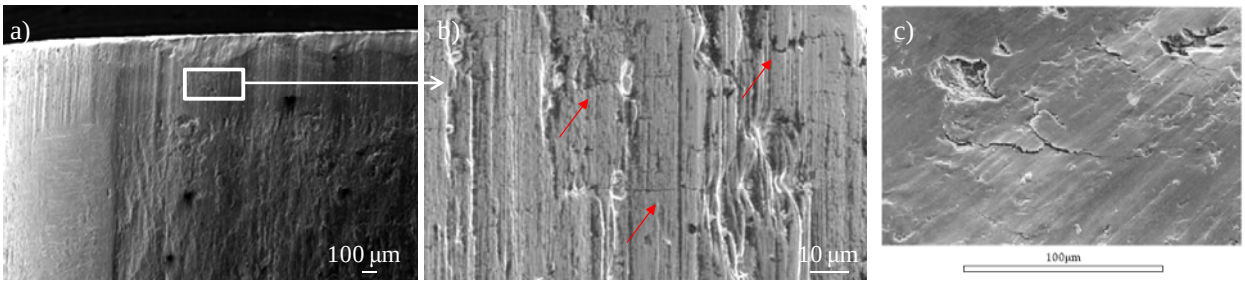

Figure 4.2.9 a) and b) cracks at the surface of a 1.2379A punch; c) example of fatigue wear reported by Stachowiak and Batchelor [STA05]

One of the main questions here is to understand the nucleation of these cracks under the high compressive stresses acting during one punch stroke. Such craters or surface asperities can create a stress field similar to that generated in a notch root under pure compressive cyclic stresses. As reported by Hsu and Wang, these types of discontinuities introduce a non-uniform stress field in the adjacent regions in which residual tensile stresses may exist despite the compressive loading [HSU10]. Previous investigations show that the extent of the tensile stress field depends on the extent of plastic yielding [FLE85]. Then crack nucleation can be caused upon unloading stage of cyclic deformation provided that the residual tensile stresses exceed the fracture strength of the material ahead of the notch root.

Propagation of such cracks, in turn, can be only explained if compressive stresses in the punch are very high, and residual tensile stresses after full unloading are generated due to plastic deformation ahead of the crack tip. These cracks nucleated from craters or other imperfections at the surface such as asperities propagate perpendicularly, as show Figure 4.2.10 in case of a 1.2379B punch and Figure 4.2.11 in case of a UNIVERSAL punch. On a micro scale real contact surfaces are not smooth and contain asperities that give rise to local point contacts and pressure spikes. Asperity contacts are important due to the tensile stresses that develop at the surface around point contacts and because the frictional traction forces intensify the plastic deformation of the surface, and cracks may nucleate there [ALF03].

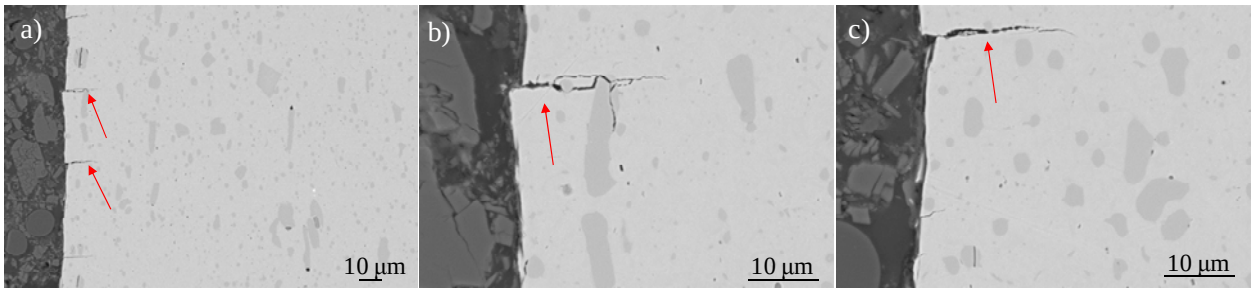

Figure 4.2.10 Examples of fatigue cracks in a 1.2379B punch nucleated from surface released particles and propagating in direction to the interior of the tool

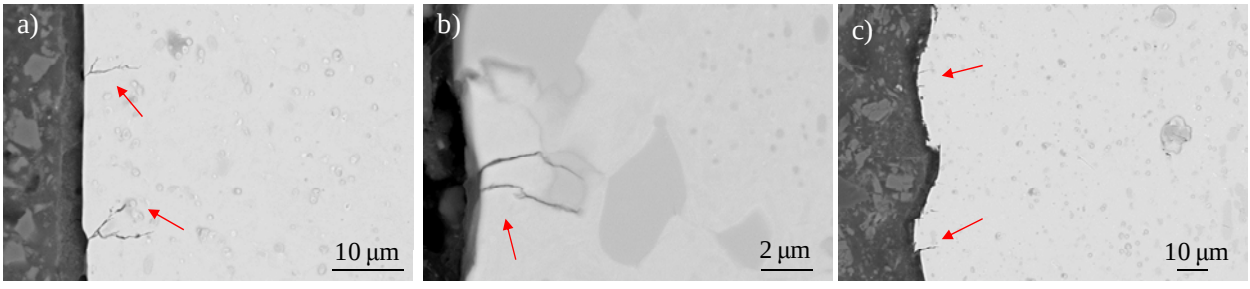

Figure 4.2.11 Examples of fatigue cracks in a UNIVERSAL punch nucleated from surface released particles and propagating in direction to the interior of the tool

In addition, another mechanism observed in this Thesis for crack initiation in tools consists in breakage of carbides as a result of plastic deformation of the matrix at their vicinity, and formation of dislocation pile ups (step 1 in Figure 4.2.12). Such dislocation pile ups trigger the development of voids, which enlarge with further deformation since they act as traps for dislocations (steps 2 and 3 in Figure 4.2.12). Crack growth does not proceed very near the surface because of the large plastic zone around its tip, but it is confined to a narrow range of depth where hydrostatic or triaxial stress is small but shear stresses are still large. All these factors favour the growth of a crack parallel to but beneath the surface (step 4 in Figure 4.2.12). Subsurface cracks nucleated at primary carbides coexist with the aforementioned cracks that nucleate from the surface in direction perpendicular to it (step 5 in Figure 4.2.12).

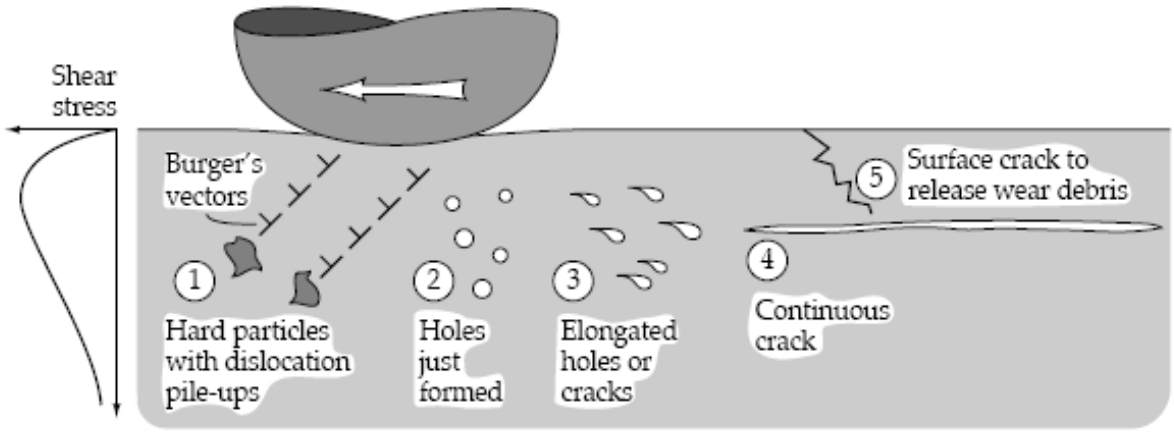

Figure 4.2.12 Illustration of a process of subsurface crack formation by growth and link up of voids [STA05]

At some unspecified point, these two types of cracks may connect and as a consequence, as shown in Figure 4.2.13, a thin laminar particle is released.

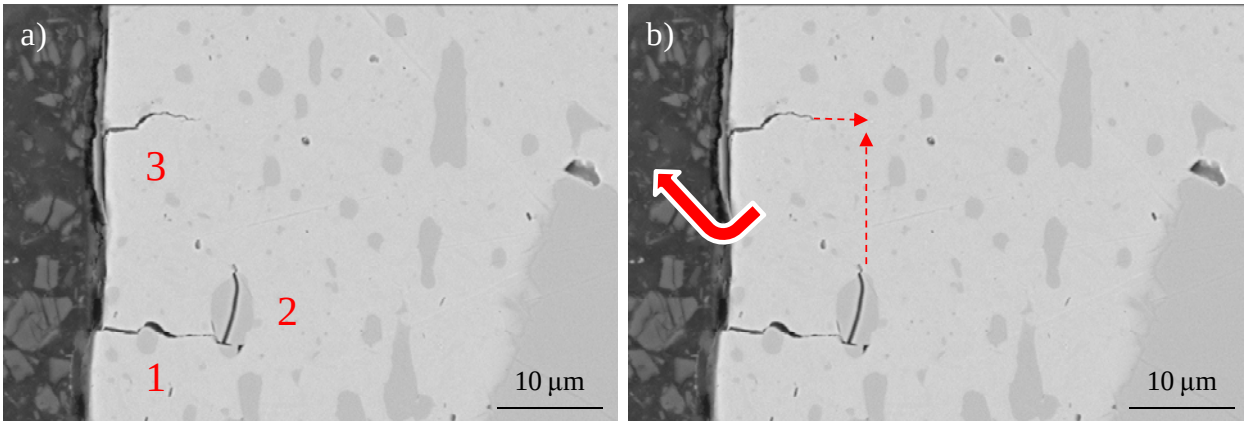

Figure 4.2.13 Cohesion of cracks number 1 and 3 (nucleated at the surface) to a crack nucleated below the surface from a broken primary carbide (number 2) in a 1.2379B punch

As schematised in Figure 4.2.14, primary cracks originated at the surface at some weak point (broken hard particle, asperity, crater, imperfection, etc.) can also propagate along weak planes such as slip planes or dislocation cell boundaries and reach the surface either because a secondary crack develops from the primary one, or alternatively the primary crack can connect with an existing subsurface crack. When the developing crack reaches the surface again, the piece of material is released.

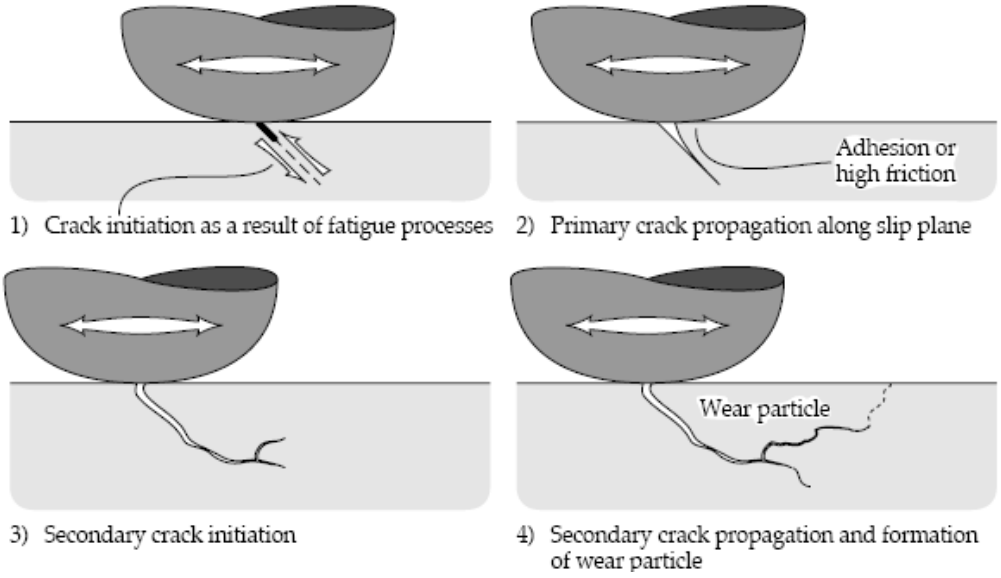

Figure 4.2.14 Schematic illustration of the process of surface crack initiation and propagation [STA05]

The mechanism explained in Figure 4.2.14 is shown in case of a 1.2379B punch in Figure 4.2.15. In this figure it can be observed that a crack initially nucleated at the surface propagates downwards and it bifurcates giving rise to secondary cracks. At a certain point, one of these secondary cracks turns its direction towards the surface, and its further propagation leads to detachment of a piece of material and to observe chipping at the cutting edge.

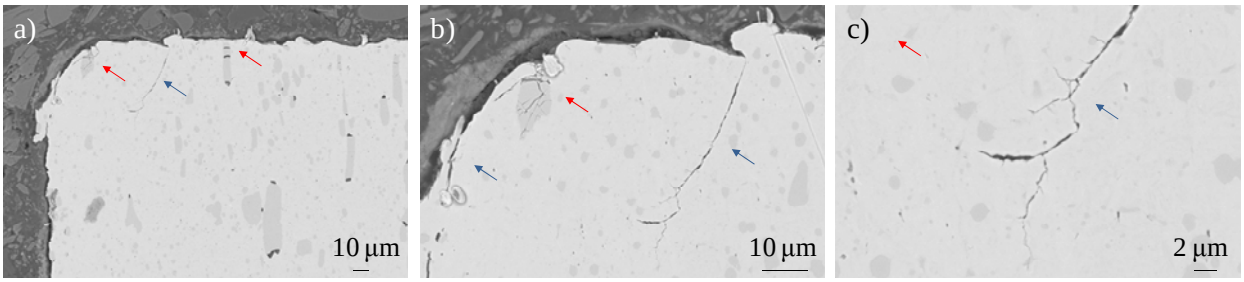

Figure 4.2.15 Process of surface crack initiation and propagation observed in the 1.2379B punch

An explanation for the change of direction of the crack can be found in a change of the stress state at the crack tip, as shown in Figure 4.2.16. In absence of any crack, at the zone where the crack is nucleated (rake face) compressive stresses in radial direction are higher than those in axial direction. Then tensile residual stresses in the radial direction are also higher than in the axial one and thus, the crack propagates vertically (perpendicular to the direction of maximum stress). At a certain depth, stresses undergo a progressive transition in which they become higher (more compressive) in the axial than the radial direction. As a result, the crack modifies its path according to the acting stress state, propagating horizontally towards the flank face. For a more in-depth analysis of the described mechanism, refer to section 4.2.2 (Figure 4.2.23).

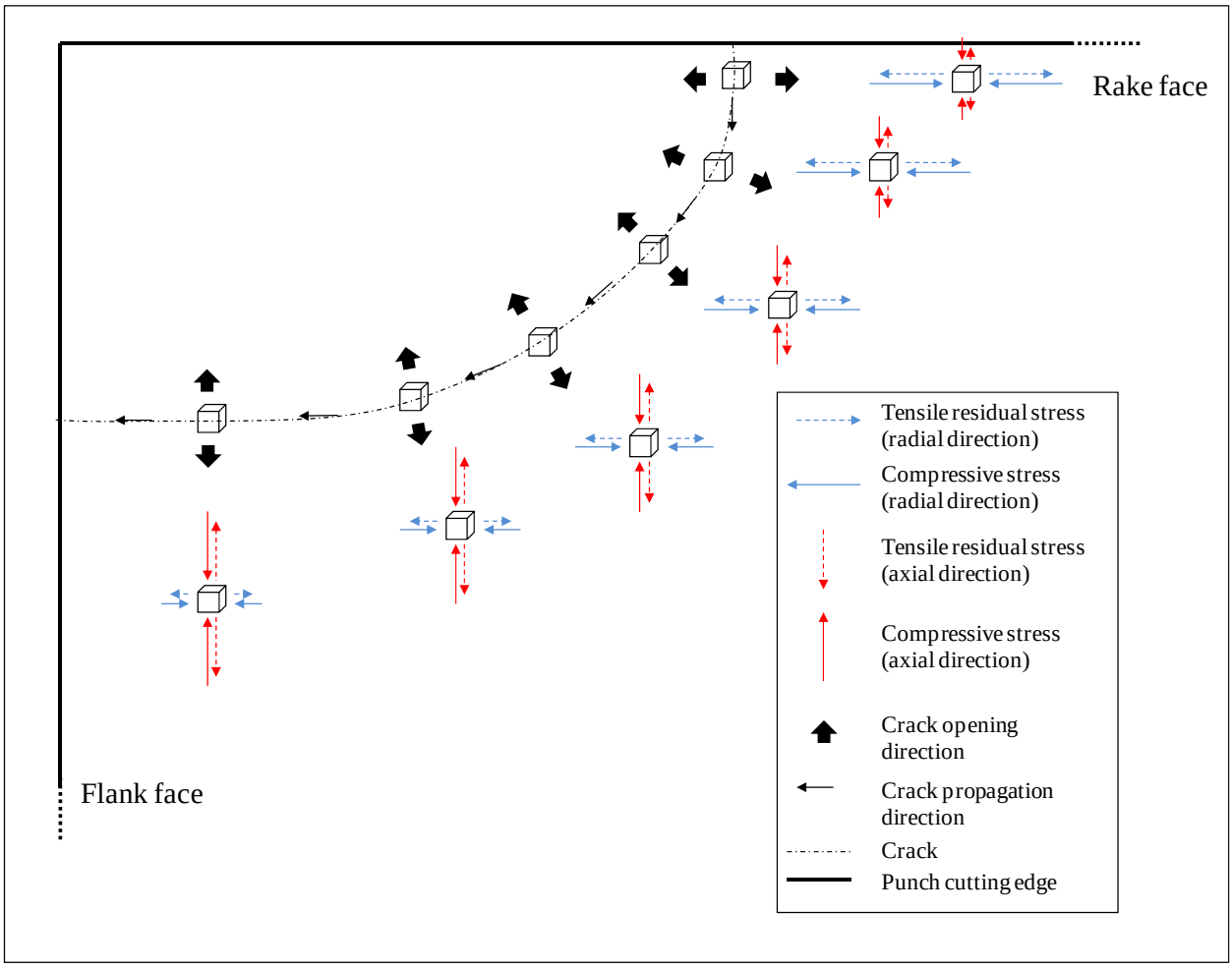

Figure 4.2.16 Schematic description of the different stress sates acting at the punch cutting edge

After the following arguments it seems plausible that chipping can take place as a result of a crack which, once nucleated at the rake face, propagates downwards and changes its growth direction towards the flank face, according to the complex stress state acting at the cutting edge. However, it is not clear yet whether the procedure for chipping formation can take place either because this crack (which propagates towards the flank face) coalesces with another one which runs in the opposite direction, or because a crack initiated at the flank face can also turn its direction to reach the rake face.

The inspection of the flank face of punches permits to observe that chipping at the cutting edge and fatigue cracks at the flank face can be two mechanisms well differentiated, and lateral cracks may not give rise to fractures by chipping since they are not able to propagate any further from the surface. Although no experimental evidence for this argument could be found in the analysed punches, Fleck et al. reported that cracks nucleated under compression loads from discontinuities at the surface are prone to get arrested, since as the crack length increases the fraction of the load cycle for which the crack is open decreases [FLE85].

Figure 4.2.17 compares fractures at the cutting edge with the lateral fatigue microcracks (denoted by red arrows). As it can be observed, microcracks appear well below the cutting edge and far from the fractured material. Therefore it is plausible that chipping is caused by cracks which, as explained before, are nucleated at the rake face and they propagate downwards to the flank face.

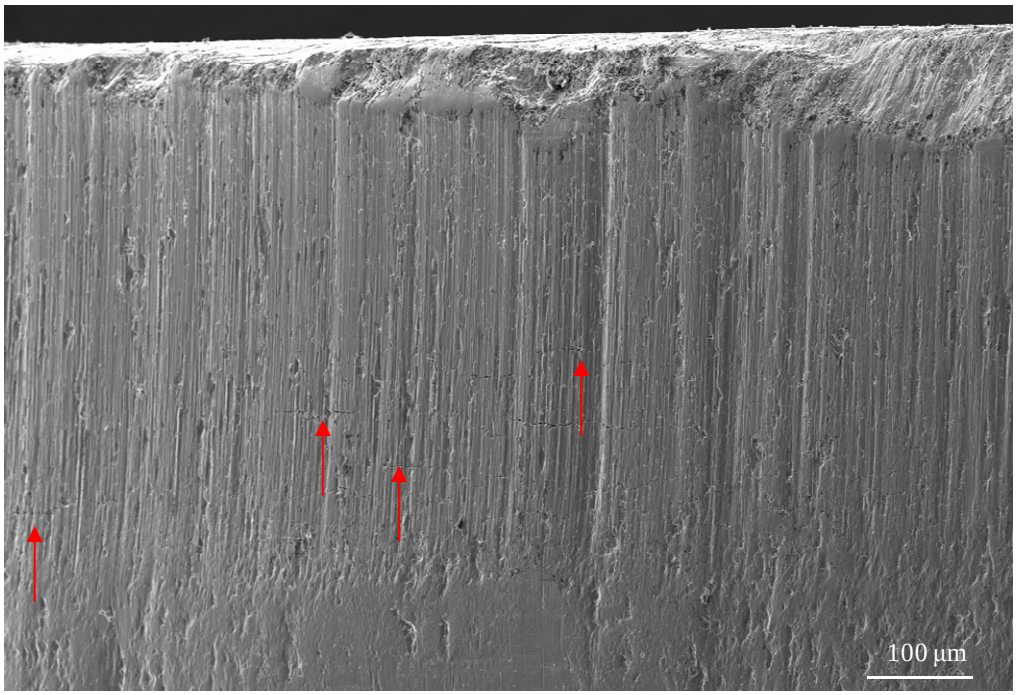

Figure 4.2.17 Image of the flank face in a 1.2379B punch where fractures at the cutting edge can be observed, as well as cracks propagating parallel to the surface (indicated by red arrows)

To summarise, Figure 4.2.18 schematises the different types of damage and the mechanisms explaining their occurrence in the studied punching tools.

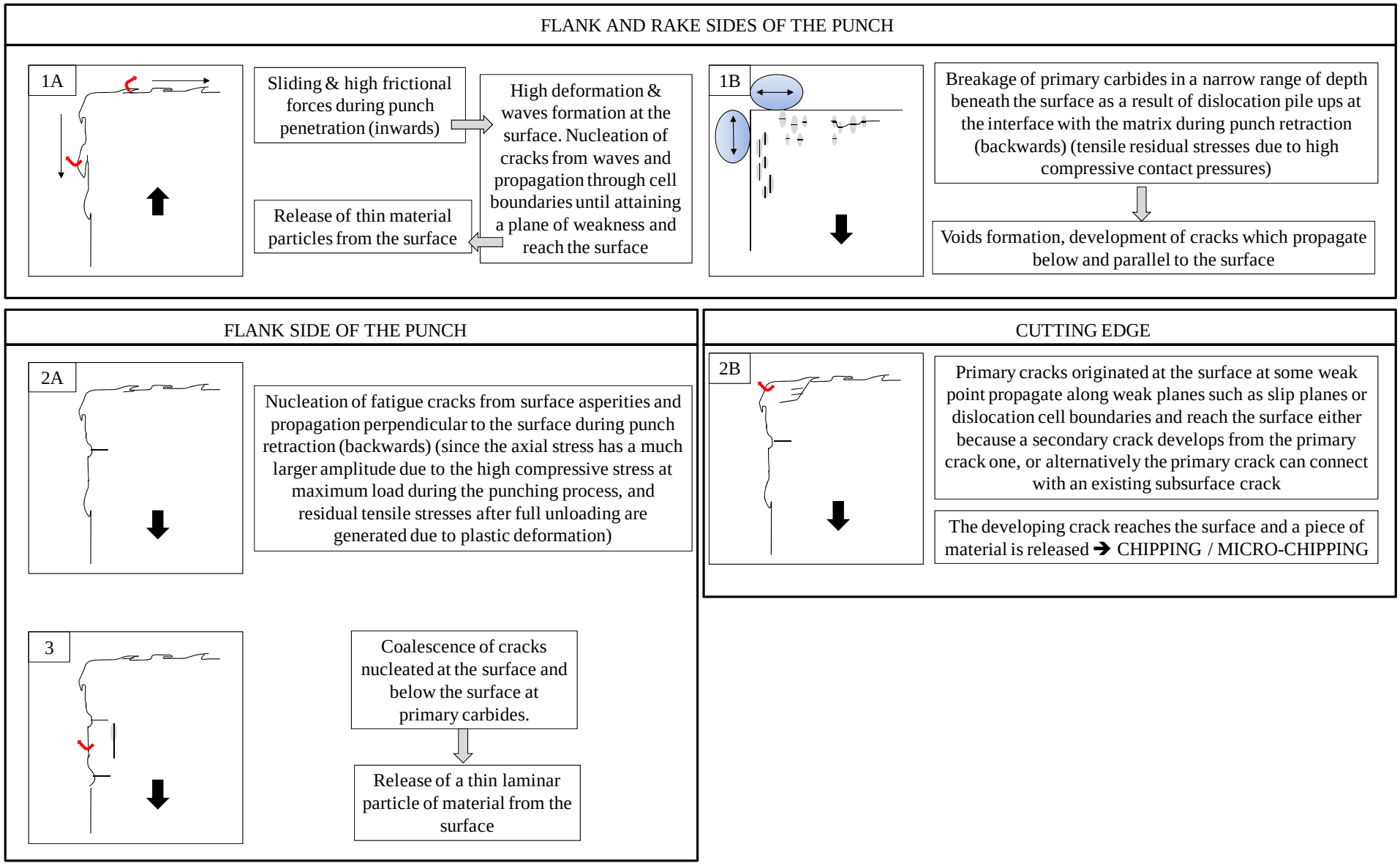

Figure 4.2.18 Summary of the different types of damage observed in punching tools of the HPC

As it can be observed in the figure above, five different types of damage are identified and they are classified into the following:

- 1A: Damage directly at the surface originated as a result of the high frictional forces during sliding against the sheet during the movement inwards of the punch. “Waves” are formed at the surface as a consequence of high deformation, and nucleation of cracks takes place because of the high strains sustained to accommodate these “waves”. Cracks propagate parallel to the surface until they reach a plane of weakness and a thin piece of material is released. In this type of mechanism the initial surface roughness of the tool plays a major role determining the sliding conditions and friction coefficient between the two bodies in contact, i.e. good surface finish and lower friction coefficients are desired. In this sense, carbides help decreasing the friction coefficient of the material, increasing the wear resistance, the yield stress and therefore, the resistance to “wave” formation and crack nucleation.

- 1B: However, due to the high contact pressures at the surface, carbides within a narrow range of depth beneath the surface are broken as a result of dislocations pile ups at the interface with the metallic matrix. Breakage of carbides is explained by the tensile residual stresses that are generated after full unloading due to plastic deformation during the backwards movement of the punch. Plastic deformation takes place because of the high compressive contact loads generated at the surface and up to some distances beneath. Such dislocation pile ups lead to the formation of voids in the matrix, from which under the repetitive sliding, cracks can nucleate and propagate below and parallel to the surface.

- 2A: At the flank side of the punch, fatigue microcracks which propagate towards the interior of the material are observed. These are nucleated from surface asperities, ahead of which a stress state similar to that created on a notch root is generated. Such cracks are found to be very shallow, as they could only be observed up to short distances from the flank face.

- 3: Detachment of a thin laminar piece of material takes place when some 2A cracks coalesce with 1B cracks.

- 2B: Chipping is explained by the nucleation of a crack at the rake face and its propagation downwards to the flank face. In this mechanism both the resistance to crack nucleation at the surface (i.e. resistance against carbide breakage, plastic deformation, formation of surface discontinuities, etc.) and the resistance to fatigue crack propagation of the tool material are important parameters. In this sense, to improve the resistance to crack nucleation, PM tool steel microstructures are desired so that there are no large broken primary carbides from which cracks can initiate. Furthermore, the yield stress of the material must be high enough to prevent plastic

deformation of the surface as a consequence of which cracks can nucleate. However, when many imperfections are initially present in tools (for instance as a result of a rough machining process), cracks originate easily and a PM microstructure can be less advantageous than an ingot cast when it comes to prevent the propagation of such cracks. *R*-curve effects should be taken into account here, in order to assess the best suitability of PM or ingot cast steels respectively. As shown in section 4.1.2, if high stresses or small cracks are involved in the fracture process, PM steels can show higher K_R than ingot cast steels up to a certain extent (since ingot cast steels suffer from *R*-curve behaviour and thus, their fracture toughness depends on the crack size). On the contrary, if nucleated cracks are long, then ingot cast steels are more advantageous since their K_{IC} is higher than PM steels.

An attempt to improve the resistance to chipping can consist in the application of a coating at the surface of the punch. In this way crack nucleation due to surface discontinuities may be reduced (the high hardness and yield stress of the coating gives low friction coefficient and high resistance to plastic deformation at the surface). However, the tests performed in this Thesis in sections 3.3.2.2 and 3.3.3 show that as the initial surface of the coated punches was very rough, fracture of the coating and detachment from the surface at early numbers of punch strokes was triggered. Furthermore, as in shearing operations of UHSS the loads and contact pressures applied are extremely high, even if the initial tool surface is very smooth the high stiffness of the coating can result in accelerated fractures only after very few strokes.

The hypothesis that voids nucleation is a necessary step in the formation of a crack suggests that materials with lower carbide or inclusion amounts, or of smaller sizes, exhibit better behaviours. This prediction has been confirmed experimentally by the increased performance of UNIVERSAL punches compared to 1.2379 or K360 (according to the lower amount and reduced sizes of carbides in UNIVERSAL with respect to the other two materials). Moreover, as follows from the results of this Thesis, UNIVERSAL shows a higher toughness when small cracks are involved. In this sense, HWS should have shown the best behaviour amongst the studied punches, due to its higher resistance to crack nucleation. However, experimental results turned out a bit different since chipping was observed in HWS after only a few strokes, even earlier than UNIVERSAL.

The previous arguments are rationalised in the following way: as discussed in this section, damage in punches is not only due to fatigue, but to fatigue wear mixed mechanisms. Under these circumstances, and taking into account the deep machining grooves initially present at the surface of punches, nucleation of cracks is triggered by surface asperities more than breakage of carbides. As according to section 1.3, the resistance to crack propagation of PM steels is neatly lower than the ingot cast steels, such nucleated cracks propagate easier through the microstructure.

Thus, as though in section 3.2.6 it was observed that HWS has higher K_R values than ingot cast steels when small cracks are involved, if cracks are longer (as it is expected if they are nucleated from machining grooves instead of carbides) they may lead to fracture faster than in ingot cast steels as K_{IC} of HWS is lower than that of ingot cast steels.

In any case, the necessity to reduce the surface roughness of tools at the initial stage is more than relevant; especially when PM steels are employed since the advantages of their PM microstructures are not full-filled in the applications.

4.2.2 Micro-mechanical analysis of slitting tools

As follows from section 3.3.3.2, fracture by chipping is the main damaging mechanism identified at the cutting edge of the lower blades. At equal numbers of strokes, the upper blades show no fractures, but the surface is affected by wear. A study of the upper and lower blades from a micro-mehcanical point of view is presented in this section and the mechanisms of nucleation and propagation of cracks in the microstructure are determined.

The cross sectional analysis of the blades reveals that different types of damage are present at the microstructure, namely two types of cracks: a first one corresponding to broken primary carbides (in direction to the stroke movement, as it shows Figure 4.2.19 in red arrows) and a second one corresponding to cracks nucleated at the surface and propagating perpendicular to the stroke movement towards the interior of the blade (Figure 4.2.19 blue arrows).

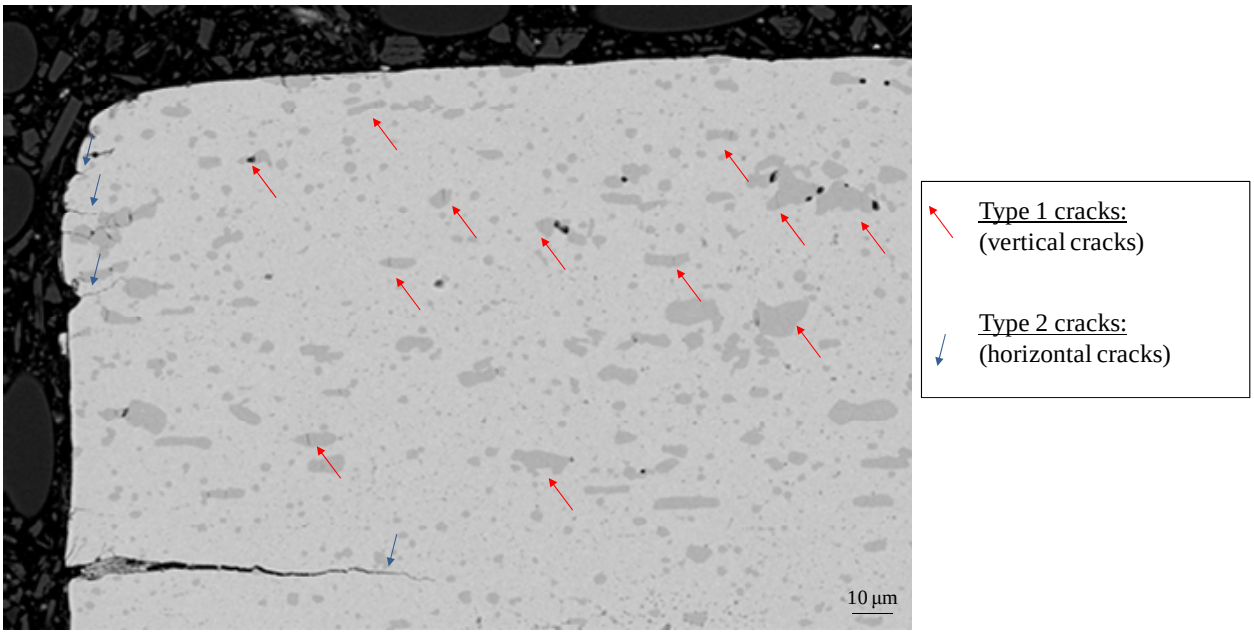

Figure 4.2.19 Cracks at the microstructure of the 1.2379 lower tool in a cross sectional analysis

These types of cracks are slightly different than those observed in punches in section 4.2.1. On the one hand, no propagating cracks are identified which, once nucleated at the rake face, run downwards to the flank face (as type 2B from Figure 4.2.18). On the other hand, hardly any damage due to “wave” formation at the surface is observed at the flank and rake sides (as type 1A of Figure 4.2.18). Only in one case, damage resembling the “waves” observed at punches surfaces is appreciated, as shown in Figure 4.2.20 a) at the flank face.

In addition, carbides are broken differently in the slitting tools. In punches, broken carbides are only identified at narrow depths below the surface but up to very distant locations with respect to the cutting edge. In slitting tools, in turn, broken carbides are only found at the zone of the cutting edge, but also at deeper locations with respect to the surface. Carbides in punches show fractures parallel to the surface on no matter the side of the punch (rake or flank); however in slitting tools, carbides break parallel to the stroke direction in all cases (near the rake and the flank faces). As shown in Figure 4.2.20 b), carbides near the rake face of the punch are broken perpendicularly to this.

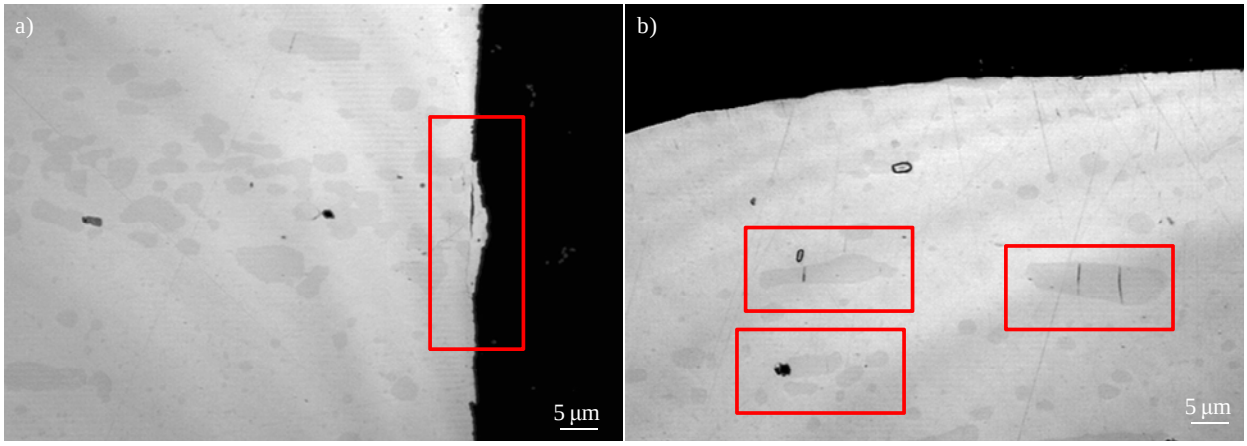

Figure 4.2.20 Crack parallel to the flank face due to “wave” formation (mechanism 1A in previous Figure 4.2.18); b) broken carbides present cracks in vertical direction, also below the rake face (in contrast to mechanism 1B in Figure 4.2.18)

From this standpoint, the breakage of carbides cannot be explained by the same mechanisms as in punches (i.e. due to residual tensile stresses generated as a result of the high compressive contact pressures) but instead, other type of stresses shall explain this occurrence. In this case, the results of von Mises stresses estimated by means show more agreement than in case of punches, at least, to predict the zones in the tool where primary carbides are broken. These are exclusively observed below the cutting edge, where the maximum von Mises stresses are registered.

Since carbides are only broken at the cutting edge and not only in the narrowest depths below the surface but up to deeper positions, as shown in Figure 4.2.19, the stresses generated inside the material instead of the contact pressures may be the responsible of their breakage (that is why FE-simulations may predict their breakage). However, all data about stress states and levels of slitting tools obtained from FE-simulations correspond to the loading stage, prior to the fracture of the sheet. In FE-models it is assumed that tools behave completely elastic during the stroke and therefore, no residual stresses are computed. This assumption may not be valid at a micro-scale, since under the high acting compressive stresses the matrix near carbides may undergo some plastic strain that can induce tensile residual stresses around them at the unloading stage.

As it is difficult to reproduce this mechanism using the FE-models employed to study the shearing process, in an attempt to estimate the possible residual tensile stresses generated around carbides in the microstructure of tool steels a FE-simulation model is especially conceived to cope with these effects. As shown in Figure 4.2.21, the microstructure of a tool steel (1.2379-type) and under the following assumptions is considered: plane strain conditions, restricted displacement on the left and lower sides and different stresses applied on the top and right sides. Carbides are assumed to behave elastically with an E as reported in Table 3.2.4 of 294 GPa. The matrix is supposed to have an E of 249 GPa (Table 3.2.5) with σ_y of 1400 MPa. The plastic curve of the matrix is estimated from compression tests with 1.2379.

Different loading states and levels are considered in Figure 4.2.21. In one case, stresses of 1300 and 2000 MPa are applied at the top and right sides (Figure 4.2.21 a)) and vice versa (Figure 4.2.21 b)), then stresses are increased to 2600 and 4000 MPa (Figures 4.2.21 c) and d)), and finally the results are compared to a case where a tensile stress at the right side of 1000 MPa is applied (Figure 4.2.21 e)).

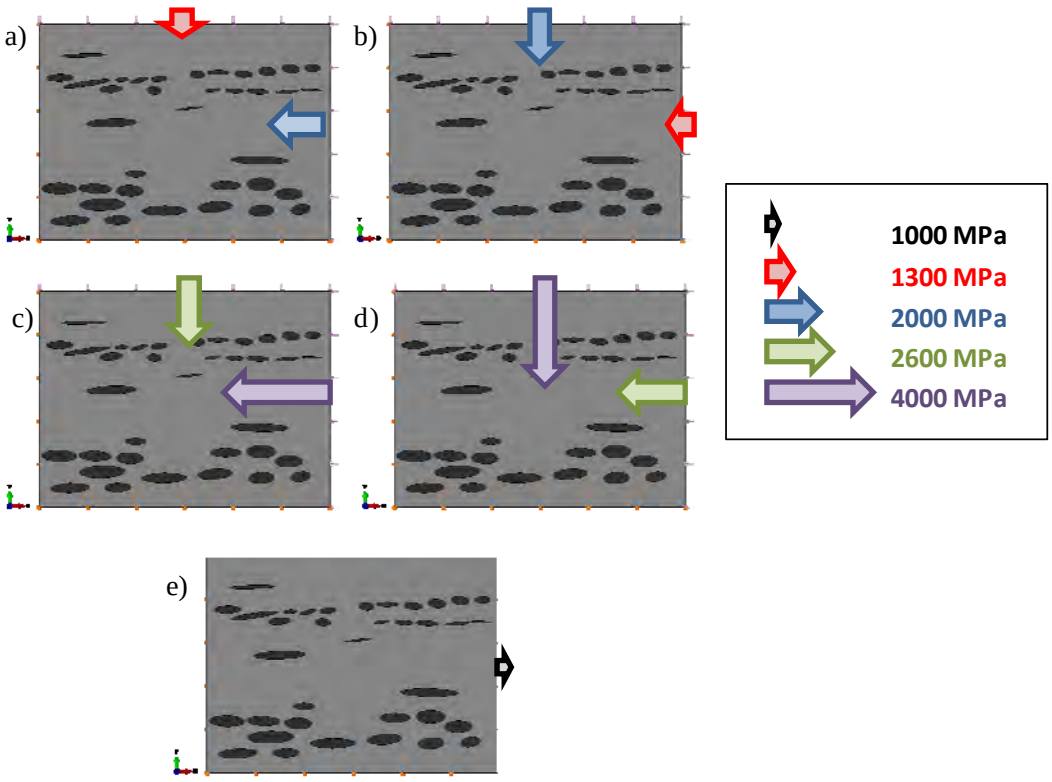

Figure 4.2.21 Schematic illustration of the FE-model to characterise residual stresses in the microstructure at the micro scale

The previous stress levels are chosen according to the results of the FE-simulation of the slitting process since as show Figures 4.2.22 and 4.2.23, near the cutting edge stresses in *Y*- direction are approximately 1,5 times higher (more negative, since all stresses are compressive) than in *X*- direction. These two stress levels owe to a first case, which may take place in the tool as follows from the FE-simulation results, and a case which a priori, stresses are somewhat higher than predicted by FE-simulations. This second case however, has been chosen since real tools may receive stresses higher than those predicted by FE-simulations. Overloads, high contact pressures, stress concentrators, and even the fact that carbides are not perfectly smooth but they have irregular geometries and shape factors lower than 1, may explain that stresses locally attain levels such as 2600 or 4000 MPa. The aim of evaluating either when stresses are maximum in *X*- or *Y*- directions is to take into account the influence of the carbide alignment with respect to the punch movement direction and the maximum load.

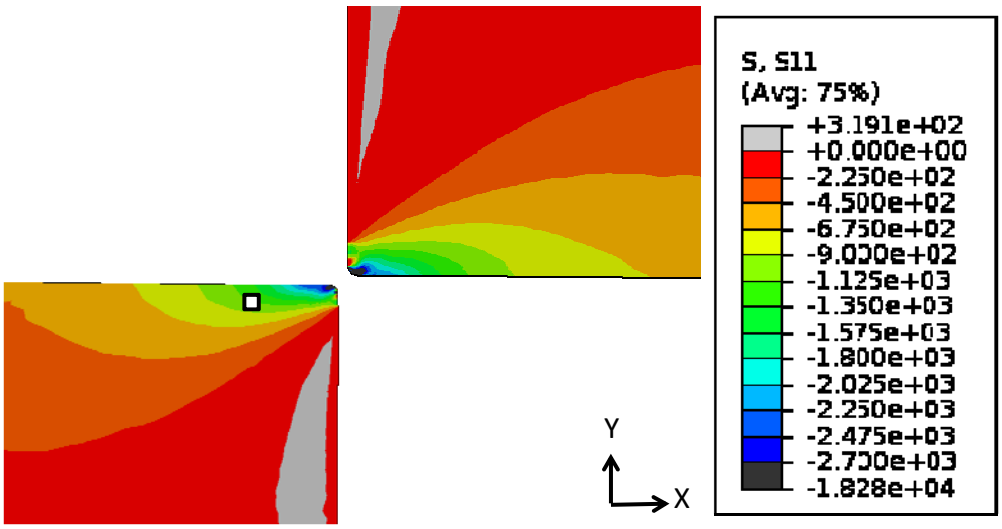

Figure 4.2.22 Stress distribution in the upper and lower tools in *X*- direction

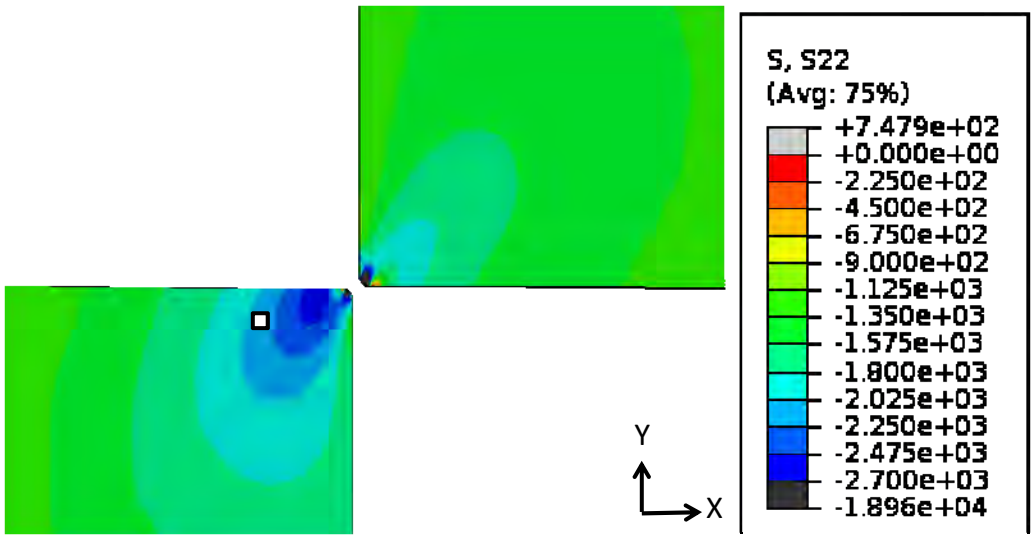

Figure 4.2.23 Stress distribution in the upper and lower tools in *Y*- direction

Figure 4.2.24 shows the stress distribution results, in terms of the von Mises stresses, at the unloaded state when compressive loads are applied (Figures 4.2.4 a) to d)) and during the tensile loading to 1000 MPa (Figure 4.2.24 e). Once the load is removed, von Mises residual stresses corresponding to the case of pressures 1300 – 2000 MPa are negligible (Figure 4.2.24 a) and b)). However, when external pressures increase to 2600 – 4000 MPa the estimated von Mises residual stresses are of about 1000 MPa (Figure 4.2.24 c) and d)).

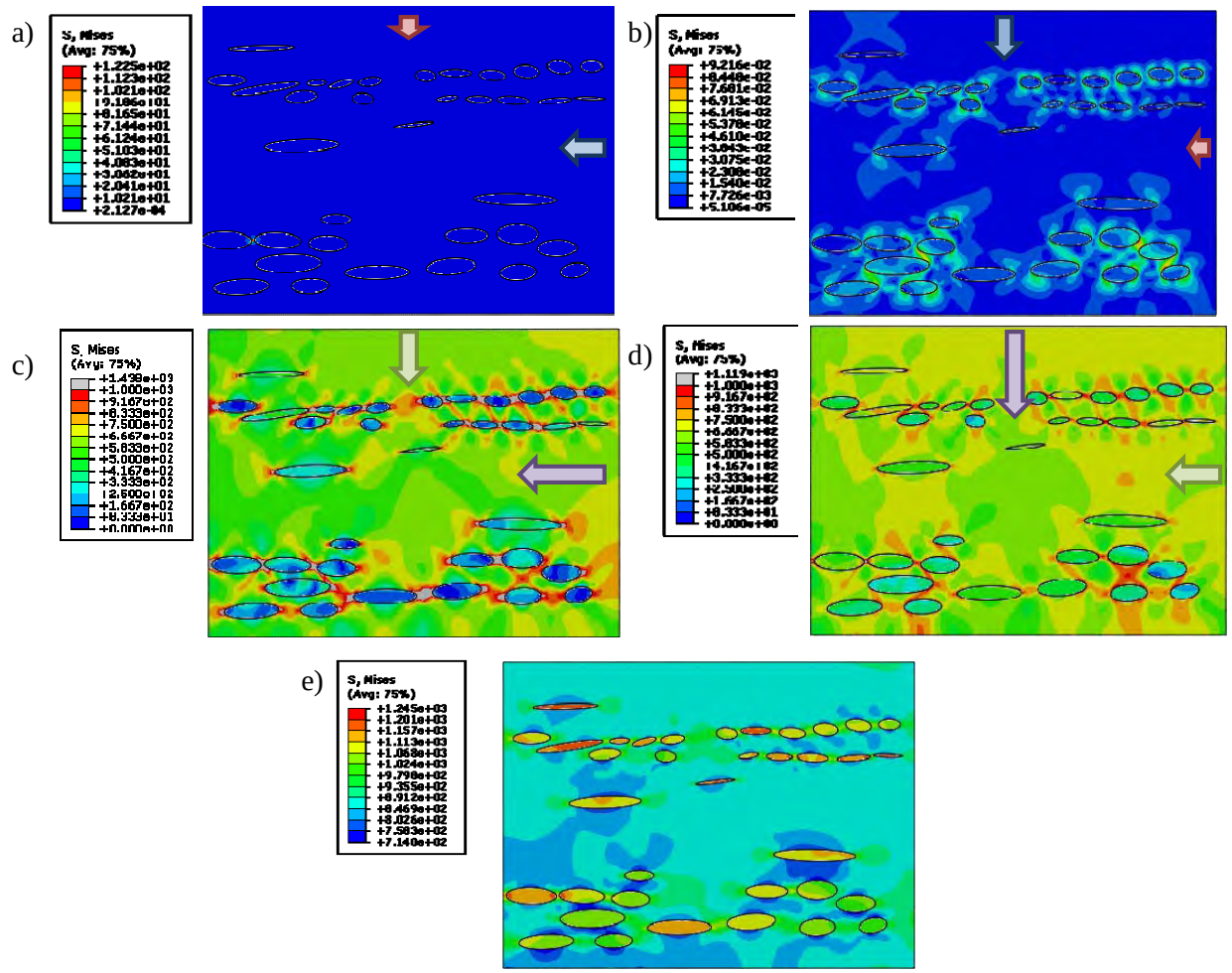

Figure 4.2.24 Von Mises stresses registered once the compressive loads defined in Figure 4.2.21 are released: a) corresponds to the results obtained with the configuration shown in Figure 4.2.21 a); b) corresponds to the results obtained with the configuration shown in Figure 4.2.21 b); c) corresponds to the results obtained with the configuration shown in Figure 4.2.21 c); d) corresponds to the results obtained with the configuration shown in Figure 4.2.21 a); e) von Mises stresses during the application of a tensile stress of 1000 MPa (Figure 4.2.21 e))

Since residual stresses are only generated in case of applying very high compressive pressures in the level of 2600 – 4000 MPa, a more detailed examination of this case is given in Figure 4.2.25, in which stresses in *X*- and *Y*- directions (S11 and S22 respectively) are plotted for the two configurations studied. As it can be observed in Figures 4.2.25 a) and b), when the compressive load is higher in *X*- direction, tensile residual stresses S22 are higher than S11 and the maximum S22 value is 600 MPa. In contrast, when the compressive load is higher in *Y*- direction (Figure 4.2.25 c) and d)) tensile residual stresses S11 are the highest and they can locally attain 1000 MPa.

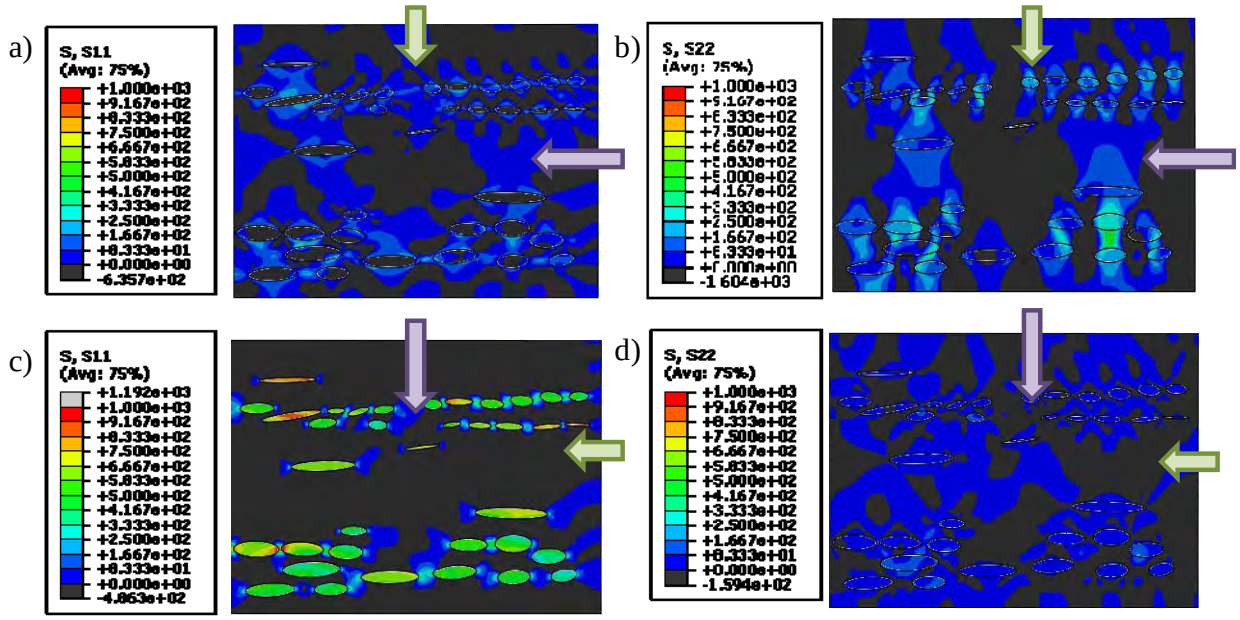

Figure 4.2.25 Stresses registered once the compressive loads defined in Figure 4.2.21 b) and c) are released: a) corresponds to the stresses in *X*- direction (S11) obtained with the configuration shown in Figure 4.2.21 c); b) corresponds to the stresses in *Y*- direction (S22) obtained with the configuration shown in Figure 4.2.21 c); c) corresponds to the stresses in *X*- direction (S11) obtained with the configuration shown in Figure 4.2.21 d); d) corresponds to the stresses in *Y*- direction (S22) obtained with the configuration shown in Figure 4.2.21 d)

The type of configuration which applies in case of the lower tools is that of Figure 4.2.21 d), since carbides are aligned perpendicular to the stroke direction, and so to the maximum acting load. Therefore as it follows from Figure 4.2.24 c), residual stresses may effectively be present in the microstructure at the unloading stage and they may attain values which, considering that they are repetitively applied, can be significantly harmful to the material behavior in fatigue. What is important to reflect after these findings is that as shows Figure 4.2.26, tensile residual stresses can explain the breakage of carbides according to the direction in which they are observed in blades (i.e. residual tensile stresses parallel to the stroke direction can explain the presence of cracks perpendicular to the stroke direction in carbides).

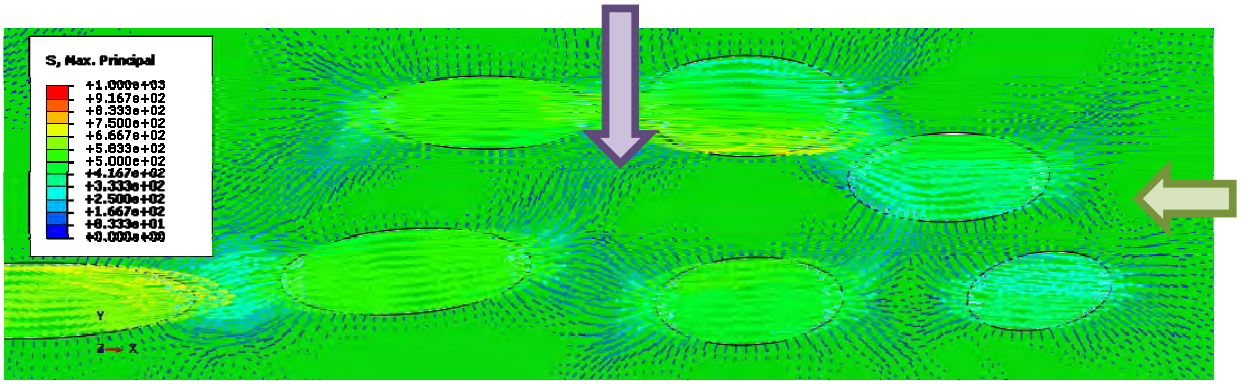

Figure 4.2.26 Detail of Figure 4.2.24 c) in which directions of maximum stresses are illustrated, and they correlate to the direction of the cracks nucleated at primary carbides in lower tools

In upper tools the estimated compressive stresses are much lower than at the lower tools and in addition, their carbide alignment is parallel to the stroke direction (as in Figure 4.2.21 c)). This configuration of carbides is advantageous since tensile residual stresses generated at the microstructure are much lower than when carbides and stroke direction are perpendicular (compare Figures 4.2.25 a) and b) for upper tools to Figures 4.2.25 c) and d) for lower tools). Therefore, accumulation of plastic strains at the matrix in these tools is not expected a priori. Accordingly, in experimental slitting tests fracture of the upper tools is mainly not observed. However, it is noteworthy that as discussed in section 4.1.1, carbides may present defects that extremely modify the stress states. According to this, in the upper tool only a few carbides are found broken but all of these are damaged, as illustrates Figure 4.2.27.

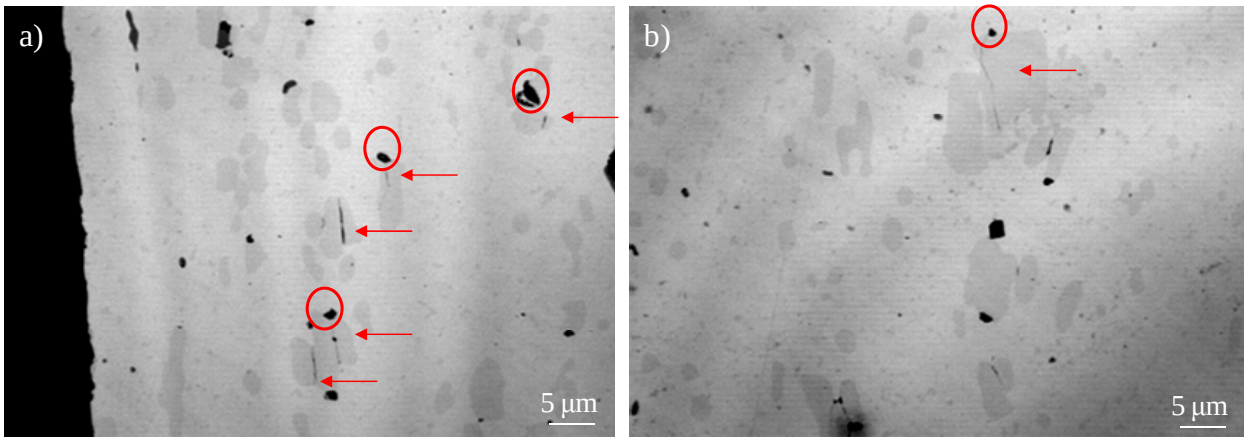

Figure 4.2.27 Broken primary carbides near the cutting edge of the upper 1.2379 tool, red arrows denote cracks nucleated because carbides present defects (encircled in red)

Hence, the arguments above prove that in case of tool steels with marked anisotropy, as ingot cast steels, it is more convenient to build blades with carbides aligned in the same direction as the stroke movement, since at the same applied load the breakage of carbides is disfavoured by the presence of lower residual tensile stresses.

Interestingly, in the cross sectional analysis of tools no cracks propagating from carbides through the matrix are observed. Only cracks nucleated at the surface propagate in the microstructure. In an attempt to find an explanation for this finding, ΔK of broken carbides at the lower tool are roughly estimated and compared to the ΔK_{TH} values (they are plotted in Figure 3.2.11). For that, ΔK values are calculated according to Equation 2.4.1 and Y values are estimated as follows from the work of Newman and Raju [NEW84]. The following considerations are assumed to determine ΔK: carbides with geometries like 1.2379 are considered, cracks have the shape of the broken carbides, $2c$ and a (the length and the depth of the crack, respectively) are equal to the mean value of D_{min} reported for 1.2379 in Table 3.1.2. The acting stresses are chosen according to the results of maximum residual tensile stresses determined from Figure 4.2.25 c).

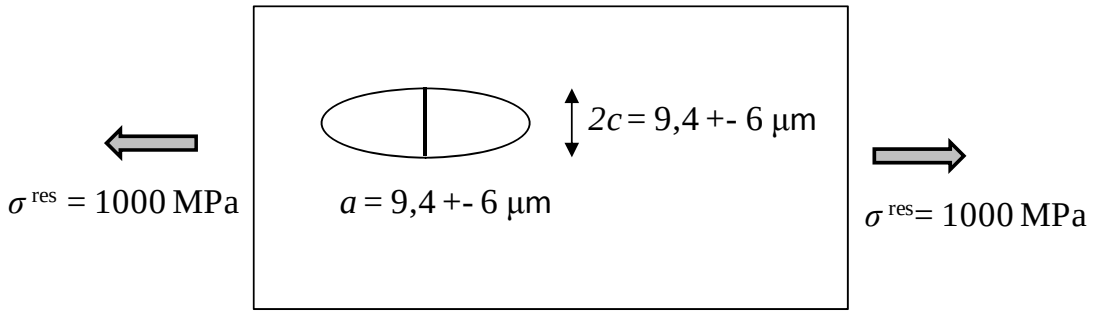

Figure 4.2.28 Schema of the parameters assumed to estimate *ΔK* at broken primary carbides of lower tools according to the carbide configuration

Calculations are done considering the scatter obtained in D_{min} values (D_{min} = 9,4 ± 6 μm so it ranges between 3,4 and 15,4 μm respectively) and in all statistically combinations possible. Results obtained are summarised in Table 4.2.1 and as follows from Figure 3.2.11 in which the determined ΔK_{TH} values for 1.2379 range between 4,0 and 4,6 MPa·m$^{1/2}$, the broken carbides are certainly not expected to give rise to propagating cracks a priori.

The estimated ΔK values are lower than ΔK_{TH} in all cases excepting for the case number 4, in which the shape of the crack is 15,4 μm both for *2c* and *a* and ΔK is 4,55 MPa·m$^{1/2}$. However, the probability that a carbide of such geometry is in the microstructure is low (1 carbide every 9, which is around 0,11 carbides satisfying this condition). In addition, taking into account that in order to propagate, a certain stress level must be acting in the crack nucleated at this broken carbide, it is hardly impossible after such approximations that a crack can propagate starting from primary carbides in these tools. In any case, in real life the microstructure is much more complicated and so they are the stress states and levels acting at the cutting edge of tools, hereby the possibility that a crack is successfully nucleated and propagates from primary carbides should not be discarded even if it has not been observed, so far.

Table 4.2.1 Estimated *ΔK* of cracks at broken primary carbides

Case	*a*, μm	*2c*, μm	σ^{res}, MPa	*Y*	ΔK, MPa·m$^{1/2}$
1	9,4	9,4	1000	1,16	3,56
2	9,4	15,4	1000	1,27	3,90
3	15,4	9,4	1000	0,99	3,89
4	15,4	15,4	1000	1,16	4,55
5	3,4	3,4	1000	1,16	2,14
6	3,4	9,4	1000	1,29	2,38
7	9,4	3,4	1000	0,80	2,45
8	3,4	15,4	1000	1,24	2,29
9	15,4	3,4	1000	0,64	2,50

However, propagating cracks do exist in tools as it was observed in Figure 4.2.19. Cracks nucleated at the surface and propagating inwards the material are observed both at the flank face of lower tools (as showed previously in Figure 4.2.19) and at the rake face of upper tools (as shows Figure 4.2.29).

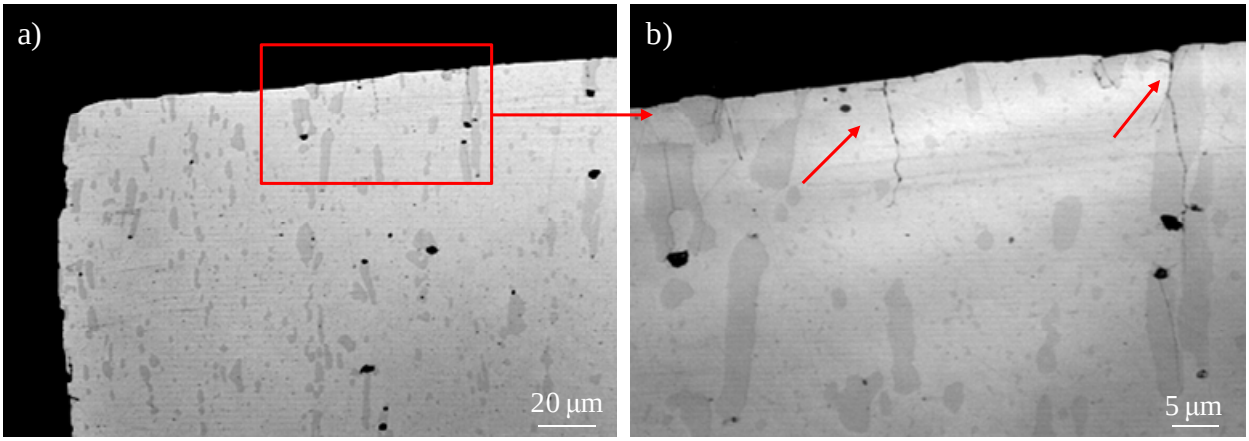

Figure 4.2.29 Cracks nucleated at the rake face of the upper tools

Cracks observed at the flank face of tools can attain long sizes at the surface (even up to millimetres as it is shown in Figures 4.2.30 and 4.2.31 after 8000 and 36000 strokes) and in the cross sectional analysis they are also found to be quite deep (sometimes measuring around 100 µm).

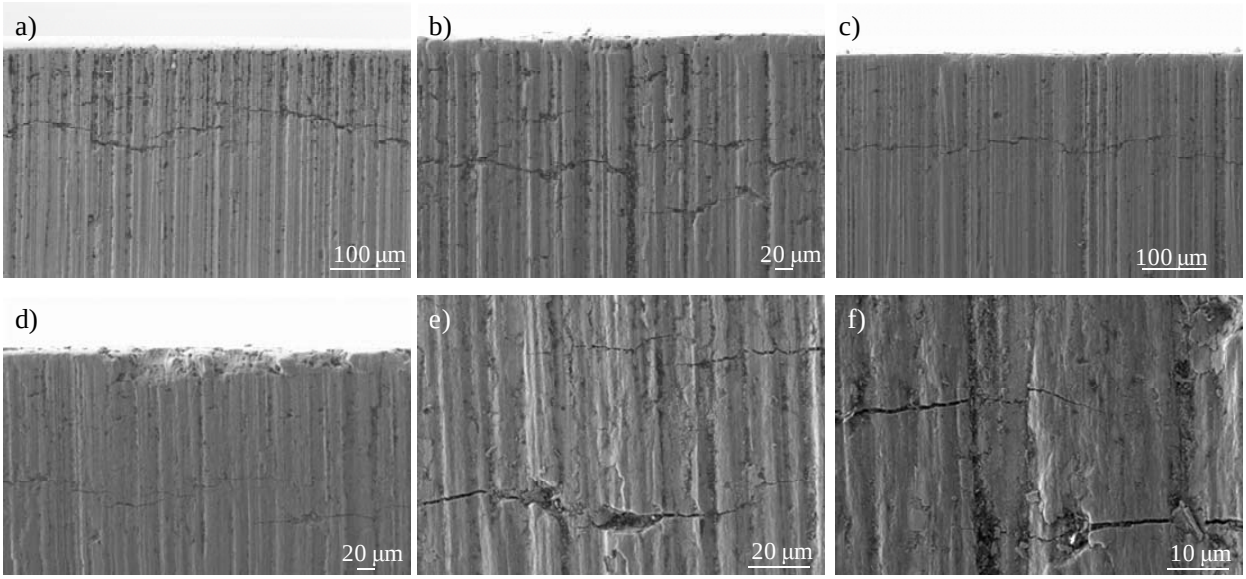

Figure 4.2.30 Cracks nucleated at the flank face of a lower 1.2379 tool at 8000 strokes

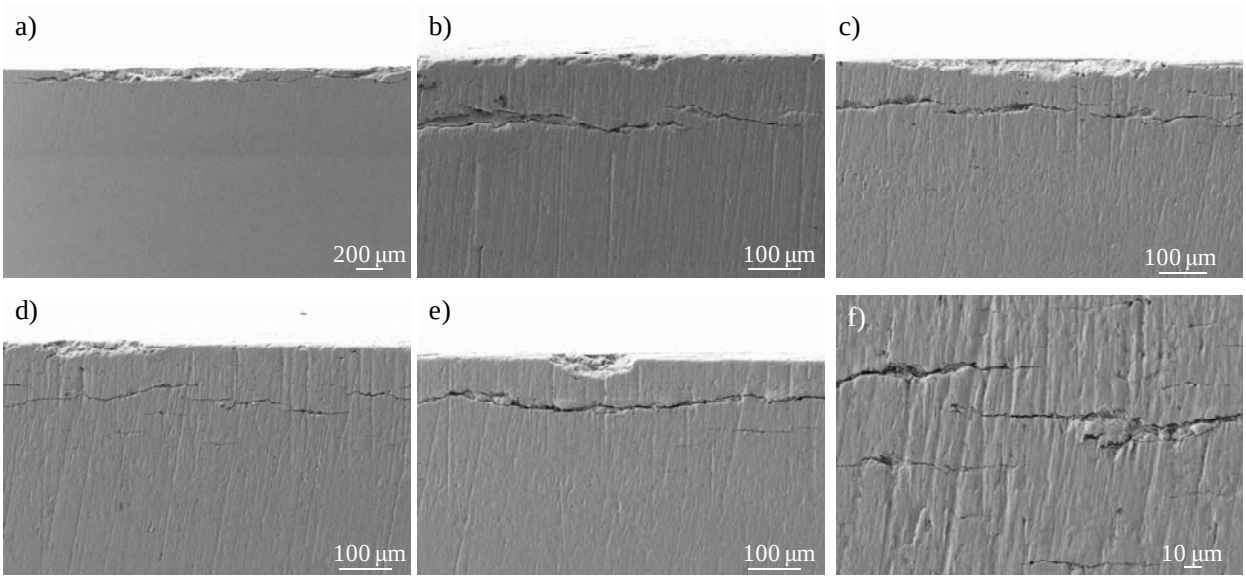

Figure 4.2.31 Cracks nucleated at the flank face of a lower 1.2379 tool at 36000 strokes

In Figure 4.2.32 it can be observed that such cracks at the flank face (Figure 4.2.32 c) and d)) are located at the same level below the cutting edge as the fractures observed. In this figure it can also be observed that these cracks grow completely flat from the flank face, but the shapes of fractures at the rake face resemble more semi-ellipses (Figure 4.2.32 a) and b)). The presence of cracks at the rake face is not as evident as that of the flank face and after the examinations of the tools, only small cracks or broken primary carbides can be identified, as shown in Figure 4.2.33. Those cracks seem to grow and coalesce at the rake face in what could resemble the semi-ellipses observed in tools.

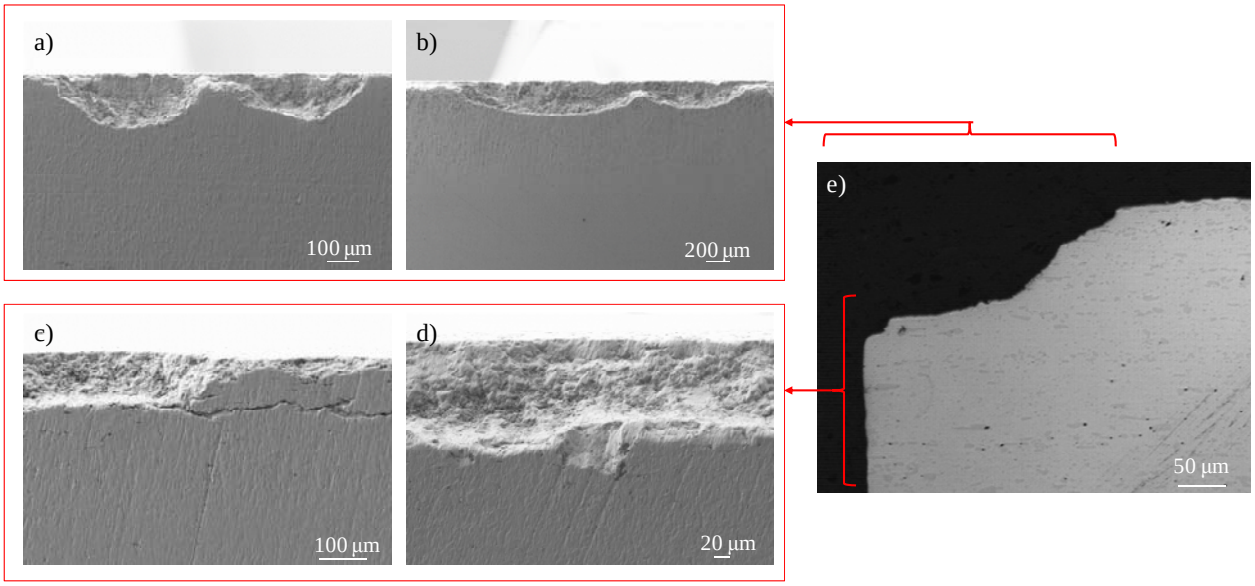

Figure 4.2.32 Fractures at the cutting edge in views from: a) and b) the rake face of the tool; c) and d) the flank side of the tool and e) cross sectional image

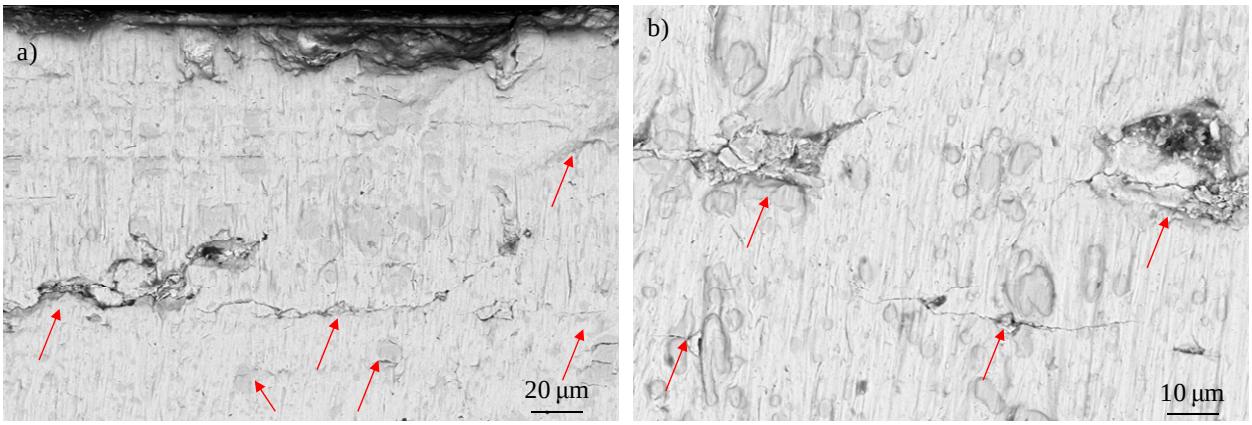

Figure 4.2.33 Cracks at the rake face of a 1.2379 lower tool near the cutting edge

In Figure 4.2.34 it can be observed that fractures all along the cutting edge have approximately the same depth and these depths correspond exactly to the location of the lateral cracks

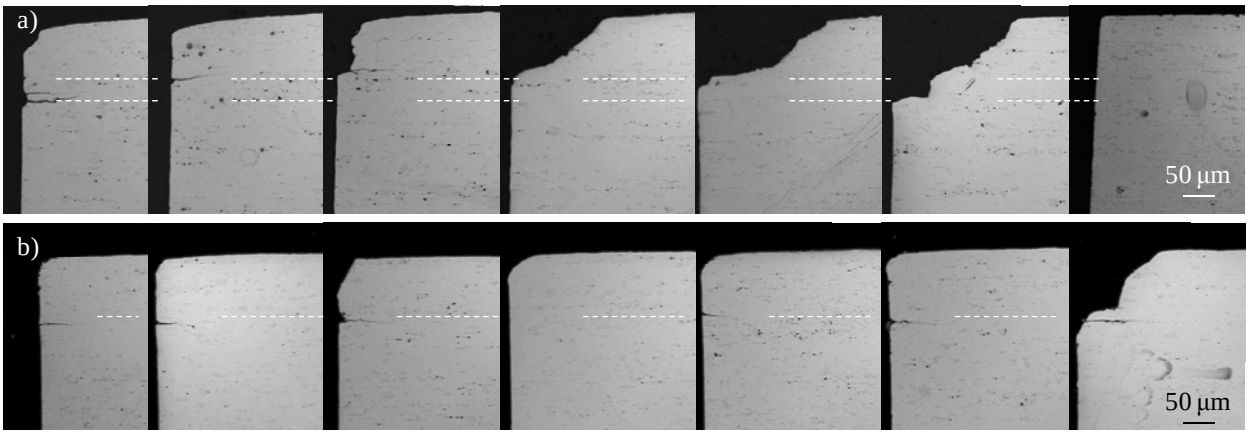

Figure 4.2.34 Cross sectional images of the cutting edge of two 1.2379 lower tools, dashed white lines denote the location of cracks nucleated at the flank face: a) after 36000 strokes and b) after 22000 strokes

As follows from the arguments above, it might be plausible that fractures observed at the cutting edge are due to the connection of both lateral cracks at the flank face and small cracks at the rake face. The fractography of the cutting edge quite indicates that lateral cracks are grown stably by fatigue but it is not sure so far whether these cracks turn their direction towards the rake face, or they coalesce with vertical cracks propagating inwards. Actually, no propagating cracks have been observed in the cross sectional analysis of lower tools despite fracture occurs.

In order to shed light on the mechanisms explaining the growth of these cracks and the occurrence of fractures, the case of slitting tools is approached from the Standing Contact Fatigue (SCF) point of view. This approximation is plausible since Alfredsson and Olsson [ALF00] examined the cracks created as a result of SCF tests and they determined that for loads above an endurance level, two different types of axi-symmetric contact fatigue cracks develop after a sufficient number of load cycles which resemble

very much the type of cracks observed in these tools. In Figure 4.2.35 a) a ring shaped surface crack can be observed, which underlines the circular region with cyclic contact and recalls the shape of the cracks observed from the top view in slitting tools in this Thesis (Figure 4.2.32 a) and b)).

These authors reported that as the overall test load level increases the distance from the contact rim grows, and a second and even a third crack may appear outside the first, as shown in Figure 4.2.35 b). Cracks are initiated at several circumferential locations around the contact rim (Figure 4.2.35 c)) creating the ring crack as they link up, analogously to the microcracks showed in Figure 4.2.33 and Figure 4.2.36, in which several circumferential cracks are observed at the cutting edge.

Alfredsson and Olsson found another type of crack as a result of SCF tests and it is the so-called sub-surface lateral crack (Figure 4.2.35 d)). The aforementioned authors observed that all lateral cracks have a shallow U-shape and the depth location is independent of the test load level. This statement is in agreement with the fact that fractures observed in slitting tools have almost the same depths below the cutting edge.

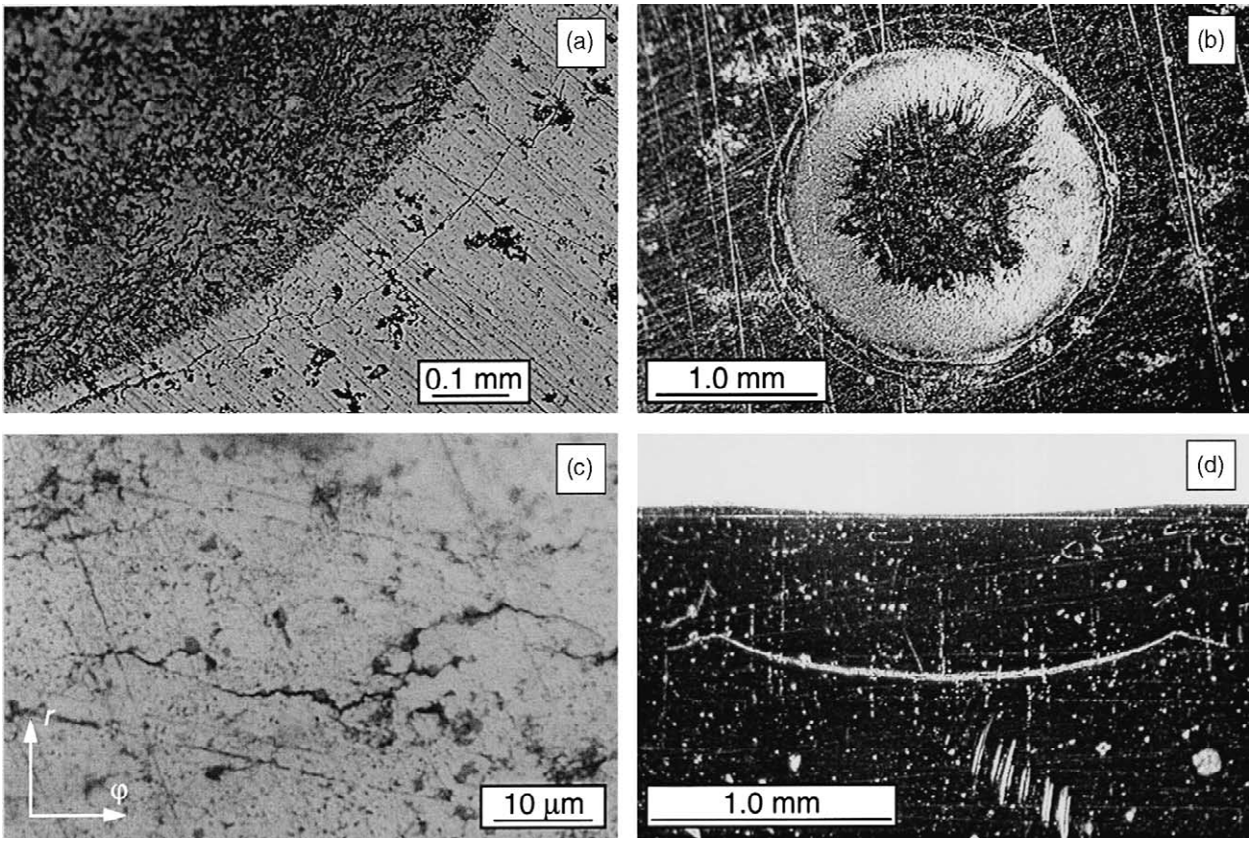

Figure 4.2.35 SCF crack results: a) top view of first ring/cone crack; b) top view of second ring/cone crack; c) initial ring/cone cracks formation and d) cut view of lateral crack [ALF01]

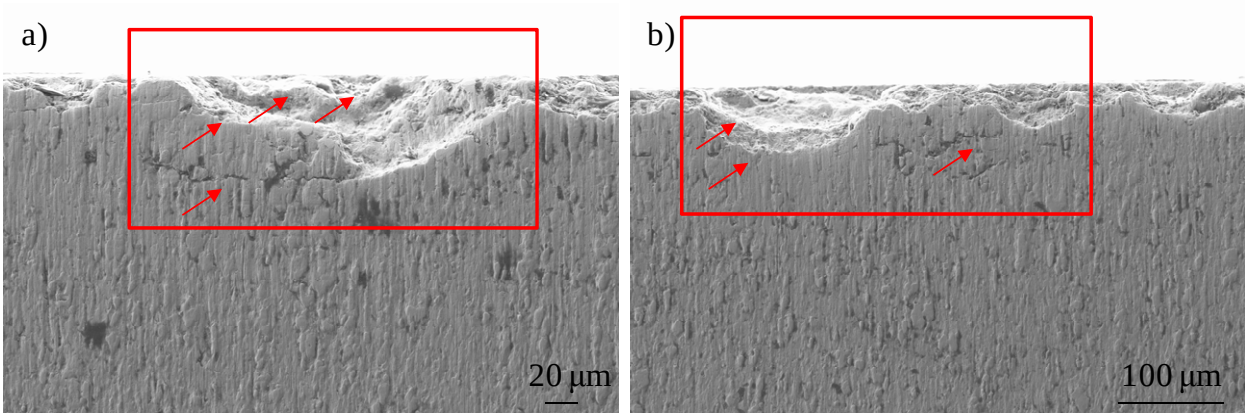

Figure 4.2.36 Several circumferential cracks are observed near fractures at the cutting edge of 1.2379 lower tools (in correspondence with Figure 4.2.34 b))

In Figure 4.2.37 it can be observed that the similitude between lateral cracks in SCF samples and cracks nucleated at the flank face of tools is very high.

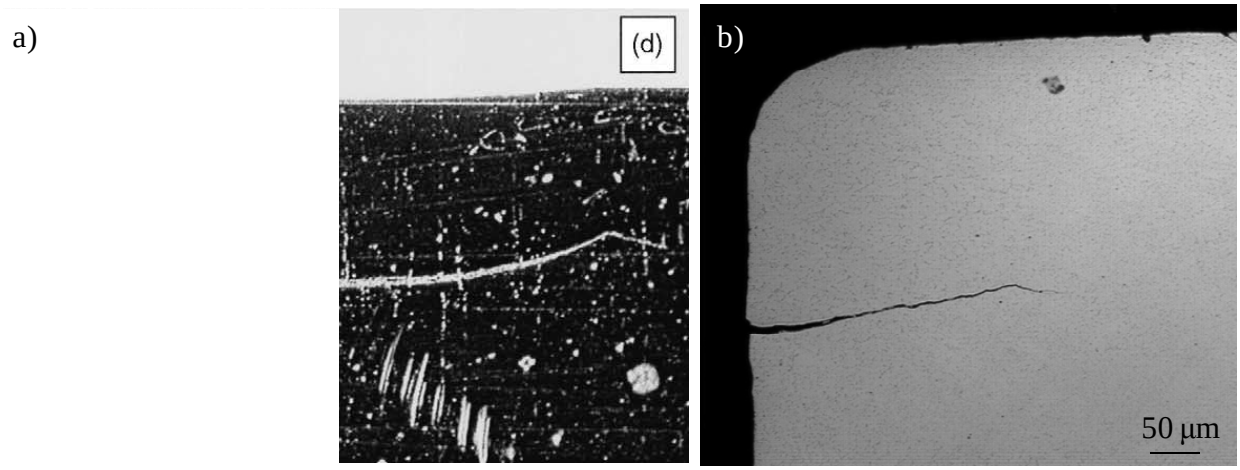

Figure 4.2.37 Lateral cracks in SCF samples resemble cracks nucleated at the flank face of tools: a) Figure 4.2.35 d) from Alfredsson and Olson [ALF01] and b) cut view of an HWS tool

Alfredsson and Olsson argued that the ring/cone crack is motivated by the tensile radial stress (Figure 4.2.38 b)). At the lateral crack position all principal stresses are compressive at maximum load. However, tensile stresses appear when the sphere is unloaded (Figure 4.2.38 a)). All principal stresses are of approximately the same numerical value at unloading, but the axial stress has a much larger amplitude due to the high compressive stress at maximum load. The lateral crack initiation is therefore explained by the tensile axial stress at unloading in combination with the large alternating stress component in the same direction. The lateral crack position and shape is a result of the inhomogeneous plastic properties of the material and the residual plastic deformation below the contact.

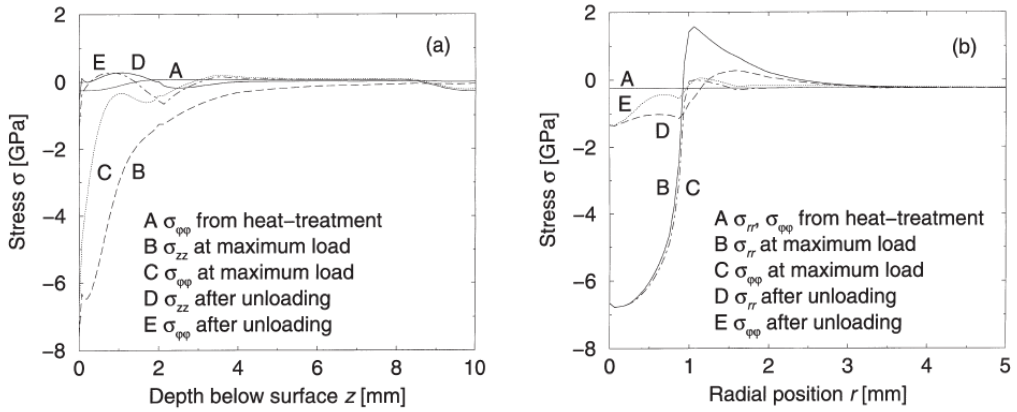

Figure 4.2.38 Principal stress distribution at P = 13,4 kN and after unloading: a) σ_{zz} and $\sigma_{\varphi\varphi}$ along the symmetry line and b) σ_{rr} and $\sigma_{\varphi\varphi}$ along the surface [ALF01]

In slitting tools, the reason for the existence of such lateral-like cracks may be first, the rough surfaces which under the high compressive stresses may cause their nucleation. Surface grooves may act as notches from which small cracks directly at the notch root are expected to be created since in absence of a crack, the stresses near the notch root can be significantly magnified with respect to the remote applied stresses. In Figure 4.2.39 the similarity of the lateral cracks in slitting tools can be compared to the case where cracks are nucleated from notches. Surface damage created by the repetitive contact loads and the high friction coefficients may also cause cracks to nucleate as follows from this mechanism.

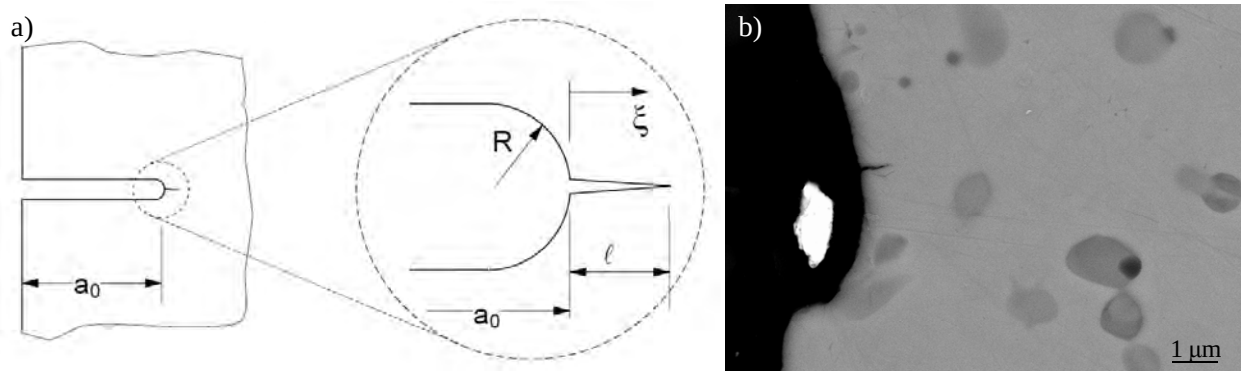

Figure 4.2.39 a) A small crack emanating from the root of a notch [FET08]; b) small crack emanating from a grinding groove in an HWS lower tool

However, in absence of such grinding defects the nucleation of cracks at the surface may still be promoted by the breakage of primary carbides, especially in case of ingot cast steels, as shown previously in Figure 3.3.84. Once cracks are opened, the modes of propagation inwards may differ depending on if they are located at the rake or flank faces. Owing to the high compression loads at the cutting edge parallel to the stroke direction, lateral-like cracks are prone to propagate faster than those ring/cone-like cracks, and as a matter of fact, that was already observed by Alfredsson and Olsson in their work on SCF.

This effect is of special importance in HWS lower tools where it is observed that at the same number of strokes than in 1.2379 or UNIVERSAL lower tools, lateral-like cracks have propagated much deeper than in UNIVERSAL and fractures have already taken place. As discussed in section 4.1 and 4.2.1, HWS has a markedly higher resistance to crack nucleation in primary carbides however, its higher fatigue sensitivity is especially detrimental when large defects such as grinding grooves are left from machining processes since cracks easily nucleate from them, and the resistance to crack propagation is lower than the ingot cast steels. Therefore, it is crucial that the grinding parameters are optimised in order to benefit of the high performance of PM steels in such applications.

To summarise, Figure 4.2.40 schematises the different types of damage and the mechanisms explaining their occurrence in the studied slitting tools.

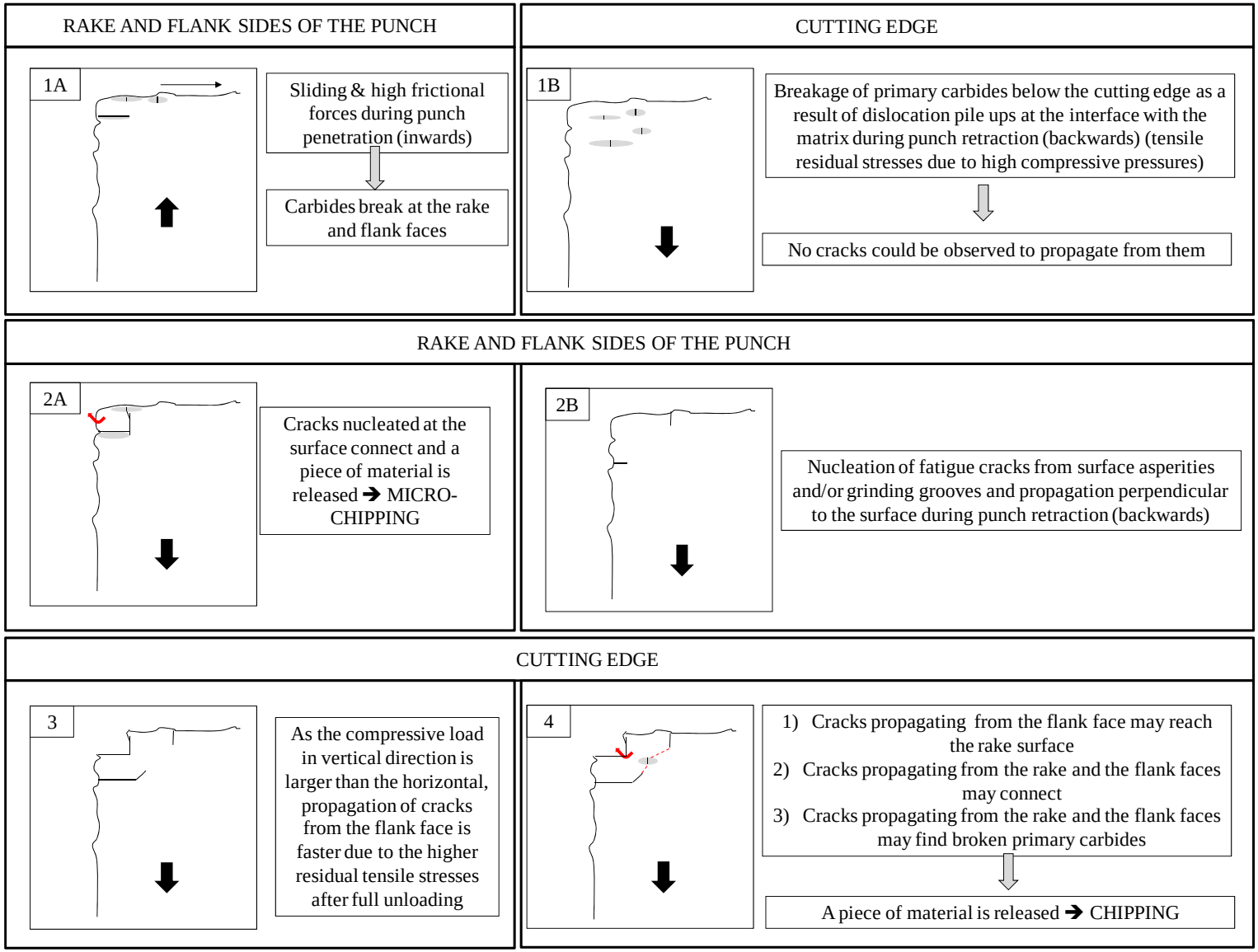

Figure 4.2.40 Summary of the different types of damage observed in the slitting tools of the HPC

As it can be observed in the figure above, damage identified in slitting tools is classified into the following:

- 1A: Damage directly at the surface originated as a result of the high frictional forces during sliding against the sheet during tool penetration. Cracks are observed at broken primary carbides of the rake and flank faces.
- 1B: Breakage of primary carbides below the cutting edge owing to the tensile residual stresses, generated as a result of the high acting compressive loads.
- 2A: Cracks nucleated at the surface from primary carbides propagate, micro-chipping is observed very near to the edge of the tool.
- 2B: Cracks nucleate at the surface from grinding grooves or asperities under the high compressive loads.
- 3: Cracks that nucleate at the flank face propagate faster than cracks that nucleate at the rake one due the high compressive loads in the stroke direction. These stresses are responsible for the higher tensile residual stresses explaining the lateral crack opening.
- 4: Cracks of step number 3 meet and chipping is observed.

Type number 1A and 1B are not observed in HWS tools, and so neither type 2A. In HWS the large cracks (compared to the microstructural size) nucleated from grinding grooves rapidly propagate and give rise to fractures. Despite ingot cast steels may contain many broken carbides and microcracks, as their resistance to crack propagation is higher than HWS, they are less sensitive to the surface roughness and in this sense they even may show a better resistance to chipping than HWS.

In presence of such marked grinding grooves, failure of tools is significantly accelerated in this type of applications dealing with such high strength sheet steels. PM tool steels are typically the most appropriated tool steel family so as to be used under such severe conditions provided that low initial surface roughness can be guaranteed. In default of satisfying this condition, the life of these tools is markedly shortened since their good resistance against crack nucleation in carbides is eclipsed by the facility that cracks develop from large defects at the surface. Therefore, the potential that PM steels offer for these applications may not be fully-operating. In contrast, probably ingot cast steels rapidly show cracks due to the presence of broken primary carbides but if the roughness of the tool is high, then they may show better performances than the PMs since their resistance to the propagation of long cracks is much higher.

PVD coatings may be a good option in these applications in order to reduce friction coefficients and delay wear phenomena as well as wear related fatigue mechanisms (i.e. when crack nucleation is due to the presence of asperities, waves, craters, etc., any imperfections created as a result of the contact between the two bodies and from cracks may priory nucleate). However, coatings are very sensitive to the roughness

of the substrate and their benefits may not be observed if the tool surface roughness is high. In this case, the coating rapidly detaches or delaminates and the overall behaviour can even be worse than in the uncoated tool. Hence, it is obvious after this investigation that the first condition to ensure the best performance of tools possible, and that tool steels show all their potential is to find and apply the optimal grinding parameters when building the tools. In this case, PM steels may be advantageously applied, and even better results may be obtained if they are coated.

4.3 Corollary

4.3.1 Considerations to the development of a model for tool life prediction: can this model be a reality?

As follows from the previous sections 4.1 and 4.2 the behaviour of tool steels in laboratory and industrial tests have been assessed from a micro-mechanical point of view. The focus has been paid on determining the influence of the microstructural constituents such as primary carbides and metallic matrix on the nucleation and propagation of cracks at a micro scale. In laboratory tests and under controlled conditions, the applied stresses at which cracks start to nucleate have been determined under monotonic loading as well as in fatigue. The propagation of such cracks has also been evaluated and it has been shown that in monotonic conditions, differences exist between the behaviour of small cracks nucleated from broken primary carbides and the behaviour of large cracks propagated following the standard test method E 399-90. In fatigue, small cracks start propagating in a tortuous manner until they attain a certain size (the size of the carbide band in which they are initially nucleated) and from this moment the growth of these cracks through the matrix turns into more stable and is rather similar to that observed for large cracks (in E 647-00 tests).

In real tools the mechanisms by which cracks nucleate and propagate are much more complicated and do not owe to one single parameter but usually, they are influenced by multiple factors such as stress states, surface roughness, microstructural discontinuities like carbides, micro-mechanical properties, etc. For this reason, the development of a robust and reliable model for predicting tool lives is very complicated as the mechanisms occurring in a tool are all linked together, acting at the same time or triggering the initiation of others.

Some of the concerns which come in mind when trying to set up a model to predict tool lives are summarised as follows:

- The first point to be considered is that not only one single type of micro-mechanism leading to damage and/or chipping is identified neither in punching nor slitting tools, but as show Figures 4.2.18 and 4.2.38 respectively, multiple damaging mechanisms are found to contribute, under

different degrees of implication, to the macroscopic failure of tools. For instance, high sliding conditions at the surface trigger both the breakage of carbides under the surface and the formation of wear particles, which create discontinuities and imperfections at the surface and can promote the nucleation of fatigue cracks from them.

- A second limiting factor regarding the development of this model is that the acting stresses cannot be determined locally in a microstructural scale for tools. The stress state at the cutting edge is highly complex and it evolves during the tool penetration and retraction movements. Von Mises equivalent stresses are typically used to quantify, by means of FE-simulation, the level and distribution of stresses in engineering components. However, in order to simplify the computation of stresses in FE-models, the test is normally stopped directly before the fracture of the sheet and tools are assumed to behave as elastic bodies and to be completely homogeneous. In this way, von Mises stresses are maximal before the fracture of the sheet and they are completely released afterwards.

But in contrast, the findings of this Thesis show that plastic deformation in the tool microstructure at the micro scale is plausible, especially at narrow depths below the contact surface and in those locations where axial compressive stresses are high. As a consequence, tensile residual stresses may be generated. The presence of primary carbides embedded in the matrix contributes to the localisation of such plastic strains at their surroundings, reason why they break. In addition, there is a major role of the friction coefficient and the sliding conditions of the sheet at the tool surface, since they trigger the formation of surface asperities. The fact that the surface is rough may explain the existence of tensile stresses at asperities even under compressive external loads, but the stresses developing locally in there are not known since they depend on the external load (which varies depending on the position of the asperity on the tool surface), on the shape of the asperity, etc. Therefore, it is difficult to set the stress value at which a crack may nucleate and after how many cycles it happens. The lack of knowledge about the local stress values responsible for effective crack nucleation in tools is a big limitation to calculate their potential life so far. Moreover, once a crack is open the singularity ahead of the tip completely modifies the stress state existing prior to its formation, and that is also something difficult to take into account since, even under compressive states, tensile stresses can be developed at the crack tip.

- In this regard, as contact pressures play an important role in tools, the fact that the surface is under constant evolution due to wearing out effects is also a limiting factor for the considerations of the model. Wear and fatigue are related processes in this tools in a way that some mechanisms are explained because of the conjunction of both; i.e. fatigue cracks are generated as a result of wear at the surface and vice versa, the propagation of fatigue cracks leads to the release of wear particles.

That means that a proper model to predict the life of tools should not disregard the wear effects on the surface since they contribute to the nucleation of fatigue cracks, and therefore a prediction of wear should also be taken into account.

- The last matter of concern is to know how the differences observed in tests with laboratory samples between small and large cracks apply also in tools. Ingot cast steels show a dependency between the toughness and the crack size, which is especially remarkable for 1.2379 and K360. In tools cracks of different sizes have been observed; lateral cracks are rather large but those responsible for the release of wear particles at the surface are very small. In fatigue however, and even if as said before the initial cracks propagate quite tortuously, small, medium and large cracks behave in a similar way, i.e. their growth can be described by similar parameters. If so, the propagation of small and large cracks is quite comparable but the K at which they can break increases together with the crack size, as shown by the R-curve results. Then it is possible that in the most stressed areas the nucleated cracks propagate and lead to failure when they are still very small, since besides the acting stress is high their effective fracture toughness is low. Only fatigue cracks which grow under more moderate stresses may attain large sizes instead (or the sizes expected after E399-90 tests on large cracks). As a result, the model should also consider the size of the nucleated crack and depending on the stress level which is acting right in there; it should continuously associate the corresponding fracture toughness value since it varies as long as the crack grows. There is a last question open on this matter and this concerns the fact that the material R-curves determined under three point bending tests really reproduce the behaviour of such cracks when they are nucleated in tools. This matter comes from the reflexion of how far is the stress state under which cracks grow in laboratory bending tests with respect with the one of real tools.

Obviously developing a model which takes into consideration all these input parameters is complex. Furthermore, the reliability and robustness of this model is hardly assured since it would have to be modified for each different operation. However, it is comforting that empirical observations in tools made from the tool steel manufacturer ROVALMA in basis of his experience after many years in this field, are completely in agreement with the findings of this investigation. Figure 4.3.1 schematises different situations taking place in tools, after ROVALMA, depending on the type of failure by chipping that they show.

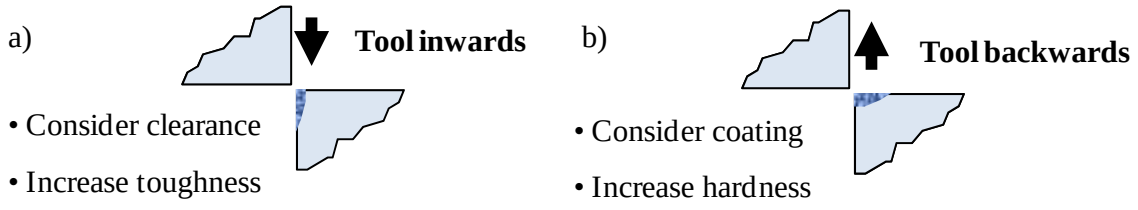

Figure 4.3.1 Schematic illustration of the different types of chippings registered empirically in basis of the long experience of the tool steel manufacturer (adapted from knowledge given by ROVALMA)

As it can be observed in the figure above, on the one hand there is the kind of damage produced when the tool moves inwards and which resembles that identified in punches (compare Figure 4.3.1 a) to Figure 4.3.2 a) and b)). In this Thesis the reasons for the formation of such cracks are discussed from an in depth micro-mechanical point of view but in analysing what the tool steel maker finds effective to preventing it: revising the shearing clearance and increasing the toughness of the tool steel, one realizes that these are in perfect agreement and can be justified using the same arguments presented in this investigation.

This type of chipping (more elongated on the flank face than on the rake one) is due to the propagation of those cracks which are nucleated at the rake face and propagate until attaining the surface on the flank. Cracks nucleated at the rake face owe to the very high contact pressures at the surface and hence, an effective way to prevent or at least, delay their nucleation is by diminishing these surface pressures. These, in turn, can be reduced by using the appropriated shearing clearance. In section 3.3.4 it is shown that an increase of clearance leads to a reduction of the load required for punching but also, to an increase of the maximum von Mises stress. This phenomenon is due to the different contact areas at the cutting edge, i.e. the contact area is smaller when higher clearances are employed. Therefore, if the clearance is too high only a narrow part of the cutting edge is receiving the load and, even if this load is lower than when using a lower clearance, it is still very high and can cause the material to be damaged early. If the clearance is too small, then loads are higher but contact areas too and the effects might be compensated. However, there is major problematic when using small clearances and this is due to the increased probability of shocks, which apart from affecting the integrity of tools they can also affect the press functionality. Then the optimal clearance value should be set for every operation.

The second recommendation made by ROVALMA concerns the increase of the toughness of the tool steel. The author of the present Thesis believes that by increase of toughness, an increase of the crack propagation resistance in fatigue and an increase of the final fracture toughness are meant. Once cracks are nucleated at the rake face, as described in section 4.2.1, their propagation depends on the resistance of the material against crack growth. Admitting that even if working at the optimal clearances, cracks may finally nucleate at the rake face due to some sort of wear damage and plastic deformation, propagation of these cracks is always a matter of concern. The ideal material would be desired to difficult the propagation of cracks or even succeed to get them arrested.

As shown in section 3.2.5, a crack only propagates provided that the acting ΔK exceeds the ΔK_{TH} of the material. It has been shown that ΔK_{TH} of small and large cracks lies approximately at the same level and it corresponds to that determined by means of standard E647-00 tests. An attempt to increase the material resistance to crack propagation consists in alternating carbide and matrix bands, in a way that once cracks attain the matrix, they require an increase of energy to continue propagating through the whole band since it is a tougher phase. In this sense and in some applications, ingot cast steels could show superior results

than PM steels. The toughness or resistance to crack propagation of the matrix in itself should also be increased by applying the appropriate heat treatment. For this, it is imperative that as explained throughout this Thesis (but further discussed in section 1.2), the small secondary precipitates embedded in the matrix have the optimal size.

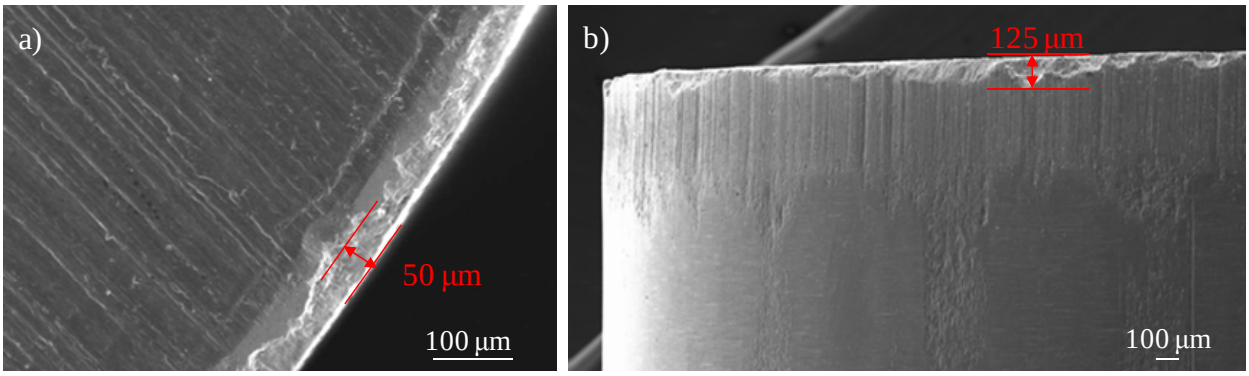

Figure 4.3.2 An example of fracture at the cutting edge of punches where similarities to Figure 4.3.1 a) can be observed: a) at the rake face and b) at the flank face

The aforementioned arguments are of especial importance in tools with non optimised surface finish and rather high initial roughness. In these cases, cracks mostly nucleate from surface imperfections and rather independently of the tool steel microstructure. Then it is particularly interesting that the tool steel has a high resistance to crack propagation (i.e. like ingot cast steels) even if that can be detrimental for the resistance to crack nucleation at primary carbides. But if the grinding process could provide the surface with a low roughness value, less than 0,5 µm, then PM steels are a good option. Breakage of carbides would definitely be delayed or prevented depending on the acting stresses, and even the effects of high contact pressures at the surface could be delayed.

On the other hand, as show Figure 4.3.1 b) in some cases chipping is more elongated on the rake face than on the flank one. Then, the application of a coating and an increase of hardness are recommended. As shown in Figure 4.3.3, this type of chipping resembles to that observed in slitting tools.

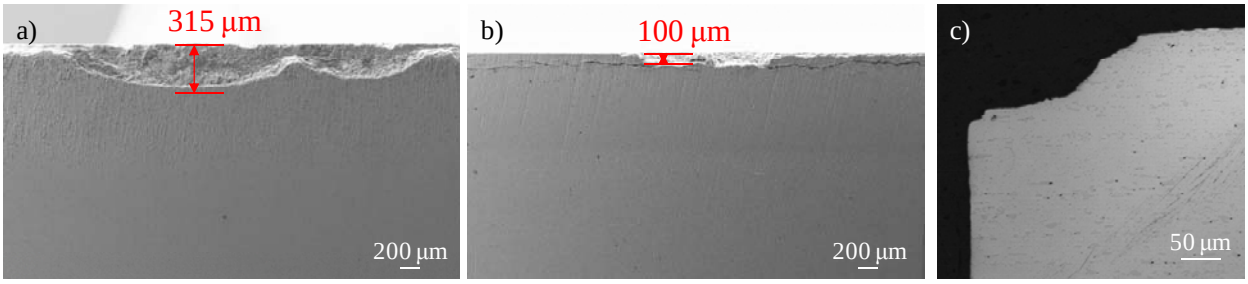

Figure 4.3.3 An example of fracture at the cutting edge of slitting tools where similarities to Figure 4.3.1 b) can be observed: a) at the rake face; b) at the flank face and c) in cross section

In these tools chipping is probably due to the propagation of fatigue cracks nucleated at the flank surface and propagating first rather horizontal, but then turning the direction under the acting stress state at the cutting edge, to finally attain the rake surface. Such cracks nucleate at the surface during the unloading stage as a result of tensile residual stresses. Hereby, a strategy to delay their nucleation consists in increasing the properties of the surface. A coating helps decreasing the friction coefficient and plastic deformation at the surface, both responsible of creating damage from which cracks are prone to nucleate. However, as shown throughout this Thesis, a critical requirement that must be satisfied so that the performance of the coated tool is successfully improved compared to the nude one is that the initial substrate surface has the lowest roughness possible. Small asperities cause tensile loads at the coating even when the external loads are compressive and hereby, the coating can easily detach from the surface (as explained in section 3.3.3.1 and Figure 3.3.64).

The recommendation of increasing the hardness of the material goes much in the same sense that applying a coating. The higher the hardness of the surface, the higher the yield stress of the material and therefore the lower the possibilities that plastic deformation occurs, that tensile residual stresses are generated and as a result, that cracks nucleate. Once again, it is very important that the surface initial roughness is low, otherwise cracks can easily nucleate from grinding grooves and the potential improvement of increasing the hardness at the surface can be detrimental, since an increase of the hardness of the material in the bulk can lead to lower toughness (as it is shown in section 1.2.2.2 An Figure 1.2.9).

In basis of this discussion and on the results presented in section 3.4, the models based on LEFM seem rather insufficient to accurately predict the life of tools. These models assume that a crack is already present in the microstructure at the cycle number one, and that it is nucleated from primary carbides or inclusion particles. However, in tools there may always be a time for crack nucleation and they do not exclusively nucleate from primary carbides or inclusions but from surface irregularities, wear particles, etc. Hence, the life of tools cannot be accurately predicted by means of these models.

In front of the lack of consistency of the models based only on LEFM to predict tool lives and as follows from the results of this Thesis, a new approach is proposed which holds the idea that the micro-mechanical properties of the metallic matrix in tool steels decrease due to the application of repetitive load. The model basically sustains the reduction of E, as some authors like Pedersen [PED97] have related the reduction of E to the accumulation of plastic strain. Cobo et al. [COB09] have reported that the drop of E with plastic deformation is based on the variation in the dislocation structure and the capability of the material to accumulate totally or partially movable dislocations, which are the responsible to produce extra microplasticity. As follows from the underlying statements, the reduction of E can be

related to a certain applied stress and number of cycles, and the lives of tools can be predicted in this way, based on micro-mechanical damage.

One of the advantages of this model is that it is based on mechanical damage instead of nucleation or propagation of cracks. Hence, any type of damage leading to a reduction of *E* at the micro level is a precursor for crack nucleation. Any type of damage means that by means of this model, not only damage as a result of broken primary carbides or inclusion particles can be detected, but also wear or plastic deformation can be taken into account since they may lead to a reduction of *E* as well. In addition, this model avoids any consideration of crack size – toughness dependency, surface roughness, stress state and level, tool geometry, shearing parameters, etc., as it only accounts for a decrease of mechanical properties of the metallic matrix, whatever it is the triggering effect.

Even though this Thesis has found a meaningful method for predicting tool lives, works have to progress in order to be able to develop a model which can accurately estimate the failure of tools. However, in the following section an example of application in industrial tools is presented.

4.3.2 An application of the micro-mechanical damage based model for life prediction of industrial tools

Tools made of HWS and employed to punch MS-W1200 2 mm thick at AUTOTECH ENG. (the performance of these tools is studied in section 3.3.2.2) were used in this part of the investigation to determine the evolution of *E* with the increase of the number of strokes. *E* was measured at different increasing distances from the cutting edge using polished specimens extracted from tools (as described in Figure 2.5.10). Specimens from four different tools were used. Tools were at different stages of their lives: at the initial stage, after 15000, 40000 and 100000 strokes, respectively.

Figure 4.3.4 present the evolution of *E* measured by means of nanoindentation through the diagonal which crosses the cutting edge of punches and up to 5 mm far from the edge. As it can be observed, *E* shows a clear decrease for distances shorter than approximately 500 μm from the punch edge at specimens after 15000, 40000 and 1000000 strokes. The examination of indentation imprints which showed a reduction of *E* reveals damage in form of plastic deformation and decohesion of primary carbides (compare Figures 4.3.5 a), b) and c) with Figure 4.3.5 d)).

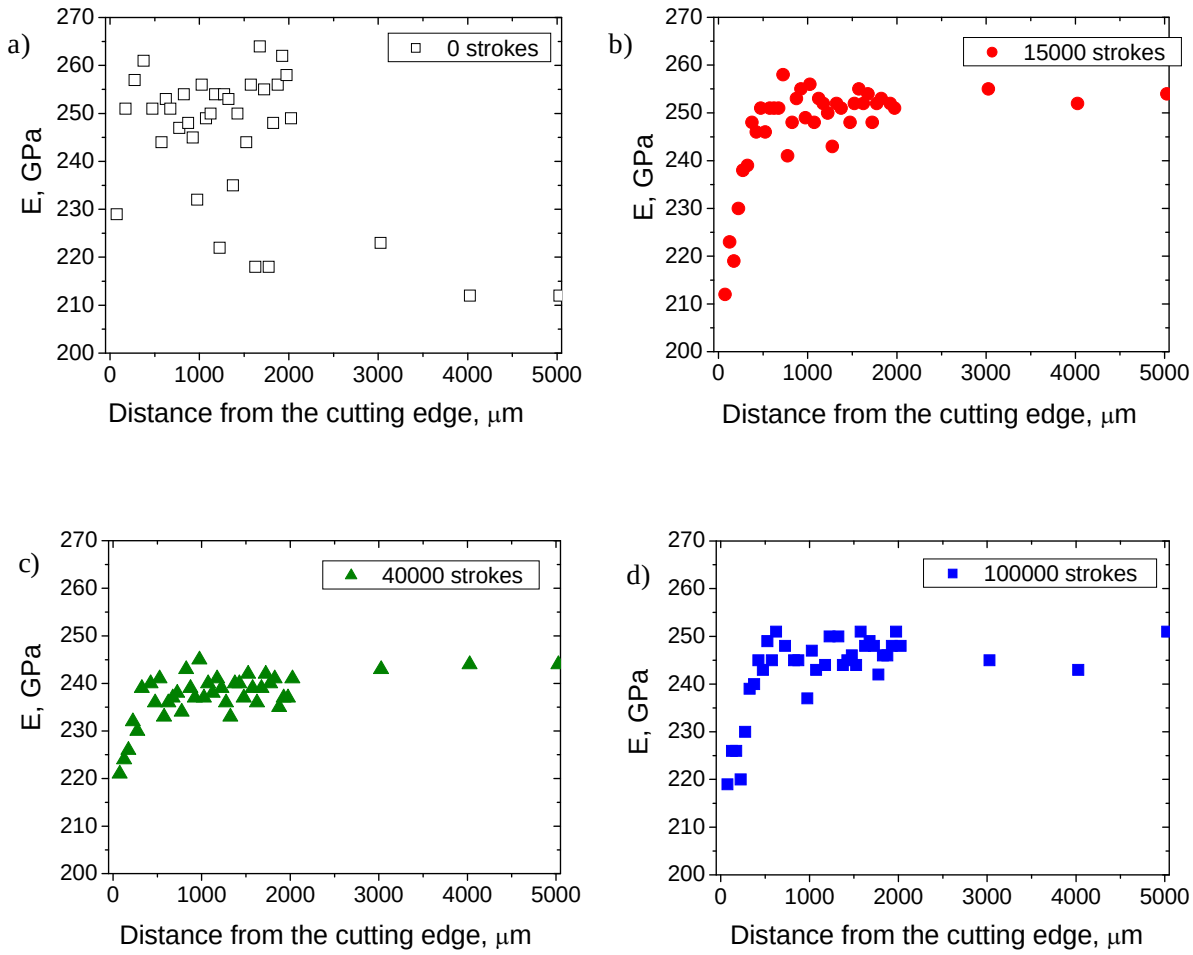

Figure 4.3.4 Evolution of *E* in HWS punches after: a) 0; b) 15000; c) 40000 and d) 10000 strokes

5. Conclusions

In this Doctoral Thesis the interrelationship between the microstructure and the mechanical behaviour of tool steels for shearing UHSS have been determined through the analysis of four different cold work tool steels: 1.2379, UNIVERSAL, K360 and HWS at 62 HRC. Micro-mechanical damage of punching and slitting tools made of these four steels has been identified, classified and rationalised in order to give the clues to improve the microstructural design of tool steels and the performance of tools for shearing UHSS.

This Thesis provides new insights into: the microstructure of ingot cast and PM tool steels and their main constituents, i.e. primary carbides and tempered martensite matrix (section 3.1), their macro- and micro-mechanical properties (sections 3.2.1 and 3.2.2), crack nucleation and growth under monotonic loads and evaluation of *R*-curve behaviour (sections 3.2.3, 3.2.4 and 3.2.6) and fatigue crack nucleation and propagation mechanisms (section 3.2.5). It also provides new insights into the mechanical and tribological behaviour of industrial and laboratory tools as well as the effects of shearing process parameters on the performance of tools and quality of sheet sheared edges (section 3.3). Finally, this Thesis analyses the suitability of LEFM based models to estimate the life of tools (section 3.4).

Damage on tools steels has been rationalised from a micro-mechanical point of view in laboratory samples (section 4.1) as well as real tools (section 4.2). The aspects that a model should consider in order to successfully predict lives of tools for shearing UHSS have been described, and as follows from the finding that *E* of the metallic matrix of tools reduces with the increase of the number of strokes, a new approach to predict tool lives has been proposed (section 4.3).

In the following lines the central and major findings of this work are revised and summarised:

<u>Microstructure and micro-mechanical properties of tool steels:</u>

- In 1.2379 there is only one type of primary carbide, M_7C_3-type, rich in Fe and Cr. In K360 there are primary carbides of the following types: M_7C_3, MC and M_6C. The chemical composition of the M_7C_3 is very similar to that of the 1.2379, with some V and Mo replacing Cr and Fe. The MC are mainly Nb carbides and the M_6C show high amounts of Mo and Fe.

- In UNIVERSAL there are M_7C_3 and MC primary carbides. M_7C_3 carbides are also similar to those of 1.2379, except for some Cr which is replaced by V and W. MC carbides are mainly formed by V. In HWS, M_7C_3, MC and M_6C are present. These carbides are supposed to present similar chemical

compositions than those of UNIVERSAL (except for the M_6C, which is assumed to be mainly formed by Mo and/or W).

- 1.2379 shows the largest carbide sizes while HWS presents the smallest carbides amongst the studied steels. M_7C_3 carbides in K360 are very close in terms of size to those of 1.2379, while those of UNIVERSAL are smaller. However, MC carbides of UNIVERSAL have larger sizes than the MC of K360. M_6C carbides of K360 are markedly smaller than the M_7C_3 and MC which are also embedded in this steel. Carbides in HWS show typical sizes for PM steels and the M_7C_3 are the largest, followed by the MC and finally, the M_6C.

- The distribution of morphology parameters suggests that carbides embedded in 1.2379 have the most irregular and elongated shapes. M_7C_3 carbides of K360 show similar morphology distributions to these, while M_7C_3 carbides of UNIVERSAL are more regular and rounded than the previous ones. MC carbides of UNIVERSAL are the most spherical amongst the ingot cast steels and they have also the highest sphericity. M_6C of K360 are quite round compared to the other two in this steel. Finally, carbides of HWS are almost like perfect spheres.

- Secondary carbides in UNIVERSAL have been classified into four different types: $Cr_{23}C_6$, $(Cr,Fe)_7C_3$, Cr_7C_3, VC and M_6C, measuring from tens to 1000 nm.

-Ingot cast steels are markedly anisotropic, especially 1.2379 and K360, while HWS shows an isotropic behaviour. The highest mechanical properties of ingot cast steels are obtained for D2 samples, in which primary carbides are oriented following the longest axis of samples.

- 1.2379 shows the lowest values of σ^R and $\Delta\sigma^{fat}$, although K360 presents only slightly better results. UNIVERSAL shows higher σ^R and $\Delta\sigma^{fat}$ than 1.2379 and K360, but HWS shows the highest values.

- Fracture and fatigue failure initiation sites are primary carbides or agglomerates of them in ingot cast steels and inclusion particles in HWS. K_{IC} and ΔK_{TH} and opposite to σ^R and $\Delta\sigma^{fat}$, are the highest in 1.2379 and the lowest in HWS. These results are in agreement with relevant literature on this field, regarding different mechanical properties on ingot cast and PM tool steels.

- E and H of M_7C_3 primary carbides in 1.2379 are higher than the M_7C_3 in UNIVERSAL and K360 but lower than the MC of the same steels. In terms of K_C, M_7C_3 of 1.2379 present similar values to MC of K360, while MC of UNIVERSAL show the highest results. No K_C is calculated for both M_7C_3 carbides of UNIVERSAL and K360, as they do not develop cracks after indentation. The

micro-mechanical properties of the metallic matrix of 1.2379, UNIVERSAL and K360 do not present significant differences.

Crack nucleation and propagation under monotonic and cyclic loads

- The nucleation of cracks in tool steels is due to the failure of primary carbides by cleavage (and inclusion particles in case of PM steels) when the stress exceeds their σ^{RC} or the matrix at their surrounding exceeds its yield stress. The yield stress of the matrix, in turn, is determined by the secondary fine carbides precipitated in the martensitic matrix during tempering. M_7C_3 primary carbides in 1.2379 and K360 present the lowest σ^{RC} results. MC carbides in K360 and M_7C_3 carbides in UNIVERSAL show similar σ^{RC}, while the MC of UNIVERSAL show higher values of σ^{RC}. HWS, in turn, shows the highest σ^{RC} results. This means that HWS has very high resistance to crack nucleation at primary carbides or inclusions compared to ingot cast steels.

- Small cracks nucleated from primary carbides in ingot cast steels are initially very shallow, but they tend to grow to semi-circular shapes as the load increases and they propagate through the matrix bands. In HWS, small cracks have already semi-circular shapes and their growth is steady through the microstructure.

- Ingot cast tool steels present *R*-curve behaviour, i.e. fracture toughness depends on the crack size. Hence, given the reduction of toughness (compared to K_{IC} values determined for long cracks through standard E 399-90 tests) in case that small cracks, or high stresses, are involved in the fracture process of ingot cast steels, it is possible that HWS shows a higher K_R even if it has a lower K_{IC}. This is a very important consideration that must be taken into account when designing tools made of ingot tool steels with high fracture resistance for applications under high stress levels, since small cracks nucleated in the microstructure have lower toughness values than those expected after K_{IC}. Therefore, different properties might be taken into consideration depending on the tool application and the acting stresses, since the behaviour of the tool steel can vary substantially. In HWS, cracks smaller than 500 μm can present higher K_R than in 1.2379 and K360. Nevertheless, if the applied stresses are low enough so that nucleated cracks can grow to longer sizes (more than 500 μm), an ingot cast steel type microstructure can show a better performance since K_{IC}, in this case, is higher than in HWS.

- AE has been successfully applied to discern fracture micro-mechanisms in tool steels. AE arises as potential technique to monitor on-line micro-mechanical damage of tool steels. Preliminary tests under monotonic loads and using laboratory specimens have shown that it is possible to correlate microstructural damage with AE signals, as well as anticipate unstable failure of specimens. The

use of AE sources could shed light to micro-mechanical damage of tools while they are working in industrial operations, so future works of this Thesis are going to progress in this direction.

- Crack propagation of short, medium and long cracks under cyclic loads can be rationalised by the mechanical parameters determined with long cracks by means of standard tests (E 647-00).

- In 1.2379 σ^{max} and σ^{RC} lie almost on the same stress level. This implies that crack nucleation in fatigue is due to a great extent, to primary carbides broken already at the first load cycles. Provided that the ΔK of these cracks at broken carbides exceeds ΔK_{TH}, the rest of the fatigue life is spent in their propagation until one of them attains the critical size for failure. The nucleation stage in 1.2379 is hereby very short compared to the number of cycles concerned for propagation. In fatigue, initial crack propagation when cracks are still confined at the carbide cluster is rather tortuous and does not show a stable growth.

- The shape of the fractured carbides determines the shape of initial cracks and therefore, the condition of $\Delta K \geq \Delta K_{TH}$ necessary so that propagation starts. As long as $\Delta K < \Delta K_{TH}$, propagation does not take place. However, if the size of nucleated cracks fulfils the aforementioned condition they successfully grow through the matrix. Once they attain a certain size (usually when they propagate out from the initial cluster) the growth is more stable and steady, independently of the primary carbides ahead. Once a stable propagation rate is attained, cracks approach semi-circular shapes and keep growing in equilibrium for the rest of the fatigue cycles.

- In UNIVERSAL σ^{max} is lower than σ^{RC}. Thus, the breakage of carbides cannot be understood because the applied stress is higher than σ^{RC} but because the strain in the matrix around the carbide is higher than the strain that carbide can withstand. This phenomenon is attributed to the cyclic softening of the metallic matrix during fatigue tests.

- HWS has a markedly lower σ^{max} compared to σ^{RC}, but as in HWS no large carbides are present, it is plausible that the matrix at the neighbourhood of inclusion particles is subjected to more distortion and stresses rise with respect to the rest of the microstructure. After an incubation period which can vary depending on the stress applied, the size of the inclusion and its location in the sample, cracks may finally nucleate due to the reduction of the matrix properties at its surroundings. Crack nucleation in HWS concerns the major part of the fatigue life since the resistance of the microstructure against crack nucleation is very high. However, once cracks are successfully nucleated, propagation stages are rather short in fatigue since the resistance of the microstructure to the propagation of cracks is relatively low. Given that the microstructure ahead of nucleated cracks

in HWS is very homogeneous, stable propagation of these into semi-circular shapes is expected already from the initial stages.

- The case of K360 D2 in turn, is rather particular since two different types of fracture modes are observed. The first type corresponds to that described for 1.2379 D2, in which fracture is initiated from primary carbides at the surface and, since $\sigma^{max} \sim \sigma^{RC}$, the incubation period for crack nucleation is expected to be rather short. The second mechanism, in turn, consists in the breakage of carbides below the surface and the propagation of cracks from them. As a result of this internal propagation of the crack, a fish-eye pattern is formed around the initial cracked particle.

Damage mechanisms of shearing tools and prediction of tool performances

- The main failure mechanism observed in tools for punching and slitting UHSS is fracture at the cutting edge by chipping.

- An analysis at the micro level has shown that different types of damage are present in tools and that they contribute to the formation of chipping at the cutting edge. Plastic deformation and nucleation of cracks at the surface of tools occurs as a result of the high frictional forces during sliding against the sheet. Cracks propagate parallel to the surface until they reach a plane of weakness and a thin piece of material is released.

- Due to the high contact pressures at the surface, carbides within a narrow range of depth beneath the surface are broken as a result of dislocations pile ups at the interface with the metallic matrix. Breakage of carbides is explained by the tensile residual stresses that are generated after full unloading due to plastic deformation during the backwards movement of the punch. Plastic deformation takes place because of the high compressive contact loads generated at the surface and up to some distances beneath. Such dislocation pile ups lead to the formation of voids in the matrix, from which under the repetitive sliding, cracks can nucleate and propagate below and parallel to the surface.

- Cracks are also nucleated from surface asperities, ahead of which a stress state similar to that created on a notch root is generated.

- Chipping is explained by the nucleation of a crack at the rake face and its propagation to the flank face, or by the coalescence of two cracks, one nucleated at the rake face and the other at the flank face.

- In presence of marked grinding grooves, failure of tools is significantly accelerated in this type of applications dealing with such high strength sheet steels. PM tool steels are typically the most appropriated tool steel family so as to be used under such severe conditions provided that low initial surface roughness can be guaranteed. In default of satisfying this condition, the life of these tools is markedly shortened since their good resistance against crack nucleation in carbides is eclipsed by the facility in which cracks develop from large defects at the surface. Therefore, the potential that PM steels offer for these applications may not be fully-operating. In contrast, probably ingot cast steels rapidly show cracks due to the presence of broken primary carbides but if the roughness of the tool is high, then they may show better performances than the PMs since their resistance to the propagation of cracks is much higher.

- Hence, after this Thesis the first condition to ensure the best performance of tools possible, and that tool steels show all their potential is to find and apply the optimal grinding parameters when building the tools. In this case, PM steels may be advantageously applied, and even better results may be obtained if they are coated.

- This Thesis has shown that some of the concerns which come in mind when trying to set up a model to predict tool lives. The first is that not only one single type of micro-mechanism leading to damage and/or chipping is identified neither in punching nor slitting tools, but multiple damaging mechanisms contribute, under different degrees of implication, to the macroscopic failure of tools.

- Second, the acting stresses cannot be determined locally in a microstructural scale for tools. In addition, the stress state and level at the cutting edge are highly complex and evolve during the tool penetration and retraction movements. The occurrence of the types of damage observed in this Thesis which cannot be solely explained by means of the acting stress state, provided by von Mises stresses estimated after FE-simulations (the most common approach to understand tool performances), calls the role of fatigue wear mixed mechanisms. These are due to sliding and high frictional forces all along the surface of tools in contact with the sheet material, which are not taken into account in FE-simulations. FE-simulation results are helpful determining macroscopically, the stress state of the punch and assess the severity of an operation with respect to another. It allows detecting the most mechanically requested zones in tools as well. However, from a micro-mechanical point of view, stresses predicted by means of macro FE-models cannot explain the type of damage observed.

- In this regard, as contact pressures play an important role in tools, the fact that the surface is under constant evolution due to wearing out effects is also a limiting factor for the considerations of the model. Wear and fatigue are related processes in these tools in a way that some mechanisms are

explained because of the conjunction of both. That means that a proper model to predict the life of tools should not disregard the wear effects on the surface since they contribute to the nucleation of fatigue cracks, and therefore a prediction of wear should also be taken into account.

- The last matter is to know how the differences observed in tests with laboratory samples between small and large cracks apply also in tools, especially to take into account *R*-curve effects on crack behaviours in tools.

- Models based on LEFM seem rather insufficient to accurately predict the life of tools. These models assume that a crack is already present in the microstructure at the cycle number one, and that if it is nucleated from primary carbides or inclusion particles. However, in tools there may always be a time for nucleation and they do not exclusively nucleate from primary carbides or inclusions but from surface irregularities, wear particles, etc. Hence, the life of tools cannot be accurately predicted by means of these models.

- A new approach is proposed which holds the idea that the micro-mechanical properties of the metallic matrix in tool steels decrease due to the application of repetitive load. The model basically sustains the reduction of *E*, which can be related to a certain applied stress and number of cycles, in a way to predict tool lives based on micro-mechanical damage. This model stands for detecting any type of damage leading to a reduction of *E* and that it is a precursor for crack nucleation. By means of this model, not only damage as a result of broken primary carbides or inclusion particles can be detected, but also wear or plastic deformation can be taken into account since they may lead to a reduction of *E* as well. In addition, this model avoids any consideration of crack size – toughness dependency, surface roughness, stress state and level, tool geometry, shearing parameters, etc., as it only accounts for a decrease of mechanical properties of the metallic matrix, whatever it is the triggering effect. Future works have to progress in order to be able to develop a model which can accurately estimate the failure of tools by means of the reduction of *E*.

List of references

[ALF00] Alfredsson B and Olsson M. Standing contact fatigue testing of a ductile material: surface and subsurface cracks, Fatigue Fract. Engng. Mater. Struct., 23 (2000) 229-240.

[ALF01] Alfredsson B and Olsson M. Applying multiaxial fatigue criteria to standing contact fatigue, International Journal of Fatigue, 23 (2001) 553-548.

[ALF03] Alfredsson B and Olsson M. Inclined standing contact fatigue, Fatigue Fract. Engng. Mater. Struct., 26 (2003) 589-602.

[ANT97] Antretter T and Fischer FD. Critical shapes and arrangements of carbides in high-speed tool steel, Materials Science and Engineering, A237 (1997) 6-11.

[ARC56] Archard JF and Hirst W. The wear of metals under unlubricated conditions, Proceedings of the Royal Society of London, Series A236, Mathematical and Physical Sciences (1956) 397-410.

[ARZ98] Arzt E. Size effects in materials due to microstructural and dimensional constraints: a comparative review, Acta Materialia, 46 (16) (1998) 5611-5526.

[BAU81] Bauer-Grosse E, Morniroli JP, Le Caer G, Frantz C. Etude des defaults de structure dans le carbure de fer métastable (Fe_7C_3) formé lors de la cristallisation d'alliages amorphes fer-carbone, Acta Metallurgica, 28(12) (1981) 1983-1992.

[BER87] Berns H, Lueg J, Trojahn W, Wähling R, Wisell H. The fatigue behavior of conventional and powder metallurgical high speed steels, Powder Metall. Int., 19 (1987) 22-26.

[BER98] Berns H, Melander A, Weichert D, Asnafi N, Broeckmann C, Groβ-Weege A. A new material for cold forging tools, Computational Materials Science, 11 (1998) 166-180.

[BOL98] Bolton JD, Gant AJ. Fracture in ceramic-reinforced metal matrix composites based on high-speed steel, Journal of Materials Science, 33 (1998) 939-953.

[BON06] Boniardi M, D'Errico F, Tagliabue C. Influence of carburizing and nitriding on failure of gears – A case study, Engineering Failure Analysis, 13 (2006) 312-339.

[BOW72] Bowman AL, Arnold GP, Storms EK, Nereson NG. The crystal structure of $Cr_{23}C_6$, Acta Cryst. B28, (1972) 3102-3103.

[CAS00] Casellas D. Influencia de la microestructura en la fatiga y fractura de circonas estabilizadas con itria y desarrollo y caracterización mecánica de materiales Y-TZP/PSZ, PhD. Thesis, Universitat Politècnica de Catalunya, Barcelona, April 2000.

[CAS07] Casellas D, Caro J, Molas S, Prado JM, Valls I. Fracture toughness of carbides in tool steels evaluated by nanoindentation, Acta Materialia,55 (2007) 4277-4286.

[COB09] Cobo R, Pla M, Hernández R, Benito JA. Analysis of the decrease of the apparent Young's Modulus of advanced high strength steels and its effect in bending simulations, Proc. of the IDDRG Conf, Eds. Levy BS, Matlock DK, Van Tyne CJ pp.109-117; Golden, CO (USA), 2009.

[CUA12] Cuadrado N, Casellas D, Anglada M and Jiménez-Piqué E. Evaluation of fracture toughness of small volumes by means of cube-corner indentation. Scripta Materialia, 66 (2012) 670-673.

[DIE61] Dieter GE Jr. Mechanical Metallurgy, Eds. McGraw-Hill Book Company and Kogakusha Company, LTD., International Student Edition, New York, 1961, 301-304.

[DOU96] Dougherty JD, Srivatsan TS, Padovan J. Cyclic stress response, strain resistance and fracture behavior of modified 1070 steel, Engng. Fract. Mech., 53 (1996) 829-847.

[DUB01] Dubar M, Dubar L, Dubois A, Verleene A, Oudin J. Wear criteria of cold forming tools, Surface Engineering, 17(2) (2001) 119-122.

[EBN01] Ebner R, Leitner H, Caliskanoglu D, Marsoner S, Jeglitsch F. Methods for characterizing the precipitation of nanometer-sized secondary hardening carbides and related effects in tool steels, Z. Metallkd., 92 (7) (2001) 820-829.

[ERD00] Erdogan F. Fracture mechanics, Int. Journal of Solids and Structures, 37 (2000), 171-183.

[ERS08] Ersoy-Nürnberg K, Nürnberg G, Golle M, Hoffmann H. Simulation of wear on sheet metal forming tools – An energy approach, Wear, 265 (2008) 1801-1807.

[FET08] Fett T. Stress intensity factors – T-streses – Weigth functions, Universitätsverlag Karlsruhe, Karlsruhe, Germany, 2008 (299-304).

[FLE85] Fleck NA, Shin CS, Smith RA. Fatigue crack growth under compressive loading, Engineering Fracture Mechanics, 21(1) (1985) 173-185.

[FUK04] Fukaura K, Yokoyama Y, Yokoi D, Tsuji N, Ono K. Fatigue of cold work tool steels: effect of heat treatment and carbide morphology on fatigue crack formation, life and fracture surface observations, Met. Mat. Trans. A, 35A (2004) 1289-1300.

[GOM97] Gomes MA, Wronski AS, Wrigth CS. Monotonic subcritical crack growth in T42 high speed steel, International Journal of Fracture, 83 (1997) 207-221.

[HAM01] Hambli R. Blanking tool wear modelling using the finite element method, Int. Journal of Machine Tolls & Manufacture, 41 (2011) 1815-1829.

[HAM03] Hambli R. BLANKSOFT: a code for sheet metal blanking processes optimization, Journal of Materials Processing Technology, 141 (2003) 234-242.

[HER83] Hertzberg RW. Deformation and fracture mechanics of engineering materials, Ed. John Wiley & Sons, 2nd edition, New York, 1983, 233-324, 353-424 and 457-618.

[HÖG] Högman B. Blanking of ultra high strength steel sheet, Proceedings of the 6th International Tooling Conference, Eds.: Bergström J, Fredriksson G, Johansson M, Kotik O, Thuvander F, Karlstad, Sweden (2002), pp. 203 – 216.

[HOR83] Horton SA, Child HC. Relationship between structure and fracture behavior in 6W-5Mo-2V type high-speed steel, Metals Technology, 10 (1983), 245-256.

[HØR02] Højerslev C, Carstensen JV, Brøndsted P, Somers MAJ. Fatigue crack behaviour in a high strength tool steel, 8th International Fatigue Congress, Eds. Blom AF, Stockholm, June 2002, pp. 352-359.

[HSU10] Hsu TY, Wang Z. Fatigue crack initiation at notch root under compressive cyclic loading, Procedia Engineering, 2 (2010) 91-100.

[JES06] Jesner G, Marsoner S, Schemmel I, Haeussler K, Ebner R, Pippan R. Damage mechanisms in materials for cold forging dies under loading conditions typical for dies, Proceedings of the 7th International Tooling Conference, vol. 1, Eds. Rosso M, Actis Grande M, Ugues D, Torino, May 2006, pp. 29-36.

[JES09] Jesner G, Pippan R. Failure Mechanisms in a fatigue-loaded high-performance powder metallurgical tool steel, Metallurgical and Materials Transactions, 40 A (2009) 810-817.

[JON08] Jonsson P, Kjellsson K, Stenberg N, Wiklund D. Laser hardened trimming tools: wear test and geometry evaluation, Proc. of the IDDRG Conf, pp.639-650; Olofström (Sweden), 2008.

[KAY96] Kayser FX. "A re-examination of Westbrook's X-ray diffraction pattern for Cr_7C_3", Materials Research Bulletin, 31(6) (1996) 635-638.

[KOG09] Koglin K and Danzl M. Car body concepts of the future, Proc. of the Int. Conf. for Innovative Developments for Lightweight Vehicle Structures, Ed. Volkswagen AG, pp. 233-260; Wolfsburg (Germany), 2009.

[KRI07] Krishnadev MR and Jain SC. Improved productivity through failure analysis: Case studies in precision forging of aerospace components, Engineering Failure Analysis, 14 (2007) 1053-1064.

[KRÖ10] Krönauer B, Hirsch M, Golle R, Hoffmann H, Golle M, Jesner G, Pelloso G, Baron L, Hermann M. Further results in blanking from –hardened ultra high strength Manganese-Boron-steels with innovative tools and tool steels; In: Proc. of the IDDRG Conf, pp.121-130; Graz (Austria), 2010.

[LAN90] Lange K. Umformtechnik Handbuch für die Industrie und Wissenschaft, Band 3: Blechbearbeitung, 2nd Edition, Springer-Verlag, Berlin Heidelberg 1990.

[LAW93] Lawn B. Fracture of brittle solids, Eds. Davis EA, Ward IM, Cambridge University Press, 2nd Edition, Cambridge, 1993, 194-248.

[LIU07] Liu, H. Method of predicting wear of a die surface, Ford Global Tecnologies, LLC., Dearborn, Mi. (2007) US007200496B2.

[LU09] Lu LT, Zhang JW, Shiozawa K. Influence of inclusion size on S-N curve characteristics of high-strength steels in the giga-cycle fatigue regime, Fatigue Fract. Engng. Mater. Struct., 32 (2009) 647-655.

[LUO99] Luo SY. Effect of the geometry and the surface treatment of punching tools on the tool life and wear conditions in the piercing of thick steel plate, Journal of Materials Processing Technology, 88 (1999) 122-133.

[MAC10] Mackensen A, Ostermair M, Hoffmann H. Investigation of a composite cast cutting tool for blanking of AHSS sheet materials, Proc. of the IDDRG Conf, pp.335-344; Graz (Austria), 2010.

[MAE08] Maekawa, S, Yasugi, K. Apparatus for detecting or predicting tool breakage, Fanuc Ltd, Yamanashi, Japan (2008) US007403868B2.

[MEL02] Melander A, Haglund S. A new model for fatigue failure due to carbide clusters, Proceedings of the 6th International Tooling Conference, Eds.: Bergström J, Fredriksson G, Johansson M, Kotik O, Thuvander F, Karlstad, Sweden (2002), pp. 699 – 710.

[MEU01] Meurling F, Melander A, Tidesten M, Westin L. Influence of carbide and inclusion contents on fatigue properties of high speed steels and tool steels, International Journal of Fatigue, 23 (2001) 215-224.

[MIS04] Miserez A, Rossoll A, Mortensen A. Fracture of aluminium reinforced with densely packed ceramic particles: link between the local and the total work of fracture, Acta Materialia, 52 (2004), 1337-1351.

[MUG02] Mughrabi H. On “multi-stage” fatigue life diagrams and the relevant life-controlling mechanisms in ultrahigh-cycle fatigue, Fatigue Fract. Engng. Mater. Struct., 25 (2002) 755-764.

[MUR02] Muro P, Gimenez S, Iturriza I. Sintering behaviour and fracture toughness characterization of D2 matrix tool steel, comparison with wrought and PM D2, Scripta Materialia, 46 (2002), 369-373.

[NAG94] Nagao Y, Knoerr M, Altan T. Improvement of tool life in cold forging of complex automotive parts, Journal of Materials Processing Technology, 46 (1994) 73-85.

[NEW84] Newman JC, Raju IS. Stress intensity factor equations for cracks in three dimensional finite bodies subjected to tension and bending loads, NASA Technical Memorandum 85793, April 1984.

[NOT10] Nothhaft K, Jocham D. Simulative Betrachtung und Optimierung des Scherschneidens pressgehärteter Stähle, internal research studies, Institute of Metal Forming and Casting, Technische Universität München, 2010.

[NOT11] Nothhaft K, Koebler C. Examination of shear cutting experiments with Ultra High Strength Steels, internal research studies, Institute of Metal Forming and Casting, Technische Universität München, 2011.

[NOW47] Nowotny H, Kieffer R. Roentgenographic investigation of carbide systems, Metallforschung, 2 (9) (1947) 257-265.

[NYS97] Nyström M, Söderlund E, Karlsson B. Plastic zones around fatigue cracks studied by ultra-low indentation technique. Int. J. Fatigue, 17(2) (1995) 141-147.

[OLI92] Oliver WC and Pharr GM. An improved technique for determining hardness and elastic modulus using load and displacement sensing indentation experiments, J. Mater. Res., 7(6) (1992) 1564-1583.

[OLI04] Oliver WC and Pharr GM. Measurement of hardness and elastic modulus by instrumented indentation: Advances in understanding and refinements to methodology, J. Mater. Res., 19(1) (2004) 3-20.

[PED97] Pedersen TO. On local damage development in cold-forging tools, Transactions of the 14th International Conference on Structural Mechanics in Reactor Technology (SMiRT 14) Lyon, France, 1997 pp. 17-22.

[PER08] Pereira MP, Duncan JL, Yan W, Rolfe BF. Contact pressure evolution at the die radius in sheet metal stamping, Journal of Materials Processing Technology, 209 (2009) 3532-3541.

[RAM93] Ramamurthi, K. System and method utilizing a real time expert system for tool life prediction and tool wear diagnosis, Texas Instruments Incorporated, Dallas, Tex. (1991) US005251144A.

[RAM99] Rammerstorfer FG, Plankensteiner AF, Fischer AD, Antretter T. Hierarchical models for simulating the mechanical behavior of heterogeneous materials: an approach to high speed tool steels, Materials Science and Engineering, A259 (1999) 73-84.

[RAN08] Randelius M. Influence of microstructure on fatigue and ductility properties of tool steels, Licentiate thesis, Materials Science and Engineering, Royal Institute of Technology, 2008 ISBN: 978-91-7178-859-7.

[RIT08] Ritchie RO, Koester KJ, Ionova S, Yao W, Lane NE and Ager III JW. Measurement of the toughness of bone: A tutorial with special reference to small animal studies, Bone, 43 (2008) 798-812.

[ROB98] Roberts G, Krauss G, Kennedy R. Tool steels, ASM International, 5th edition, Materials Park OH, 1998.

[SHA09] Sharpe R, Smokers R. Assessment with respect to long term CO_2 emission targets for passenger cars and vans, AEA Energy & Environment, Report to the European Commission, ENV/C.5/FRA/2006/0071, 2009.

[SHI01] Shiozawa K, Lu L, Ishihara S. S-N curve characteristics and subsurface crack initiation behavior in ultra-long life fatigue of a high carbon-chromium bearing steel, Fatigue Fract. Engng. Mater. Struct., 24 (2001) 781-790.

[SHI06-1] Shiozawa K, Morii Y, Nishino S. Subsurface crack inititiation and propagation mechanism under the supper-long fatigue regime for high speed tool steel (JIS SKH51) by fracture surface topographic analysis, JSME Int. Journal A, 49(1) (2006) 1-10.

[SHI06-2] Shiozawa K, Morii Y, Nishino S, Lu L. Subsurface crack initiation and propagation mechanisms in high-strength steel in a very high cycle fatigue regime, International Journal of Fatigue, 28 (2006) 1521-1532.

[SO08] So H, Hoffmann H, Golle R. Scheidstrategien zum wirtschaftlichen Zerteilen pressgehärteter Stahlbleche, Merklein M, Tagungsband zum 3. Erlanger Workshop Warmblechumformung, Meisenbach Bamberg, Germany, 2008.

[SO09] So H, Hoffmann H, Golle, R. Blanking of press hardened ultra high strength steel, Proc. of the Hot Sheet Metal Forming of High-Performance Steel, pp.137-146; Luleå (Sweden), 2009.

[SOH08-1] Sohar CR, Betzwar-Kotas A, Gierl C, Weiss B, Danninger H. Gigacylce fatigue behavior of a high chromium alloyed cold work tool steel, International Journal of Fatigue, 30 (2008) 1137-1149.

[SOH08-2] Sohar CR, Betzwar-Kotas A, Gierl C, Weiss B, Danninger H. Fractographic evaluation of gigagycle fatigue crack nucleation and propagation of a high Cr alloyed cold work tool steel, International Journal of Fatigue, 30 (2008) 2191-2199.

[SOH08-3] Sohar CR, Betzwar-Kotas A, Gierl C, Weiss B, Danninger H. Influence of surface residual stresses on gigacycle fatigue response of high chromium cold work tool steel, Mat.-wiss. U. Werkstofftech., 39(3) (2008) 248-257.

[STA05] Stachowiak GW, Batchelor AW. Engineering tribology, 3rd edition, Ed. Elsevier Butterworh-Heinemann, Burlington, MA, USA, 2005 (571-593).

[TOR95] Torizawa, Y, Shimizu, S, Okabe, M. Apparatus for predicting tool life, Okuma Corporation, Nagoya, Japan (1995) US005428556A.

[UDD06] Uddeholm, SSAB Swedish Steel; Soluciones para utillajes de trabajo en frío para aceros avanzados de alta resistencia. Guía de selección. Agosto 2006.

[VAN04] Vander Voort GF, Manilova EP, Michael JR and Lucas GM. Study of Selective Etching of Carbides in Steel, Fortschritte in der Metallographie 36, Sonderbande der Praktischie Metallographie 36, Deutsche Gesellschaft fur Materialkunde e.V., Frankfurt, Germany, 2004, 255-260.

[VAN08] Van Ratingen MR. The changing outlook of Euro NCAP, Euro NCAP, Airbag 2008, 2008.

[VIN02] Vinter Dahl K. Fractography analysis of tool samples used for cold forging, Risø National Laboratory, Roskilde, 2002 (Risø-R-1359 (EN)) ISBN 87-550-P102-1.

[YAM09] Yamada K, Wakayama S. AE monitoring of microdamage during flexural fracture of cermets, EURO PM2009 Conference Proceedings, vol.1, Ed. EPMA, Copenhagen, October 2009, pp. 247-252.

[YOK03] Yokoi D, Tsujii N, Fukaura K. Effects of tempering temperature and stress amplitude on low-cycle fatigue behavior of a cold work tool steel, Materials Science Research International, 9 (3) (2003) 216-222.

[YOS06-1] Yoshida H, Itoh S. Method of predicting damage of dies, Daido Steel Co., LTD., Nagoya, Japan (2006) US200602300881A1.

[YOS06-2] Yoshida H, Itoh S, Okajima T., Method of predicting damage of dies, Daido Steel Co., LTD., Nagoya, Japan (2006) US20060266125A1.

[WAS09] Advanced high strength steel (AHSS) application guidelines (v4.1), WorldAutoSteel; 2009.

[WAY94] Wayne SF, O'Nei, DA, Zimmermann CE, Val Y. Method and system for designing a cutting tool, Valenite Inc, Madison Heights, Mich. (1994) US005377116A.

[WEI61] Weibull W. Fatigue testing and analysis of results, Pergamon Press (1961), 16-7.

Published articles

Nothhaft K, Suh J, Golle M, Picas I, Casellas D, Volk W. *Shear cutting of press hardening steel: influence of punch chamfer on process forces, tool stresses and sheared edge qualities*, Production Engineering, 6 (2012) 413-420.

Martínez-González E, Picas I, Casellas D, Romeu J. *Analysis of fracture resistance of tool steels by means of Acoustic Emission*, Journal of Acoustic Emission, 28 (2010) 163-169.

Picas I, Cuadrado N, Casellas D, Goez A, Llanes L. *Microstructural effects on the fatigue crack nucleation in cold work tool steels*, Procedia Engineering, 2 (2010) 1777-1785.

Articles published in conferences

Inngebrand A, Valls I, Molas S, Picas I, Casellas D. *New tool steel with very high levels of toughness for cutting of press hardened steel and other demanding applications*, Proceedings of the 9th International Tooling Conference, Eds. Leitner H, Kranz R, Tremmel A (Leoben 2012) pp. 235-240 (ISBN 978-3-901384-52-3).

Picas I, Martínez-González E, Casellas D, Romeu J. *Analysis of Micro-mechanical Damage in Tool Steels Coupling Fracture Tests and Acoustic Emission*, Proceedings of the 19th European Conference on Fracture, (Kazan 2012) (ISBN 978-5-905576-18-8).

Picas I, Muñoz R, Lara A, Hernández R, Casellas D. *Effect of the cutting process in the mechanical and fatigue properties of press hardened 22MnB5 steel*, Proceedings of the 3rd International Conference on Hot Sheet Metal Forming of High-Performance steel, Eds. Oldenburg M, Steinhoff K, Prakash B, (Kassel 2011) pp. 85-92 (ISBN 978-3-942267-17-5).

Picas I, Hernández R, Casellas D, Valls I. *Influence of the microsctructure in the tribo-mechanical behavior of UHSS cutting tools*, Proc. of the IDDRG 2011 International Conference, (Bilbao 2011).

Picas I, Cuadrado N, Casellas D, Goez A, Llanes L. *Efecto de la microestructura en la nucleación y propagación de fisuras en aceros de herramienta de trabajo en frío*, XXVIII Encuentro del grupo español de fractura, Ed. Secretaría del grupo español de fractura (Gijón 2011) pp. 217-22 (ISSN 0213-3725).

Picas I, Cuadrado N, Casellas D, Goez A, Llanes L. *Influence de la microstructure dans les mécanismes de nucléation de fissures de fatigue dans des aciers pour outils de travail à froid*, Matériaux 2010, (Nantes 2010) (ISBN978-2-9528-1403-4).

Martínez-González E, Picas I, Casellas D, Romeu J. *Analysis of fracture resistance of tool steels by means of Acoustic Emission*, 29th European Conference on Acoustic Emission Testing (Vienna 2010) (ISBN: 978-3-200-01956-0).

Picas I, Hernández R, Casellas D. *Strategies to increase the tool performance in punching operations of UHSS*, 50th Anniversary Conference: Tools and Technologies for the Processing of Ultra High Strength Steels, IDDRG 2010 Conference Proceedings, Ed. Kolleck R (Graz 2010), pp. 325-344 (ISBN 978-3-85125-108-1).

Laumann T, Picas I, Grané M, Casellas D, Riera MD, Valls I. *Hard cutting of tailored hardened 22MnB5*, 50th Anniversary Conference: Tools and Technologies for the Processing of Ultra High Strength Steels, IDDRG 2010 Conference Proceedings, Ed. Kolleck R (Graz 2010), pp. 355-362 (ISBN 978-3-85125-108-1).

Picas I, Hernández R, Casellas D, Valls I. *Cold cutting of microstructurally tailored hot formed components*, Proceedings of the 2nd International Conference on Hot Sheet Metal Forming of High-Performance steel, Eds. Oldenburg M, Steinhoff K, Prakash B, (Luleå 2009) pp.115-125 (ISBN 978-3-937524-84-9).

Hernández R, Picas I, Llobet A, Casellas D. *Estimation of tool performance during cold forming of AHSS*, Proceedings of the IDDRG 2009 International Conference, Eds. Levy BS, Matlock DK, Van Tyne CJ (Golden 2009) pp.703-714 (ISDN 978-0-615-29641-8).

Casas B, Casellas D, Picas I, Rodriguez N, Valls I. *Improvement of wear resistance of PM tool steels through microstructural design*, Proceedings of the 8th International Tooling Conference, Eds. Beiss P,

Broeckmann C, Franke S, Keysselitz B (Aachen 2009) pp. 643-650 (ISBN 10: 3-8613-0701-4, ISBN 13: 978-3-8613-0701-3).

Goez A, Picas I, Valls I, Casas B, Casellas D, Llanes L. *Fatigue strength of cold work tool steels: microstrutcture – critical flaws correlation*, Proceedings of the 8th International Tooling Conference, Eds. Beiss P, Broeckmann C, Franke S, Keysselitz B (Aachen 2009) pp. 651-660 (ISBN 10: 3-8613-0701-4, ISBN 13: 978-3-8613-0701-3).

Picas I, Hernández R, Casellas D, Casas B, Valls I. *Mechanical performance of cold forming tools*, Proceedings of the 8th International Tooling Conference, Eds. Beiss P, Broeckmann C, Franke S, Keysselitz B (Aachen 2009) pp. 1037-1048 (ISBN 10: 3-8613-0701-4, ISBN 13: 978-3-8613-0701-3).

Casellas D, Picas I, Castellà M, Goez A, Llanes L, Casas B, Valls I. *Effect of carbides properties and microstructural characteristics on crack nucleation and propagation in cold forming tools*, Proceedings of the 8th International Tooling Conference, Eds. Beiss P, Broeckmann C, Franke S, Keysselitz B (Aachen 2009) pp. 479-490 (ISBN 10: 3-8613-0701-4, ISBN 13: 978-3-8613-0701-3).

Picas I, Hernández R, Casellas D, Valls I. *Aplicación de la mecánica de la fractura para optimizar la relación desgaste-tenacidad en herramientas de corte en frío de aceros de alta resistencia*, XXVI Encuentro del Grupo Español de Fractura, Ed. Secretaría del Grupo Español de Fractura (Santander 2009) pp. 611-616 (ISSN 0213-3725).

Goez A, Picas I, Torres Y, Casellas D, Llanes L. *Comportamiento a Fractura de aceros para trabajo en frío: influencia de la microestructura*, XXVI Encuentro del Grupo Español de Fractura, Ed. Secretaría del Grupo Español de Fractura (Santander 2009) pp. 136-141 (ISSN 0213-3725).

Picas I, Hernández R, Casellas D, Casas B, Valls I. *Tool performance in cutting of hot stamped steels*, Proceedings of the 1st International Conference on Hot Sheet Metal Forming of High-Performance steel, Eds. Oldenburg M, Steinhoff K, Prakash B, (Kassel 2008) pp. 179-190 (ISBN 978-3-937057-18-7).

Picas I, Pérez R, Lara A, Prado JM. A new methodology to determine the plastic anisotropy using optical strain measuring systems: application on AHSS sheet strips and tubes, Proceedings of the IDDRG 2008 conference, (Olofström 2008) pp. 69-79 (ISBN 978-91-633-2948-7).

Picas I, Casellas D, Llobet A, Hernández R, Riera MD, Valls I, Casas B. *Mechanical performance of tools in cold forming of high strength steels*, International Conference on New Developments in Advanced High-Strength Sheet Steels Proceedings, Eds. Association for Iron & Steel Technology (Orlando 2008) pp. 390-400 (ISBN 978-1-886362-99-4).

Casellas D, Picas I, Goez A, Torres Y, Llanes L, Valls I, Casas B. *Microstructural effects on the fatigue resistance of cold work tool steels for shaping AHSS*, , International Conference on New Developments in Advanced High-Strength Sheet Steels Proceedings, Eds. Association for Iron & Steel Technology (Orlando 2008) pp. 401-408 (ISBN 978-1-886362-99-4).

Articles submitted

Lara A, Picas I, Casellas D. *Effect of the cutting process on the fatigue behaviour of press hardened steels*, Journal of Material Processing Technology 2012; 00:0000-0000.

Picas I, Martínez-González E, Casellas D, Romeu J. *Analysis of Micro-mechanical Damage in Tool Steels Coupling Fracture Tests and Acoustic Emission*, Meccanica 2012; 00:0000-0000.

Picas I, Casellas D, Llanes L. *Analysis of monotonic subcritical crack growth in tool steels*, Materials Science and Engineering 2012; 00:0000-0000.